DYNAMIC MODELING OF THE HYDROLOGIC PROCESSES IN AREAS OF DISCONTINUOUS PERMAFROST

A

DISSERTATION

Presented to the Faculty

of the University of Alaska Fairbanks

in Partial Fulfillment of the Requirements

for the Degree of

DOCTOR OF PHILOSOPHY

By

William Robert Bolton, B.A., M.S.

Fairbanks, Alaska

August 2006

DYNAMIC MODELING OF THE HYDROLOGIC PROCESSES IN AREAS OF DISCONTINUOUS PERMAFROST

By

William Robert Bolton

RECOMMENDED:

Advisory Committee Chair

Chair, Department of Civil Engineering

APPROVED:

Dean, College of Engineering and Mines

Dean of the Graduate School

August 22, 2006

Date

Abstract

The overarching hypothesis of this dissertation is *"in the sub-arctic environment, the presence or absence of permafrost is dominant influence on hydrologic processes."* The presence or absence of permafrost is the defining hydrologic characteristic in the sub-arctic environment. Discontinuous permafrost introduces very distinct changes in soil hydraulic properties, which introduce sharp discontinuities in hydrologic processes and ecosystem characteristics. Hydraulic properties vary over short and long time scales as the active layer thaws over the course of a summer or with changes in permafrost extent. The influence of permafrost distribution, active layer thaw depth, and wildfire on the soil moisture regime and stream flow were explored through a combination of field-based observations and computer simulations. Ice-rich conditions at the permafrost table do not allow significant percolation of surface waters, which result in saturated soils near the ground surface and limited subsurface storage capacity, compared to well-drained non-permafrost sites. The removal of vegetation by wildfire results in short-term (<10 years) increases in moisture content through reduced evapotranspiration. Long-term (>10 years) drying of soils in moderate to severe wildfire sites is the result of an increased active layer depth and storage capacity. A spatially-distributed, process-based hydrologic model, TopoFlow, was modified to allow spatial and temporal variation in the hydraulic conductivity and porosity of soils. By continual variation of the hydraulic conductivity (proxy for permafrost distribution and active layer thaw depth) and porosity (proxy for storage capacity), the dynamic soil properties found in the sub-arctic environment are adequately represented. The sensitivity of TopoFlow to changes in permafrost condition, vegetation regime, and evapotranspiration is analyzed. The net result of the field observations and computer simulations conducted in this research suggest the presence or absence of permafrost is the dominant influence on soil moisture dynamics and has an important, but secondary role in the stream flow processes.

Table of Contents

List of Figures

List of Tables

Acknowledgements

Throughout my graduate career, I have been fortunate to work and interact with a number of wonderful people and researchers. I would like to thank my major advisor, Dr. Larry Hinzman, for his continuous encouragement, support, and enthusiasm throughout my program. Larry's door was always open for me to ask questions, talk about problems, and offer advice and solutions to the topic of the day. I would also like to thank Dr. John Fox for his encouragement, support, and advice during our long discussions about all things science and not. Dr. Douglas Kane and Dr. Terry Chapin provided many useful suggestions during the development of my project and throughout the writing process. Dr. Kenji Yoshikawa was instrumental to the success of all parts of my graduate program. Dr. Julia Boike helped provide the focus needed to finish. Dr. Scott Peckham provided insight to the TopoFlow model. Tim Howe provided valuable statistical advice. Many thanks go to Michael Lilly for introducing me to Larry Hinzman and for opening the door to this field.

I am thankful to all the people who spent many long (and great) days helping with me in the field: Trevor White, Hansel Klausner, Jeremiah Drage, Andy Monaghan, Crane Johnson, Julie Knudson, Bob Busey, Brandon Peltier, Rachel Halstead, Joni Wilm, Shawna Laderach, Matt Stone, Matt Fraver, Wendy Davis, Byron Roys, Gordon MacIntosh, Jennifer Benning, Baozhong Liu, John Galligher, Peter Cleary, Glory Rae Erickson, Neal Mead, Dr. Jock Irons, Dave and Michelle Claar, Ivan Romanovsky, Ann Farris, Kevin Petrone, Dr. Larry Hinzman, and Dr. Kenji Yoshikawa. Rob Gieck and Bub Mueller provided valuable advice, insight, and knowledge while planning my field program and instrumentation.

I would also like to thank fellow graduate student Kevin Petrone for the help in CPCRW and our scientific discussions. Paul Overduin kept me going through the INRA experiment / program. Norma Haubenstock helped me keep (or at least try) some sort of perspective. Ryan Woodard among other things taught me how to be a humble loser of 'The Race,' and all things Linux.

Finally, I would like to thank Ann. Without her support, help, and understanding, I would not have been able to begin or complete this endeavor. Thank you.

This research was largely supported by the National Science Foundation FROSTFIRE, Long-Term Ecological Research, and Arctic System Science Freshwater Integration projects.

The Inland Northwest Research Alliance provided a two-year graduate fellowship through its Subsurface Science Research Initiative. Additional support was provided by the University of Alaska Graduate School, the University of Alaska Center for Climate Change, and the Alaska Section of the American Water Resources Association.

Chapter 1
Introduction: Soil moisture and climate change in the Alaskan boreal forest

1.1 Climate change in the high latitudes

The body of evidence is mounting that the Arctic, including Alaska, is now experiencing an unprecedented degree of environmental change [*Chapman and Walsh*, 1993; *Serreze et al.*, 2000; *IPCC*, 2001; *ACIA*, 2005; *Hinzman et al.*, 2005]. The Arctic has warmed 0.098°C per decade from 1861-2000. More recently, the Arctic has warmed 0.364°C per decade for the 1977-2001 time period [*Jones and Moberg*, 2003] (both rates are statistically significant at the 95% level). In Alaska, the mean annual surface air temperature (Figure 1.1) has increased $2-3^{o}C$ over the past half century, with greater warming ($3-5^{o}C$) occurring during the winter (December - February) months [*Chapman and Walsh*, 1993; *Serreze et al.*, 2000; *ACIA*, 2005]. Widespread changes in precipitation, particularly during the winter months, have also been documented [*Kattsov and Walsh*, 2000; *Anisimov and Fitzharris*, 2001]. Most climate stations with a long-term record (> 40 years) in Alaska and Western Canada have observed a slight increase in precipitation [*Hinzman et al.*, 2005].

The mean global air temperature for the 2005 calendar year is the warmest on record (using instrumental data) for the past century – largely attributed to the anomalous warm temperatures experienced throughout the Arctic [*Hanson et al.*, 2006]. With the six warmest years occurring in the past eight years, coupled with a significant decrease in the Arctic Ocean ice cover [*Overpeck et al.*, 2005; *Stroeve et al.*, 2005], increases in the length of snow-free days [*Chapin et al.*, 2005; *Hinzman et al.*, 2005], and a northward movement of the tree-line into the arctic [*Chapin et al.*, 2005], many believe this warming trend will continue into the foreseeable future [*IPCC*, 2001; *ACIA*, 2005].

Associated with increases in surface temperature, the permafrost temperatures in the boreal forest region of Alaska have also increased [*Osterkamp and Romanovsky*, 1999; *Osterkamp*, 2003]. The permafrost condition in this region is unstable, as the permafrost temperature is very close to the melting point of ice, often $-1^{o}C$ or warmer [*Yoshikawa et al.*, 2002]. Increased surface temperatures in combination with an unstable thermal regime has resulted in a reduction in areal permafrost coverage and an increase in active layer depth (the layers of soil above the permafrost that freezes and thaws annually) [*Jorgenson et al.*,

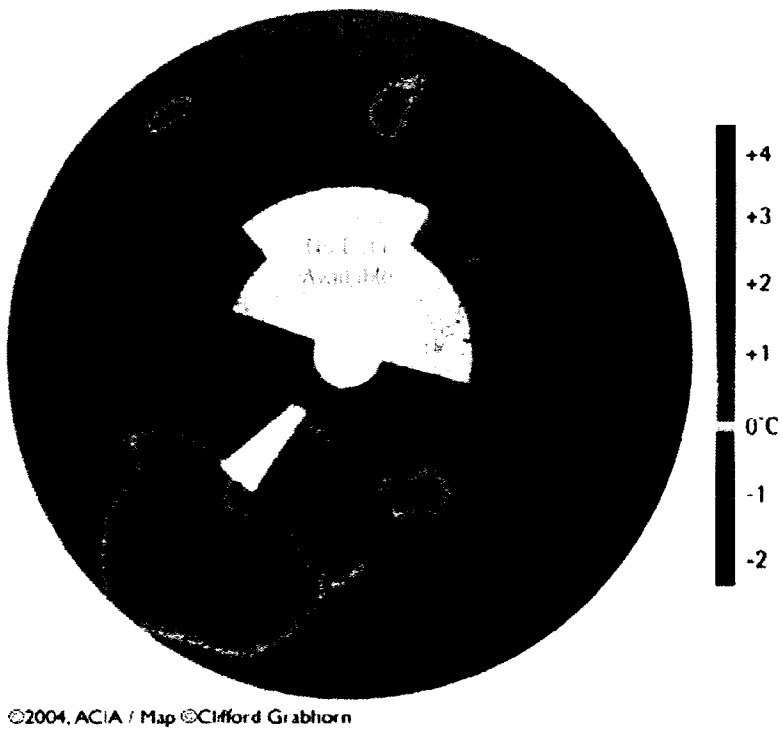

Figure 1.1: Observed air temperature change in the Arctic from 1954-2003. The left panel shows the annual change in air temperature. The right panel shows the winter (December - February) change in air temperature. Figures from *ACIA* [2005].

2001; *Serreze et al.*, 2002; *Yoshikawa et al.*, 2003; *Zhang*, 2005]. The observed change in the climate and thermal regimes have been reflected in the arctic hydrologic system, including later freeze-up and earlier break-up dates of rivers [*Magnuson et al.*, 2000], increased arctic river runoff [*Peterson et al.*, 2002], increased river baseflow in Russian rivers [*Peterson et al.*, 2002; *Yang et al.*, 2002], shrinking (or draining) of lakes [*Smith et al.*, 2005], and an increase in thermokarst development [*Osterkamp and Romanovsky*, 1999; *Osterkamp et al.*, 2000; *Jorgenson et al.*, 2001]. As the thermal and hydrologic systems are fully coupled systems, it is not surprising the hydrologic system has responded to the changes in thermal regime [*Hinzman et al.*, 1991, 2005; *Walsh et al.*, 2005].

Compared to more temperate regions, the northern latitudes are more sensitive to a changing climate. This is due to several factors, including the reduction of surface albedo. The surface albedo is expected to be reduced through a decrease in sea ice cover, temporal and spatial reductions in snow cover, and a northward expansion of the boreal forest [*ACIA*, 2005; *Chapin et al.*, 2005]. Based on general circulation model(GCMs) projections, increases in air temperature (particularly winter) and precipitation (both summer and winter) that are expected to continue into the next century (Figure 1.2)[*IPCC*, 2001; *ACIA*, 2005].

1.2 Importance of soil moisture and stream flow

The soil moisture regime plays an important role in a number of processes related to climate change including land-atmosphere interactions, soil respiration, permafrost distribution, and the frequency and severity of wildfires.

1.2.1 Land-atmosphere interaction

The energy exchange between the land, oceans, the sea ice, and atmosphere controls the Earth's climate system on local, regional, and global scales [*Eugster et al.*, 2000]. Soil moisture is the single most important terrestrial factor controlling the surface energy balance after the presence or absence of snow cover. The partitioning of available energy (net radiation minus the ground heat flux) into sensible and latent heat is largely controlled by the soil moisture content [*Betts et al.*, 1999]. Furthermore, soil moisture also is a control on the net solar (short wave) radiation, as the albedo of bare soils, lichen, and *Sphagnum* increase with decreasing moisture content [*Eugster et al.*, 2000].

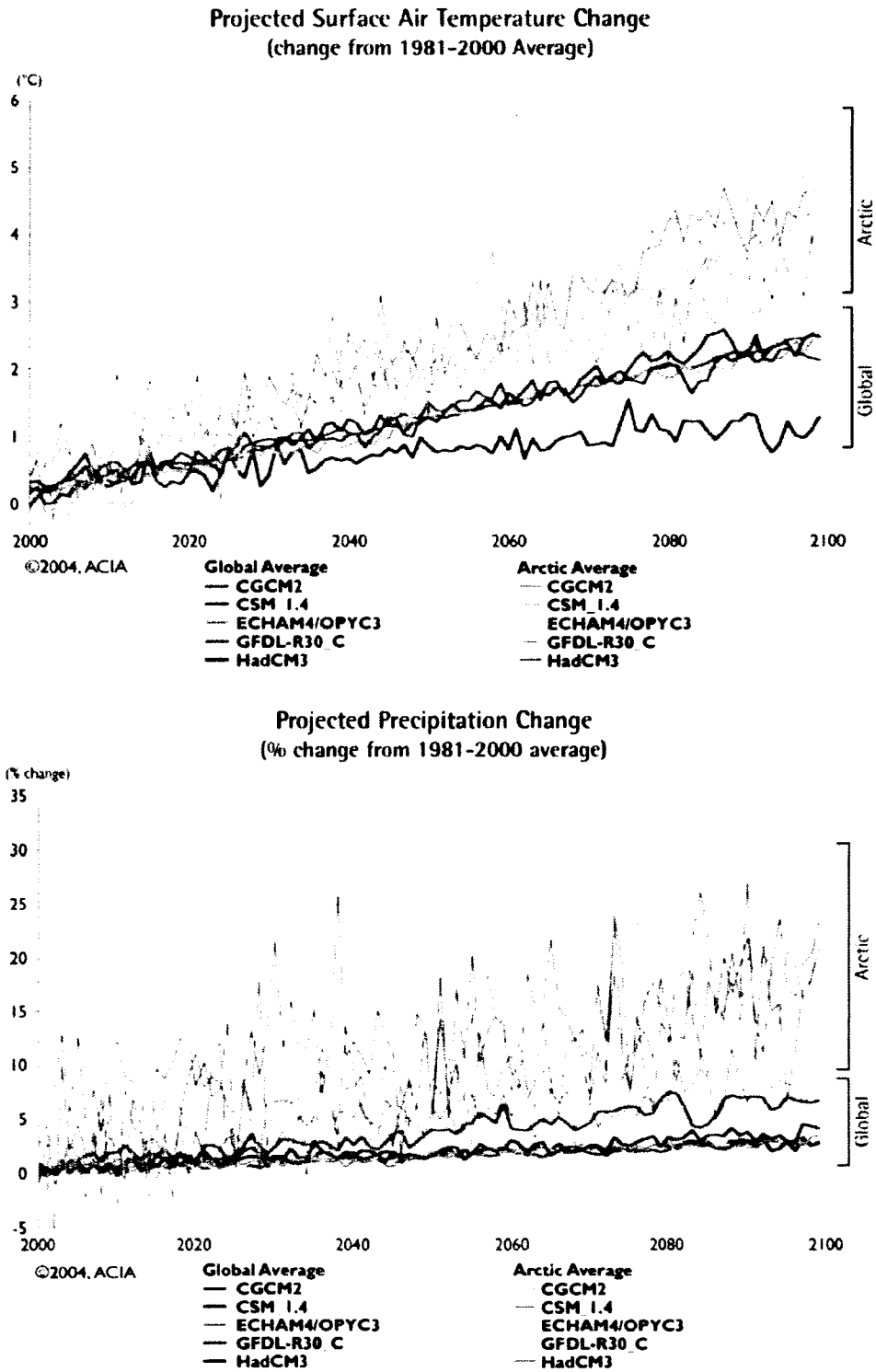

Figure 1.2: Average projected surface air temperature (upper panel) and precipitation (lower panel) from the five Arctic Climate Impact Assessment models. Heavy lines indicate global averages while light lines represent the projected change in the arctic region. Figures from *ACIA* [2005].

The role of soil moisture in the climate system has recently received increased attention. *Chapin et al.* [2000] recently suggested the relationship between the climate and soil moisture is a major knowledge gap in arctic and boreal forest research in North America. The global climate modeling community has also identified soil moisture as a significant factor in the land surface energy flux. These fluxes show steep gradients on both the regional and sub-grid scales in part due to the heterogeneous distribution of soil moisture [*Douville*, 2003].

1.2.2 Soil respiration

In the sub-arctic environment, soil respiration is typically slow due to low ground temperatures [*French et al.*, 1997]. As a result, the boreal forest has sequestered more than 37% of the total terrestrial carbon [*Smith et al.*, 1993; *Kasischke et al.*, 1995]. If surface temperatures increase as expected, the rate of soil respiration will increase. Soil moisture is important to this process as either carbon dioxide (CO_2) or methane (CH_4) are produced as a by-product in the soil respiration process [*Moore*, 1983; *Callaghan and Jonasson*, 1996; *Friborg et al.*, 2003]. In soils that are well drained (low soil moisture), aerobic decomposition of organic matter produces CO_2. In poorly-drained soils, anaerobic conditions prevail, which promotes the production of CH_4. Increasing the flux of either CO_2 or CH_4, both strong greenhouse gases, will result in a positive feedback, with increased emissions of either CO_2 or CH_4, resulting in increased surface temperatures. This will in turn further promote increases in soil respiration.

1.2.3 Permafrost distribution

Soil moisture is a major component in permafrost aggradation and degradation due to the thermal properties of water. Permafrost distribution is influenced by a number of factors such as landscape, soil types, and vegetation [*Haugen et al.*, 1982]. The presence and thickness of an organic layer overlying permafrost is one of the most important factors in the aggradation and degradation of permafrost [*Viereck*, 1982]. The thermal conductivity of soil is a function of moisture content, soil density, and temperature. Although an increase in soil moisture increases thermal conductivity of the soils (enhancing degradation of per-

mafrost in a warming climate), an increase in soil moisture also results in increased evaporation from the soil surface. Increases in the latent heat flux (from increased evaporation) will result in a decreasing soil temperature and a condition of permafrost maintenance or possible aggradation.

1.2.4 Wildfire

The frequency and severity of wildfires primarily depend upon the moisture condition (in part, soil moisture) of the fire fuels [*Rowe and Scotter*, 1973]. Wildfires have been a natural part of the boreal forest ecosystem history [*Rowe and Scotter*, 1973]. Fires in the boreal forest have both immediate and long-term impacts on the ecosystem due to effects on the surface energy balance, the water balance, and underlying permafrost. The effect of wildfire on soil moisture depends on the severity of fire, the soil type, and the presence of permafrost. Due to the fragile state of the permafrost regime, slight changes in either the energy or water balance may lead to threshold changes in the permafrost condition or ecosystem function (i.e. changing vegetation and soil moisture condition).

In the boreal forest, the fire return interval has been estimated to be between 50-500 years [*Yarie*, 1981; *Dyrness et al.*, 1986; *Kasischke et al.*, 1995]. Under a warming climate scenario, it has been hypothesized the frequency and severity of wildfires will increase due to warmer and drier conditions [*Van Wagner*, 1988; *Flannigan and Van Wagner*, 1991]. The total area burned in the North American boreal forest has more than doubled (10-year averages) from the 1960s through the 1990s, while the area burned in the contiguous United States has remained at nearly the same level over the same time period [*Kasischke et al.*, 2006].

1.2.5 Stream flow

The Arctic Ocean is the only ocean in the world in which its terrestrial contributing area is greater than the surface area of the ocean itself [*Vörösmarty et al.*, 2000]. Changes in the freshwater contribution (amount and timing) to the Arctic Ocean may affect the sea-ice formation process and alter the thermohaline circulation pattern [*Arnell*, 2005; *Walsh et al.*, 2005], potentially changing the climate system on local, regional, and global scales.

The boreal forest has an important role in the freshwater discharge to the Arctic Ocean, as the majority of the terrestrial contributing area originates within the boreal forest [*McGuire and Chapin*, 2006]. The timing and amount of precipitation, changes in permafrost dynamics, ecosystem changes (moving treeline, vegetation shifts), and disturbance (natural such as wildfire or man-made such as the building of dams) have all been identified as potential mechanisms leading to a shift in the freshwater budget of the Arctic Ocean [*McGuire and Chapin*, 2006]. *McGuire and Chapin* [2006] claim a major challenge to the research community is "to establish the link between permafrost changes of the boreal forest in response to a warming climate and changes in the discharge of freshwater into the Arctic Ocean." As mentioned earlier, increases in runoff from the major Russian rivers to the Arctic Ocean have already been documented [*Peterson et al.*, 2002; *Serreze et al.*, 2002; *Yang et al.*, 2002].

1.3 Research hypothesis

The overarching hypothesis for my research is ***'in the sub-arctic environment, the presence or absence of permafrost is the dominant influence on watershed hydrological processes'***. The sub-arctic is located in the transition zone between the Arctic and more temperate environments. As such, most of the current or expected changes to the hydrologic system, due to a changing climate, will be be experienced most dramatically and first in this region. For this reason, this study focuses on the hydrologic processes throughout the sub-arctic region.

The TopoFlow model is the product of several investigators efforts, including the present author. In this dissertation research, my primary objective is to develop a spatially-distributed, process-based numerical model, in order to describe, simulate, and predict the hydrological processes everywhere throughout a sub-arctic watershed. The aim of this model is to explore the effects of vegetation and soil type, distribution of permafrost, and amount and timing of precipitation on the hydrologic response in this region. More specifically, the following research objectives are explored in this research:

- To analyze field-based soil moisture patterns in areas underlain with permafrost and in permafrost-free areas
- To analyze stream discharge patterns in watersheds underlain with differing propor-

tions of permafrost

- To analyze the water balance components in the sub-arctic region and identify the important hydrologic processes in watersheds with varying permafrost extent
- To analyze the short- and long-term impacts of wildfire on the soil moisture regime in Interior Alaska
- To describe and apply a spatially-distributed, process-based hydrologic model in order to simulate spatial and temporal water balance components in the (sub-)arctic environment, including stream flow, snowmelt, evapotranspiration, infiltration & percolation, and groundwater flow.

1.4 Research questions

Based upon the objectives of this research, a number of research questions were formulated with the purpose of identifying a number of important issues.

1. *What are the differences in the soil moisture regime in areas underlain with permafrost compared to areas free of permafrost?* In the sub-arctic environment, understanding and being able to make accurate predictions of the soil moisture regime is essential to linking the terrestrial system to the local and regional climatic processes. The relationship between the climate system and the soil moisture distribution and active layer development has been identified by *Chapin et al.* [2000] as a major gap in boreal forest research.
2. *What are the important hydrologic processes in the sub-Arctic environment?* In light of the expected increases in both temperature and precipitation, it is important to understand and predict the feedback mechanisms of the water cycle [*Kane and Hinzman*, 2004]. In the sub-arctic, small changes in the natural system may lead to dramatic threshold changes to many of the hydrologic processes including stream flow, soil moisture dynamics, and evapotranspiration.
3. *Does vegetation type influence the soil moisture regime and stream flow patterns?* In the boreal forest, deciduous vegetation have latent fluxes which correspond to the equilibrium evaporation rate, while the latent heat flux of coniferous vegetation only

approaches 25-50% of the equilibrium evaporation rate [*Baldocchi et al.*, 2000; *Eugster et al.*, 2000]. Are the differences in vegetation types, through differences in evapotranspiration rates, translated to differences in the soil moisture and stream flow regimes?

4. *What are the short- and long-term impacts of wildfire on the soil moisture regime in Interior Alaska?* In the North American boreal forest, the area burned has more than doubled in the last 40 years [*Kasischke et al.*, 2006]. It has been hypothesized that in a warmer climate in the boreal forest, the frequency and severity of wildfires will continue to increase [*Hinzman et al.*, 2003].

5. *By spatially and temporally varying hydraulic conductivity and porosity of the soils, is it possible to simulate the hydrologic response in an area of discontinuous permafrost?* Simulation of the hydrologic processes is challenging due to rapidly changing thermal (permafrost versus non-permafrost, active layer development) and hydrologic (hydraulic conductivity and storage capacity) conditions in both time and space (x, y, and z-dimensions). Is it possible to accurately represent the permafrost regime, in hydrologic terms, by simply varying (both spatially and temporally) the hydraulic conductivity (proxy for permafrost distribution) and porosity (proxy for storage capacity) with active layer development?

6. *What are the consequences of climate change on the hydrologic response in the sub-arctic environment?* Once a hydrologic model is able to adequately simulate the present hydrologic processes of a sub-arctic watershed, it can be used to explore the impacts of a changing climate through applying different climate scenarios (via permafrost distribution, active layer development, air temperature, and precipitation).

I address these questions in two parts: 1) an extensive field data collection program, and 2) adaptation and application of a process-based, spatially-distributed numerical model to the sub-arctic environment. Three sub-basins of the Caribou-Poker Creeks Research Watershed (CPCRW), located 48 km north of Fairbanks, Alaska, have been the primary focus of my research. These sub-basins vary in areal extent of permafrost from approximately 3 to 53% [*Haugen et al.*, 1982; *Yoshikawa et al.*, 1998]. Formal descriptions (including site

maps) of CPCRW are found in Sections 2.1 and 3.2.

1.5 Outline of chapters

The reccurring question throughout this thesis (Chapters 2 - 5, Appendix A) is: How does the distribution of permafrost influence the soil moisture regime and hydrologic processes in a sub-arctic environment? The core chapters of this thesis are organized as a series of publications designed to address this question as well as the research questions described above. Each of these publications represents a step toward the modification and application of a numerical model capable of simulating the hydrologic processes in regions of discontinuous permafrost.

The sub-arctic environment can be characterized as being located in the zone of discontinuous permafrost. Although the distribution of permafrost in this region is site specific, it dominates the response of many of the hydrologic processes, including stream flow, soil moisture dynamics, and water storage processes. In Chapter 2 of this disertation, I analyze the stream flow response to precipitation events over the course of a summer [*Bolton et al.*, 2000]. The objectives of this chapter were to 1) compare the stream flow response to precipitation events in watersheds of varying permafrost coverage, and 2) investigate changes in stream flow composition over the same period using hydrograph separation techniques. Additionally, comparisons of soil moisture dynamics in an area underlain with permafrost and an area free of permafrost are presented.

The permafrost in Interior Alaska is warm and unstable when thawed (often between -1°C and 0°C [*Yoshikawa et al.*, 2002]) as these soils are usually ice-rich. With the expected changes in air temperature and precipitation (Section 1.1), it is important to be able to understand and predict the feedback mechanisms of the water cycle [*Kane and Hinzman*, 2004], where small changes in the natural system may result in dramatic, threshold changes in the hydrology, ecology, and surface energy balance, with subsequent climatological impacts on local and regional (and potentially global) scales. In 2004, a workshop was held to collect and synthesize the water balance components from 39 research watersheds located in or near the circumpolar north [*Kane and Yang*, 2004]. In Chapter 3, a long-term (1978-2003) water balance analysis of the three sub-watersheds of CPCRW is presented [*Bolton et al.*, 2004]. The focus of this study was to synthesize the water balance components from

watersheds of varying permafrost with the intent of identifying key similarities and differences in these components with permafrost coverage.

In Chapter 4, I describe the structure and formulation of a process-based hydrologic model, TopoFlow [*Bolton et al.*, In prep.-b]. TopoFlow is largely based upon the ARHYTHM model [*Hinzman et al.*, 1995; *Zhang et al.*, 2000], which was developed at the Water and Environmental Research Center, University of Alaska Fairbanks. The purpose of TopoFlow is to describe and predict the hydrologic processes everywhere throughout a watershed. In Chapter 5, the TopoFlow model is modified in order to represent the discontinuous permafrost condition of the sub-arctic environment [*Bolton et al.*, In prep.-a]. In order to represent the discontinuous permafrost condition, I vary the soil properties (hydraulic conductivity and porosity) of each model layer as proxies for permafrost distribution and soil storage capacity of the active layer. In this chapter, a sensitivity analysis testing the simulated hydrologic runoff to changes in air temperature, precipitation, permafrost distribution, active layer depth, and vegetation type and distribution is conducted.

Wildfires in the boreal forest have been a natural part of ecosystem. Wildfires have both immediate and long term effects on the ecosystem due to changes in the surface energy balance, water balance, and permafrost regime. The short-term effects of wildfire on soil moisture and thermal regimes, in both cold and temperate regions, have been well documented [*Tiedemann et al.*, 1979; *Klock and Helvey*, 1976; *Moore and Keeley*, 2000]. In Appendix A, the immediate through long-term effects of wildfire to the permafrost regime throughout Interior Alaska are explored [*Yoshikawa et al.*, 2002]. In this paper, soil moisture measurements are collected and analyzed at 11 different wildfires, with dates of ignition ranging from 1924 through 2000 (measurements collected during the active burn). This study was conducted as part of a larger interdisciplinary fire disturbance project called FROSTFIRE [*Hinzman et al.*, 2003].

Figure 2.6 has been modified from the original figure to include statistical information not previously published. Figures A.6 and A.7 were originally prepared for publication, but were not included in the final published manuscript. Other slight modifications have been made in Chapters 2 - Appendix A in order to fit the thesis format.

References

ACIA (2005), *Impacts of a warming Arctic: Arctic Climate Impact Assessment*, 1046 pp., Cambridge University Press.

Anisimov, O., and B. Fitzharris (2001), *Polar regions (Arctic and Antarctic)*, chap. *Climate Change 2001: Impacts, Adaptation, and Vulnerability*. Contribution of Working Group II to the Third Assessment report of the Intergovernmental Panel on Climate Change, pp. 801–841, Cambridge University Press.

Arnell, N. (2005), Implications of climate change for freshwater inflows to the Arctic Ocean, *Journal of Geophysical Research, 110*, D07105. doi:10.1029/2004JD005348.

Baldocchi, D., F. M. Kelliher, T. Black, and P. Jarvis (2000), Climate and vegetation controls on boreal zone energy exchange, *Global Change Biology, 6*(Supplement 1), pp. 69–83.

Betts, A. K., M. Goulden, and S. Wofsy (1999), Controls on evaporation in a boreal spruce forest, *Journal of Climate, 12*, 1601–1618.

Bolton, W., L. Hinzman, and K. Yoshikawa (2000), Stream flow studies in a watershed underlain by discontinuous permafrost, in *Proceedings Water Resources in Extreme Environments*, edited by D. Kane, pp. 31–36.

Bolton, W., L. Hinzman, and K. Yoshikawa (2004), Water balance dynamics of three small catchments in a sub-arctic boreal forest, in *Northern Research Basins Water Balance (Proceedings of a workshop held at Victoria, Canada, March 2004)*, edited by D. L. Kane and D. Yang, IAHS Series of Proceedings and Reports Number 290, pp. 213 – 223.

Bolton, W. R., L. D. Hinzman, and D. L. Kane (In prep.-a), Evaluating the hydrologic response to changing watershed characteristics and climate in the subarctic, *Journal of Geophysical Research - Biogeosciences*.

Bolton, W. R., S. D. Peckham, and L. Hinzman (In prep.-b), Toward understanding the hydrologic processes in a watershed dominated by discontinuous permafrost, *Journal of Geophysical Research - Biogeosciences*.

Callaghan, T., and S. Jonasson (1996), Arctic terrestrial ecosystems and environmental change, in *The Arctic and Environmental Change*, edited by P. Wadhams, J. Dowdeswell, and A. Schofield, pp. 59–76, Gordon and Breach.

Chapin, F., A.D. McGuire, J. Randerson, R. Pielke, D. Baldocchi, S.E. Hobbie, N. Roulet, W. Eugster, E. Kasischke, E.B. Rastetter, S.A. Zimov, and S.W. Running. (2000), Arctic and boreal ecosystems of western North America as components of the climate system, *Global Change Biology*, *6*(Supplement 1), 211–223.

Chapin, F.S., M. Sturm, M.C. Serreze, J.P. McFadden, J.R. Key, A.H. Lloyd, A.D. McGuire, T.S. Rupp, A.H. Lynch, J.P. Schimel, J. Beringer, W.L. Chapman, H.E. Epstein, E.S. Euskirchen, L.D. Hinzman, G. Jia, C.L. Ping, K.D. Tape, C.D.C. Thompson, D.A. Walker, and J.M. Welker. (2005), Role of land-surface changes in the Arctic summer warming, *Science*, *310*, 657–660.

Chapman, W., and J. Walsh (1993), Recent variations in sea ice and air temperature in high latitudes, *Bulletin American Meteorology Society*, *74*, 33–47.

Douville, H. (2003), Assessing the influence of soil moisture on seasonal climate variability with AGCMS, *Journal of Hydrometeorology*, *4*, 1044–1066.

Dyrness, C., L. Viereck, and K. Van Cleve (1986), *Forest Ecosystems in the Alaskan Taiga*, chap. Fire in taiga communities of interior Alaska, pp. 74–86, Springer-Verlag.

Eugster, W., W.R. Rouse, R.A. Pielke, J.P. McFadden, D.D. Baldocchi, T.G.F. Kittel, F.S. Chapin, G.E. Liston, P.L. Vidale, E. Vaganov, and S. Chambers. (2000), Land-atmosphere energy exchange in arctic tundra and boreal forest: available data and feedbacks to climate, *Global Change Biology*, *6*(Supplement 1), 84–115.

Flannigan, M., and C. Van Wagner (1991), Climate change and wildfire in Canada, *Canadian Journal of Forest Research*, *21*, 66–72.

French, N., E. Kasischke, J. Michalek, and L. Bourgeau-Chavez (1997), Monitoring the effects of fire on soil temperature and moisture in boreal forest ecosystems using satellite imagery, in *Proceedings of the International Symposium on Physics, Chemistry, and Ecology in Seasonally Frozen Soils*, edited by I. Iskandar, E. Wright, J. Radke, B. Sharratt, P. Groenevelt, and L. Hinzman, pp. 551–557, Fairbanks, Alaska.

Friborg, T., H. Soegaard, T. Christensen, C. Lloyd, and N. Panikov (2003), Siberian wetlands: Where a sink is a source, *Geophysical Research Letters, 30*, 2129.

Hanson, J., R. Ruedy, M. Sato, and K. Lo (2006), Global temperature trends: 2005 summation, http://data.giss.nasa.gov/gistemp/2005/, Goddard Institute for Space Studies.

Haugen, R., C. Slaughter, K. Howe, and S. Dingman (1982), Hydrology and climatology of the Caribou-Poker Creeks Research Watershed, Alaska, *CRREL Report 82-26*, US Army Corps of Engineers Cold Regions Research and Engineering Laboratory.

Hinzman, L., D. Kane, R. Gieck, and K. Everett (1991), Hydrologic and thermal properties of the active layer in the Alaskan Arctic, *Cold Regions Science and Technology, 19*, 95–110.

Hinzman, L., D. Kane, and Z. Zhang (1995), A spatially distributed hydrologic model for arctic regions, in *International GEWEX Workshop on Cold-Season/Region Hydrometeorology. Summary Report and Proceedings*, no. 15 in Int. GEWEX Project Office Publication, pp. 236–239.

Hinzman, L., N.D. Bettez, F.S. Chapin, M.B. Dyurgerov, C.L.Fastie, B. Griffith, R.D. Hollister, A. Hope, H.P. Huntington, A.M. Jensen, G.J. Jia, T. Jorgenson, D.L. Kane, D.R. Klein, G. Kofinas, A.H. Lynch, A.H. Lloyd, A.D. McGuire, F.E. Nelson, W.C. Oechel, T.E. Osterkamp, C.H. Racine, V.E. Romanovsky, R.S. Stone, D.A.Stow, M. Sturm, C.E. Tweedie, G.L. Vourlitis, M.D. Walker, D.A. Walker, P.J. Webber, J.M. Welker, K.S. Winker, and K. Yoshikawa (2005), Evidence and implications of recent climatic change in northern Alaska and other arctic regions, *Climatic Change, 72*, 251–298.

Hinzman, L. D., M. Fukuda, D. V. Sandberg, F. S. Chapin III, and D. Dash (2003), FROSTFIRE: An experimental approach to predicting the climate feedbacks from the changing boreal forest regime, *Journal of Geophysical Research, 108*(D1),8153, doi:10.1029/2001JD000415.

IPCC (2001), Climate change 2001: Synthesis report. summary for policymakers., *Tech. rep.*, Intergovernmental Panel on Climate Change.

Jones, P., and A. Moberg (2003), Hemispheric and large-scale surface air temperature variations: An extensive revision and an update to 2001, *Journal of Climate, 16*, 206–223.

Jorgenson, M., C. Racine, J. Walters, and T. Osterkamp (2001), Permafrost degradation and ecological changes associated with a warming climate in central Alaska, *Climate Change, 48*, 551–571.

Kane, D., and L. Hinzman (2004), Monitoring extreme environments: Arctic hydrology in transition, *Water Resources Impact, 6*(1), 24–27.

Kane, D. L., and D. Yang (Eds.) (2004), *Northern Research Basins Water Balance*, IAHS Publication 190, International Association of Hydrological Sciences.

Kasischke, E., N. Christensen, and B. Stocks (1995), Fire, global warming, and the carbon balance of boreal forests, *Ecological Applications, 5*, 437–451.

Kasischke, E. S., T. S. Rupp, and D. L. Verbyla (2006), Fire trends in the Alaskan boreal forest, in *Alaska's Changing Boreal Forest*, edited by F. S. Chapin, M. W. Oswood, K. Van Cleve, L. A. Viereck, and D. L. Verbyla, Long-Term Ecological Research Network Series, chap. 17, pp. 285–301, Oxford University Press.

Kattsov, V., and J. Walsh (2000), Twentieth-century trends of arctic precipitation from observational data and a climate model simulation, *Journal of Climate, 13*, 1362–1370.

Klock, G., and J. Helvey (1976), Soil-water trends following wildfire on the Entiat Experimental Forest, in *Annual Proceedings Tall Timbers Fire Ecologic Conference*, 15, pp. 193–200.

Magnuson, J., D. Robertson, B. Benson, R. Wynne, D. Livingstone, T. Arai, R. Assel, R. Barry, V. Card, E. Kuusisto, N. Granin, T. Prowse, K. Steward, and V. Vuglinski (2000), Historical trends in lake and river ice cover in the northern hemisphere, *Science, 289*, 1743–1746.

McGuire, A. D., and F. S. Chapin (2006), Climate feedbacks in the Alaskan boreal forest, in *Alaska's Changing Boreal Forest*, edited by F. S. Chapin, M. W. Oswood, K. Van Cleve, L. A. Viereck, and D. L. Verbyla, Long-Term Ecological Research Network Series, Chap. 19, pp. 309–322, Oxford University Press.

Moore, C., and J. Keeley (2000), Long-term hydrologic response of a forested catchment to prescribed fire, in *Proceedings Water Resources in Extreme Environments*, edited by D. Kane, pp. 37–42, American Water Resources Association, Anchorage, Alaska.

Moore, R. D. (1983), On the use of bulk aerodynamic formulae over melting snow, *Nordic Hydrology, 14*(4), 193–206.

Osterkamp, T. (2003), A thermal history of permafrost in alaska, in *Proceedings of the Eighth International Conference on Permafrost, 21-25 July 2003*, pp. 863–868, Balkema Publishers.

Osterkamp, T., and V. Romanovsky (1999), Evidence for warming and thawing of discontinuous permafrost in Alaska, *Permafrost and Periglacial Processes, 10*, 17–37.

Osterkamp, T., L. Viereck, Y. Shur, M. Jorgenson, C. Racine, A. Doyle, and R. Boone (2000), Observations of thermokarst and its impact on boreal forests in Alaska, USA, *Arctic, Antarctic and Alpine Research, 32*, 303 – 315.

Overpeck, J., M. Sturm, J.A. Francis, D.K. Perovich, M.C. Serreze, R. Benner, E.C. Carmack, F.S. Chapin, S.C. Gerlach, L.C. Hamilton, L.D. Hinzman, M. Holland, H.P. Huntington, J.R. Key, A.H. Lloyd, G.M, MacDonald, J. McFadden, D. Noone, T.D. Prowse, P. Schlosser, and C. Vörösmarty (2005), Arctic system on trajectory to new, seasonally ice-free state, *EOS, Transactions American Geophysical Union, 86*(34), 309,312–313.

Peterson, B., R. Holmes, J. McClelland, C. Vörösmarty, R. Lammers, A. Shiklomanov, I. Skiklomanov, and S. Rahmstort (2002), Increasing river discharge to the Arctic Ocean, *Science, 298*, 2171–2173.

Rowe, J., and G. Scotter (1973), Fire in the boreal forest, *Quaternary Research, 3*, 444–464.

Serreze, M., D. Bromwich, M. Clark, A. Etringer, T. Zhang, and R. Lammers (2002), Large-scale hydro-climatology of the terrestrial arctic drainage system, *Journal of Geophysical Research, 108*(D2), D01,108.

Serreze, M., J. Walsh, F. Chapin, T. Osterkamp, M. Dyurgerov, V. Romanovsky, W. Oechel, J. Morison, T. Zhang, and R. Barry (2000), Observational evidence of recent change in the northern high latitude environment, *Climatic Change, 46*, 159–207.

Smith, L., Y. Sheng, G. MacDonald, and L. Hinzman (2005), Disappearing arctic lakes, *Science, 308*, 1429.

Smith, T., W. Cramer, R. Dixon, R. Neilson, and A. Solomon (1993), The global terrestrial carbon cycle, *Water, Air and Soil Pollution, 70*, 19–37.

Stroeve, J., M. Serreze, F. Fetterer, T. Arbetter, W. Meiser, J. Maslanik, and K. Knowles (2005), Tracking the Arctic's shrinking ice cover: another extreme September minimum in 2004, *Geophysical Research Letters, 32*, L04,501, doi:10.1029/2004GL021810.

Tiedemann, A., C. Conrad, J. Dieterich, J. Hurnbeck, W. Megahan, L. Viereck, and D. Wade (1979), Effects of fire on water – a state-of-knowledge review, *General Technical Report WO-10*, U.S. Department of Agriculture Forest Service, 28 p.

Van Wagner, C. (1988), The historical pattern of annual burned area in Canada, *Forest Chronicle, 64*, 182–185.

Viereck, L. (1982), Effects of fire and firelines on active layer thickness and soil temperatures in Interior Alaska, in *Proceedings of the 4th Canadian Permafrost Conference*, pp. 123–134, Ottawa.

Vörösmarty, C., B. Fekete, M. Meybeck, and R. Lammers (2000), A simulated topological network representing the global system of rivers at 30-minute spatial resolution (stn-30), *Global Biogeochemical Cycles, 14*, 599–621.

Walsh, J. E., O. Anisimov, J.O.M. Hagen, T. Jakobsson, J. Oerlemans, T.D. Prowse, V. Romanovsky, N. Savelieva, M. Serreze, A. Shiklomanov, I. Shiklomanov, S. Solomon, A. Arendt, D. Atkinson, M.N. Demuth, J. Dowdeswell, M. Dyurgerov, A. Glazovsky, R.M. Koerner, M. Meier, N. Reeh, O. Sigurosson, K. Steffen, and M. Truffer (2005) Cryosphere and hydrology, in *Arctic Climate Impact Assessment*, edited by C. Symon, L. Arris, and B. Heal, Chap. 6, pp. 184–242, Cambridge University Press.

Yang, D., D. Kane, L. Hinzman, X. Zhang, T. Zhang, and H. Ye (2002), Siberian Lena River hydrologic regime and recent change, *Journal Geophysical Research, 107*(D23), 4694, doi:10.1029/2002JD002,542.

Yarie, J. (1981), Forest fire cycles and life tables: A case study from Interior Alaska, *Canadian Journal of Forest Research, 11*, 554–562.

Yoshikawa, K., L. Hinzman, N. Ishikawa, C. Collins, and V. Lunardini (1998), Air and ground temperature models at Caribou-Poker Creeks Research Watershed, in *Proceedings of the 49th AAAS Arctic Science Conference*, Fairbanks, Alaska.

Yoshikawa, K., W. Bolton, V. Romanovsky, M. Fukuda, and L. Hinzman (2002), Impacts of wildfire on the permafrost in the boreal forest of Interior Alaska, *Journal of Geophysical Research, 107*(8148: doe:10.1029/2001JD000438), printed 108(D1), 2003.

Yoshikawa, K., D. White, L. Hinzman, D. Goering, K. Petrone, W. Bolton, and N. Ishikawa (2003), Water in permafrost: Case study of aufeis and pingo hydrology in discontinuous permafrost, in *International Conference on Permafrost, Proceedings 8*, vol. 2, edited by M. Phillips, S. Springman, and L. Arenson, pp. 1259–1264.

Zhang, T. (2005), Spatial and temporal variability in active layer thickness over the Russian Arctic drainage basin, *Journal of Geophysical Research, 110*, D16,101.

Zhang, Z., D. Kane, and L. Hinzman (2000), Development and application of a spatially-distributed Arctic hydrological and thermal process model (ARHYTHM), *Hydrological Processes, 14*, 1017–1044.

Chapter 2

Stream flow studies in a watershed underlain by discontinuous permafrost*

Abstract

Permafrost plays an important role in the hydrology of sub-arctic watersheds. Ice-rich conditions at the permafrost table do not allow significant percolation, resulting in a slightly increased response time to precipitation events, limited subsurface storage, and low base flows between precipitation events. The Caribou-Poker Creeks Research Watershed (CPCRW), located 48 km north of Fairbanks, Alaska, is underlain by discontinuous permafrost along north-facing slopes and valley bottoms. Spring snowmelt is a major hydrologic event of the year but accurate discharge measurements have been difficult to obtain due to extensive aufeis formation at the stream gauging stations. Although spring snowmelt is usually a major hydrologic event of the year, maximum stream discharge was recorded during a major rainfall event in June. Comparison of the specific discharges from the C2, C3, and C4 sub-watersheds which are underlain, respectively, with 3.5, 53.2, and 18.8% permafrost, show that the C3 sub-watershed had higher peak specific discharges and a lower specific base flow compared to the C2 and C4 sub-watersheds. However, as the active layer depth (the layer of soil above the permafrost the thaws and freezes seasonally) increased throughout the summer, the C3 sub-watershed displayed decreasing peak specific discharges, the result of increased subsurface storage, during precipitation events. Recession analysis indicate the contribution of subsurface water during precipitation events from the C3 and C4 sub-watersheds increased throughout the summer as the active layer increased in thickness, while the contribution from the subsurface flow in the low permafrost basin remained nearly constant.

KEY TERMS: stream flow runoff, permafrost, active layer, research watershed, specific yeild, stream recession.

---

*W.R. Bolton, L. Hinzman, and K. Yoshikawa. 2000. Stream flow studies in a watershed underlain by discontinuous permafrost. in D.L. Kane (ed.), Proc. Water Resources in Extreme Environments, American Water Resources Association. pp 31-36.

2.1 Introduction

Permafrost plays an important role in the hydrology of sub-arctic watersheds. Ice-rich conditions do not allow significant percolation at the permafrost table, resulting in a slightly increased time to peak discharge to precipitation events (including snowmelt), limited subsurface storage, and low base flows between precipitation events compared to permafrost free areas. Soil moisture content is also important to hydrologic processes. The soil moisture level determines the rate of infiltration that can occur during precipitation events. Once the soil is saturated, surface water will not be able to infiltrate into the subsurface, resulting in overland flow. The soil moisture content is affected by many factors including vegetation type, soil type, presence of permafrost, amount and timing of precipitation, slope, and drainage conditions.

The Caribou-Poker Creeks Research Watershed is located 48 km north of Fairbanks (65°10'N, 147°30'W) and encompasses an area of 101.5 km^2 (Figure 2.1). CPCRW was established in 1969 in response to the need for sub-arctic hydrologic information [*Slaughter*, 1971] following the Fairbanks flood in 1967. Permafrost in CPCRW is discontinuous, generally found along north facing slopes and valley bottoms [*Haugen et al.*, 1982; *Nelson*, 1978]. Thicknesses of organic soils overlying permafrost soils range between 20-50 cm [*Slaughter and Kane*, 1979]. Soils free of permafrost are generally found on south to southwest facing slopes. The organic soils in non-permafrost areas are less than 15 cm thick. The areas of C2 (5.2 km^2), C3 (5.7 km^2), and C4 (11.4 km^2) sub-watersheds of CPCRW are underlain, respectively, with 3.5, 53.2, and 18.8% permafrost [*Haugen et al.*, 1982].

The objectives of this paper are to (1) compare stream flow response to precipitation events in the C2 (LoP), C3 (HiP), and C4 (MedP) sub-watersheds, and (2) using hydrograph separation techniques, investigate the changes in stream flow composition in areas of discontinuous permafrost. Four summer storms in the 1999 field season were used for analysis.

2.1.1 Field methods

Stream stage was recorded at the LoP, HiP, and MedP sub-watersheds using Campbell Scientific CR10X data loggers and a Microswitch 5-psi pressure transducer. Five consecutive measurements were averaged every hour and recorded. Stage measurements were

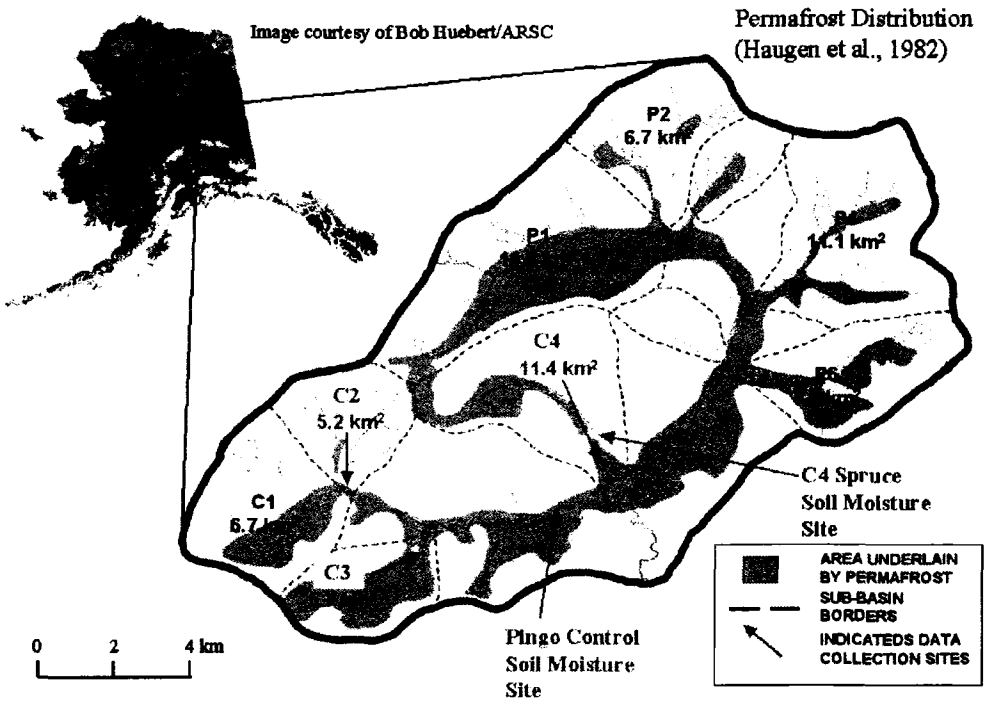

Figure 2.1: Caribou-Poker Creeks Research Watershed location and permafrost distribution.

taken at the MedP sub-watershed on a 30-minute interval after 7 July 1999. Parshall flumes were used at each sub-watershed to obtain continuous discharge data. Discharge measurements were made using USGS standard methods at different stage levels to confirm the discharge data obtained from the data logger. Periodic stream flow measurements were conducted from the initiation of snowmelt until late September when freeze-up occurred. Pressure transducers and data loggers were installed immediately following melt from the flumes. Hourly rainfall measurements were collected adjacent to each stream gauging station (through 24 August 1999). In the LoP and HiP sub-watersheds, rainfall was collected using a tipping-bucket rain gauge. In the MedP sub-watershed, was instrumented with a weighing-bucket rain gauge.

Snow measurements conducted include snow depth, snow water equivalent, and snow ablation. Snow water equivalent measurements were made using an Adirondack snow sampler. At each site, 10 snow water equivalent and 50 snow depth measurements were averaged following the double-sampling technique of *Rovansek et al.* [1993]. Extensive snow surveys were conducted in mid-March, followed by periodic measurements through the completion of snowmelt.

Soil moisture content is measured at 5 locations in CPCRW. At each site, Campbell Scientific CS615 soil moisture probes were installed horizontally into small pits and connected to a Campbell Scientific CR10(X) data logger that recorded on hourly intervals. The data obtained from the CS615 probes were used to calculate the dielectric constant of the soil. The *Topp et al.* [1980] equation for mineral soils and *Stein and Kane* [1983] equation for organic soils were then applied to obtain the soil moisture content. Four of the soil moisture stations are located within the MedP sub-watershed. These sites are located in a valley bottom, a spruce stand, a birch stand, and along a shrubby ridge. The fifth soil moisture site is located adjacent to Caribou Creek in a mixed birch/spruce stand, which is underlain by permafrost. Factors such as vegetation type, slope, presence of permafrost, and aspect were considered in site locations. The total depth of each soil moisture pit varied between 37 cm and 70 cm, with 4 to 6 soil moisture probes installed at each location. Soil moisture probes were installed in the surface duff layer, the organic soil, and at regular intervals through the mineral soil.

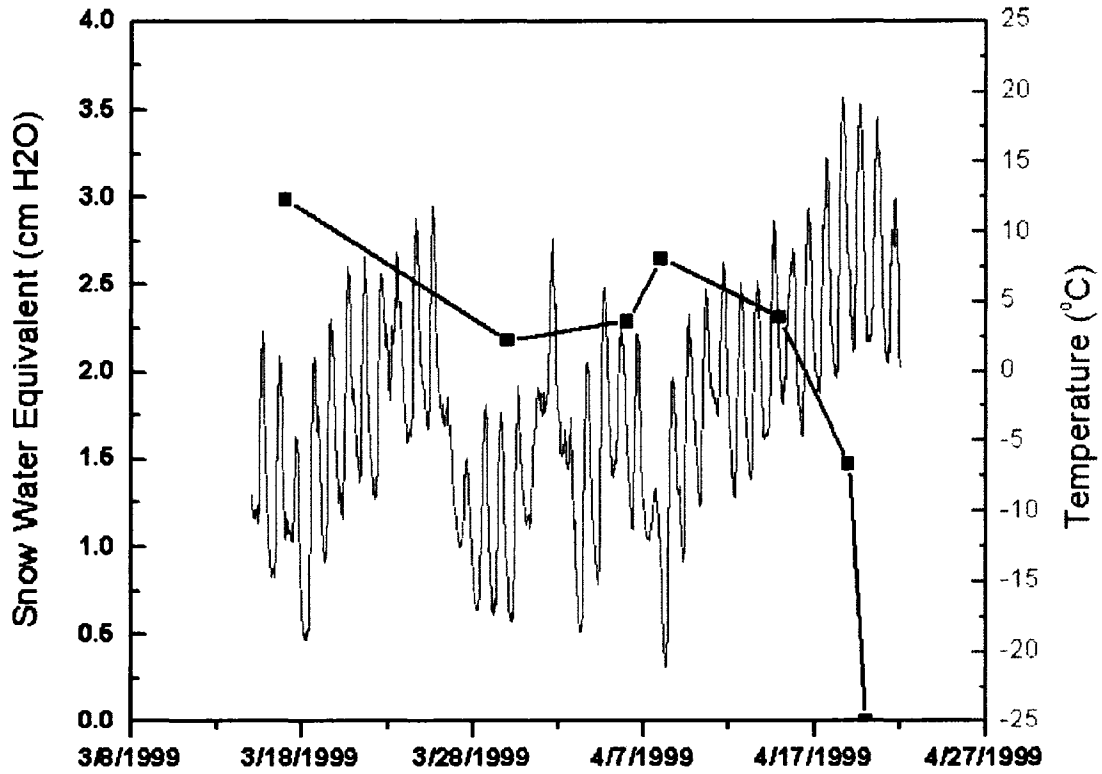

Figure 2.2. Snow ablation near the stream outlet of the C4 sub-watershed.

2.2 Results

2.2.1 Snowmelt

Spring snowmelt is a major hydrological event of the year, although accurate discharge measurements have been difficult to obtain due to extensive aufeis formation at the stream gauging stations, causing the flow to become dispersed outside of the normal channels. Snow precipitation accounted for approximately 30-40% of the yearly total of incoming precipitation. Ablation of the snow pack occurred over a 2-3 week period. However, over the final 4-5 days, rapid ablation of the remaining snow pack (over 50% of the maximum snow water equivalent) occurred during a period of sustained temperatures above 0°C (Figure 2.2).

2.2.2 Summer storms

Comparison of the specific discharges during precipitation events shows the HiP sub-watershed consistently displays the highest peak specific discharges, while the LoP sub-watershed consistently displays the lowest peak specific discharge (Figure 2.3). Although the spring snowmelt is a major hydrologic event of the year, the maximum stream specific discharge was recorded during a major precipitation event in June (Storm 1). Figure 2.4 indicates that this precipitation event occurred before any significant thawing of the mineral soils of the active layer, a period when the soil storage capacity is near its minimum. In areas underlain by permafrost, thawing of the active layer throughout the summer potentially increases the soil water capacity (dependent upon whether these soils are saturated or drained when thawed), potentially decreasing surface water runoff during large precipitation events (Storms 1-4, Figure 2.3). Between precipitation events, the HiP sub-watershed displayed the lowest specific baseflow while the LoP sub-watershed consistently displayed the highest specific baseflow.

2.2.3 Hydrograph separation

In areas underlain by permafrost, the depth of the active layer limits the amount of sub-permafrost water that eventually contributes to stream flow. As the active layer thaws, the potential storage capacity of the soils increases, resulting in increased subsurface water contributing to stream flow. Using the graphical separation techniques, described by *McNamara et al.* [1997], the fraction of subsurface water contributing to storm events can be determined. This technique is difficult to use on overlapping storm events, which happened frequently during the 1999 field season. Discharge measurements were averaged over 6 hour periods to aid in this analysis. During the 1999 field season, the amount of old water contributing to the LoP sub-watershed remained fairly consistent, while the amount of subsurface water contributing to both the HiP and MedP sub-watersheds increased throughout the summer (Table 2.1, Figures 2.5, 2.6). These results are generally consistent with the results obtained by *McNamara et al.* [1997] in an area of continuous permafrost.

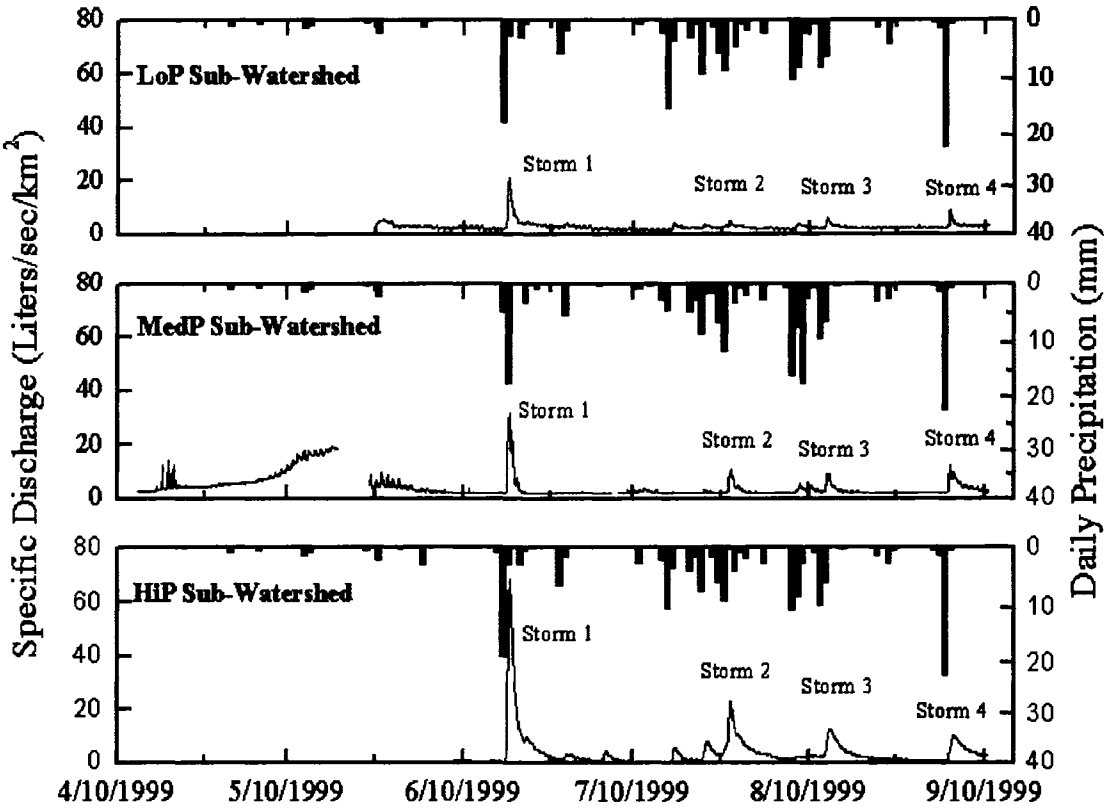

Figure 2.3: Specific discharge hydrograph and precipitation for the LoP, MedP, and HiP sub-watersheds.

Table 2.1. Results of hydrograph separation.

Sub-Watershed	Storm Event	Date	Total Discharge (m^3)	Subsurface Water (%)
LoP	1	6/6	15,965	68
	2	ND	ND	ND
	3	8/12	4,937	76
	4	9/2	5,315	74
HiP	1	6/6	56,555	17
	2	7/25	27,384	46
	3	8/12	18,893	51
	4	9/2	17,147	66
MedP	1	6/6	35,103	25
	2	7/25	16,854	57
	3	8/12	14,980	59
	4	9/3	35,644	88

ND, not determined due to complex hydrograph.

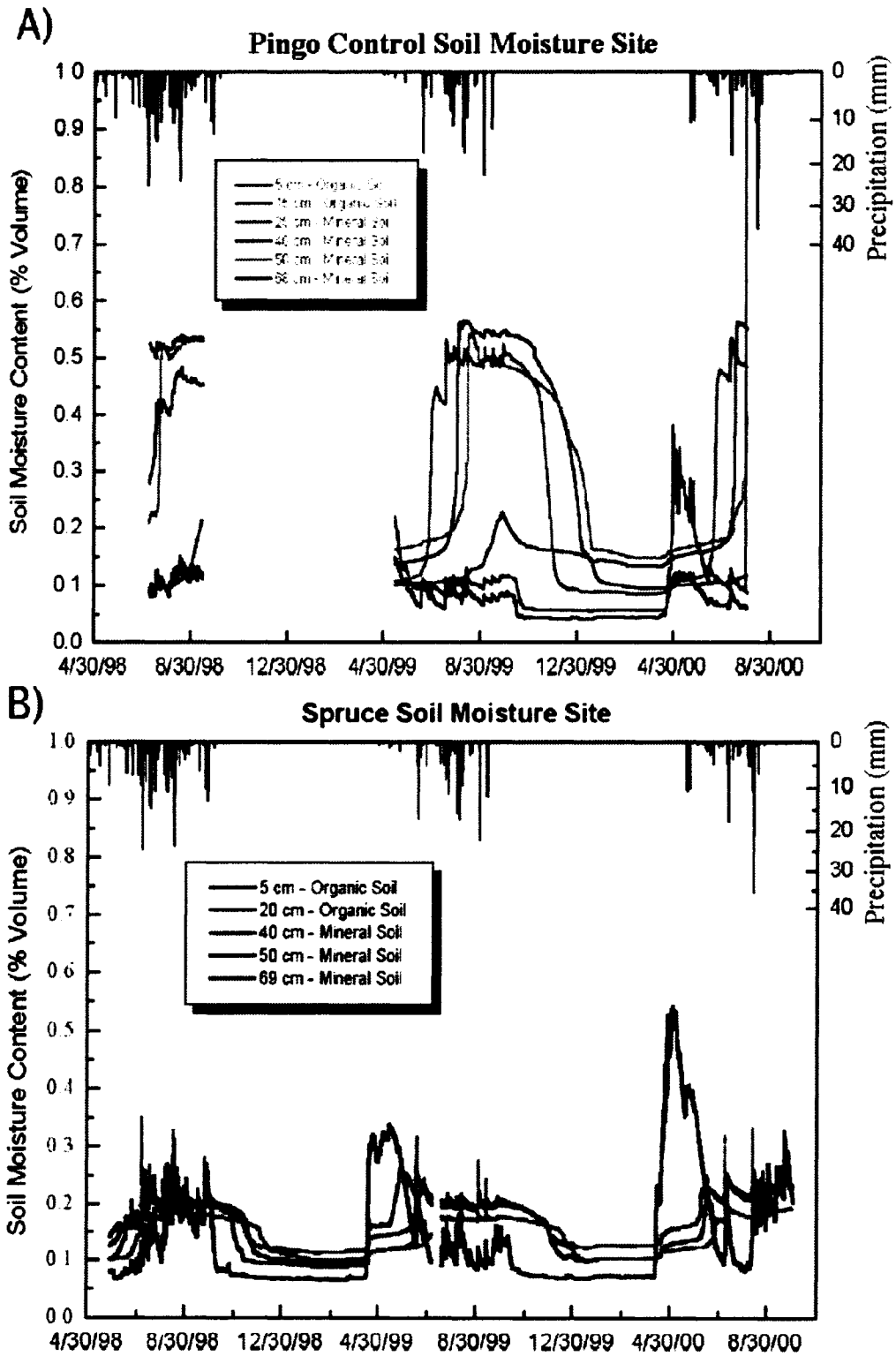

Figure 2.4: Soil moisture contents in (a) an area underlain by permafrost and (b) an area free of permafrost.

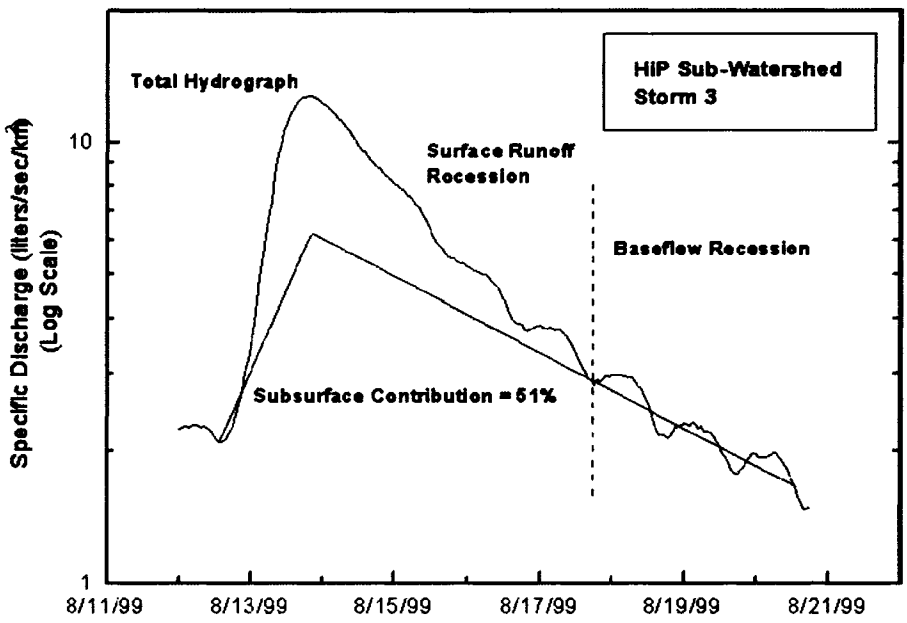

Figure 2.5. Storm 3, HiP sub-watershed graphical hydrograph separation.

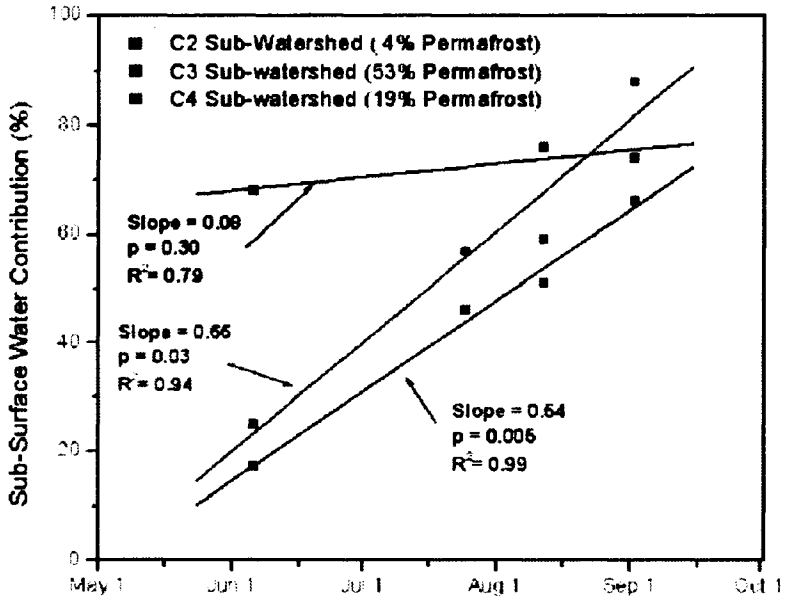

Figure 2.6. Subsurface water contribution from the LoP, MedP, and HiP sub-watersheds.

2.3 Conclusion

Spring snowmelt is usually a significant hydrologic event each year in these watersheds, although the peak discharges observed in this study were recorded during a major rainfall event in June, before the active layer had thawed substantially. Ice-rich conditions at the permafrost table inhibit significant percolation to the subsurface soils, resulting in a decreased infiltration rate and increased interflow at the organic / mineral soil interface during rainfall events compared to areas free of permafrost. Soil moisture contents of mineral soils in areas underlain by permafrost remained near saturation throughout the summer, displaying little response to rainfall events, while the soil moisture contents in areas free of permafrost remained drier, displaying a greater response to rainfall events. The C3 sub-watershed [containing the highest amounts of permafrost] displayed higher peak specific discharges (watershed discharge divided by basin area), a lower specific baseflow, and a slower response time during rainfall events compared to the C2 and C4 sub-watersheds. As the active layer began to thaw, increasing the soil water storage capacity, the C3 sub-watershed displayed decreasing peak specific discharges during large rainfall events. Hydrograph separation analysis indicate the subsurface water contribution to the storm hydrographs from the C2 sub-watershed [containing the lowest amount of permafrost] during precipitation events was about 70% throughout the summer. The subsurface water contribution from the C3 and C4 sub-watersheds increased throughout the summer from amounts as low as 17% to those approaching 88%.

2.4 Acknowledgements

Support for this research was provided under grants from the National Science Foundation LTER Program (Grant No. DEB-9707461), the Japan Marine Science and Technology Center (JAMSTEC) under the YuWEx program, and the Alaska Section of the American Water Resources Association.

References

Haugen, R., C. Slaughter, K. Howe, and S. Dingman (1982), Hydrology and climatology of the Caribou-Poker Creeks Research Watershed, Alaska, *CRREL Report 82-26*, US Army Corps of Engineers Cold Regions Research and Engineering Laboratory.

McNamara, J., D. Kane, and L. Hinzman (1997), Hydrograph separations in an rctic watershed using mixing model and graphical techniques, *Water Resources Research, 33*(7), 1707–1719.

Nelson, G. (1978), Hydrologic information for land-use planning, Fairbanks vicinity, Alaska, *Open-File Report 78-959*, U.S. Geological Society.

Rovansek, R., D. Kane, and L. Hinzman (1993), Improving estimates of snowpack water equivalent using double sampling, in *Proceedings of the 50th Eastern Western Snow Conference*, edited by M. Ferrick and T. Pangburn, pp. 157–163.

Slaughter, C. (1971), Caribou-Poker Creeks Research Watershed: Background and current status, *Special Report 157*, CRREL.

Slaughter, C., and D. Kane (1979), Hydrologic role of shallow organic soils in cold climates, in *Canadian Hydrology Symposium: Proceedings, 79-Cold Climate Hydrology*, pp. 380–389.

Stein, J., and D. Kane (1983), Monitoring the unfrozen water content of soil and snow using time domain reflectometry, *Water Resources Research, 19*(6), 1537–1584.

Topp, G., J. Davis, and A. Annan (1980), Electromagnetic determination of soil water content: measurements in coaxial transmission lines, *Water Resources Research, 16*(3), 574–582.

Chapter 3

Water balance dynamics of three small catchments in a sub-arctic boreal forest*

Abstract

This study examines the water balance components from three small sub-arctic watersheds near Fairbanks, Alaska, U.S.A., which vary in permafrost coverage from 3 to 53%. The results show that the presence or absence of permafrost affects many of the water balance components, particularly stream flow runoff and groundwater storage. The average annual precipitation is 410 mm, 2/3 of which is rain. Evapotranspiration, derived using the Priestley-Taylor method, averages between approximately 200-310 mm. During the snowmelt and summer runoff periods, the presence of poorly-drained permafrost limits infiltration of surface waters, generating higher runoff than in comparable well-drained non-permafrost soils. Lower storm flow, but higher baseflow is consistently observed in the C2 (3% permafrost coverage) and C4 (18% permafrost coverage) sub-basins when compared to the C3 (53% permafrost coverage) sub-basin. In the sub-arctic region, many of the storage processes (subsurface storage, interception, and stream icings) are critically important to the water balance, but are the least well quantified.

KEY TERMS: Alaska; boreal forest; Caribou-Poker Creeks Research Watershed; discontinuous permafrost; water balance

3.1 Introduction

The global climate has been warming [*Chapman and Walsh*, 1993] and the northern latitudes are particularly sensitive to climate change, with expected increases in both air temperature (particularly winter) and precipitation (both winter and summer)[*IPCC*, 2001]. Permafrost in Interior Alaska is relatively warm (often between -1°C and 0°C) and unstable, as these soils are often ice-rich [*Yoshikawa et al.*, 2002]. In light of a changing climate, it is critically important to collect long-term hydrological data to better understand and predict the feedback mechanisms of the water cycle [*Kane and Hinzman*, 2004]. Hydrological responses

*W.R. Bolton, L. Hinzman, and K. Yoshikawa, Water balance dynamics of three small catchments in a Sub-Arctic boreal forest, *Northern Research Basins Water Balance* (Proceedings of a workshop held at Victoria, Canada, March 2004), IAHS Publication 290, pp. 213-223, 2004.

Table 3.1: Physical hydrologic characteristics of selected sub-basins of study in the Caribou-Poker Creeks Research Watershed (modified from *Haugen et al.*, 1982).

Basin	C2	C3	C4
Area (km^2)	5.2	5.7	11.4
Aspect	S	NE	SSE
Elevation (m)	323–738	274–770	226–686
Total stream length	2.2	2.6	5.0
Drainage density (km km^2)	0.70	0.73	0.70
% Area below 305 m	0.0	0.1	5.9
% Area between 305 and 488 m	29.0	39.5	27.3
% Area between 488 and 640 m	38.0	51.4	50.9
% Aarea above 640 m	33.0	9.1	15.9
% Area underlain by permafrost	3.5	53.2	18.8

in watersheds with discontinuous permafrost are particularly important as these regions will display dramatic, threshold changes in hydrology, ecology and surface energy balance as permafrost degrades. The presence or absence of permafrost is a dominant factor controlling surface and groundwater hydrology, with consequent impacts to local biological, ecological and climatological processes. Understanding the controls that permafrost exerts on hydrological processes may improve projections of watershed responses under a warmer climate. The focus of this study is to synthesize the water balance components from three small watersheds of varying permafrost coverage in Interior Alaska.

3.2 Watershed description

The Caribou-Poker Creeks Research Watershed (CPCRW) (Figure 3.1), the site chosen for this study, is located 48 km north of Fairbanks, Alaska (65°10'N, 147°30'W). Located in the boreal forest, CPCRW encompasses an area of 101.5 km^2 and is underlain with discontinuous permafrost. The three sub-watersheds of CPCRW selected for this study are C2 (5.2 km^2), C3 (5.7 km^2), and C4 (11.4 km^2). Each sub-watershed is underlain, respectively, with approximately 3, 53, and 19% permafrost (Table 3.1) [*Haugen et al.*, 1982; *Yoshikawa et al.*, 1998].

Permafrost in CPCRW is generally found along north facing slopes and valley bottoms [*Haugen et al.*, 1982]. Soils free of permafrost are generally found on south to southwest fac-

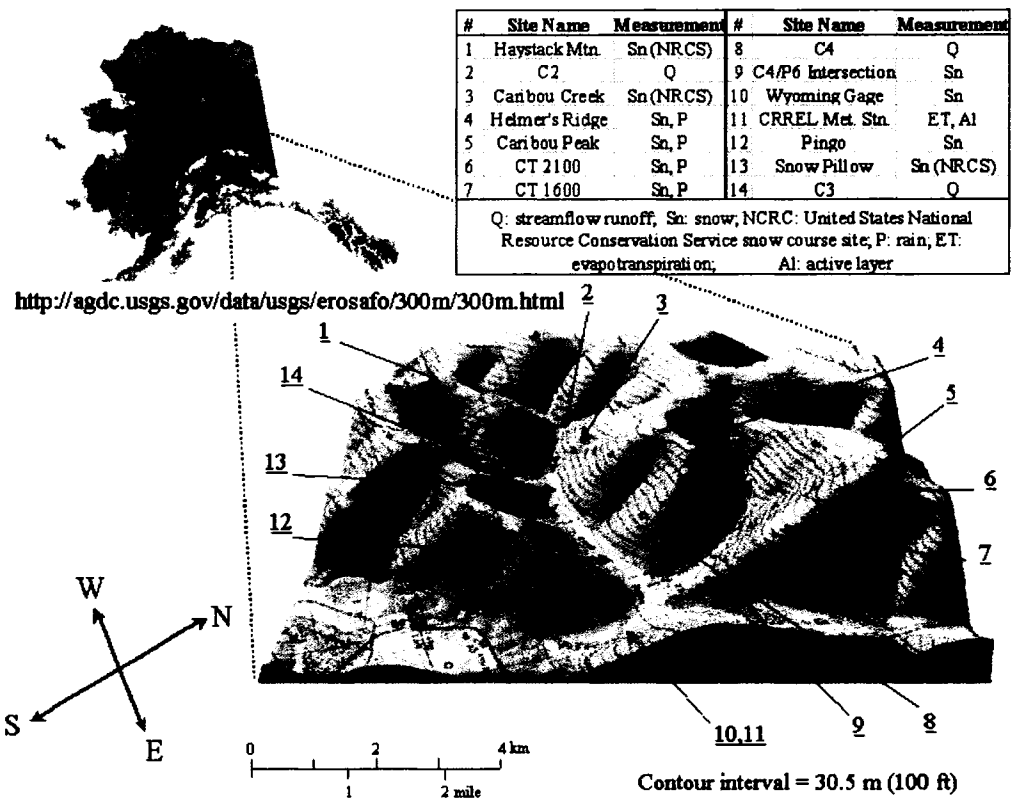

#	Site Name	Measurement	#	Site Name	Measurement
1	Haystack Mtn.	Sn (NRCS)	8	C4	Q
2	C2	Q	9	C4/P6 Intersection	Sn
3	Caribou Creek	Sn (NRCS)	10	Wyoming Gage	Sn
4	Helmer's Ridge	Sn, P	11	CRREL Met. Stn.	ET, Al
5	Caribou Peak	Sn, P	12	Pingo	Sn
6	CT 2100	Sn, P	13	Snow Pillow	Sn (NRCS)
7	CT 1600	Sn, P	14	C3	Q

Q: streamflow runoff, Sn: snow; NCRC: United States National Resource Conservation Service snow course site; P: rain; ET: evapotranspiration; Al: active layer

Figure 3.1: Site location and measurement locations of the Caribou-Poker Creeks Research Watershed

ing slopes. Permafrost distribution is influenced by a number of factors such as landscape, soil type, and vegetation cover [*Haugen et al.*, 1982]. In CPCRW, the thermal condition of the permafrost is unstable, varying from -3 to 0°C, with thickness ranging from 0-120 m [*Yoshikawa et al.*, 2003]. The maximum active layer thickness averages 0.52 m (2000 - 2002) at a low elevation point in the center of the watershed (Figure 3.1, Site 11).

Vegetation in CPCRW consists of black spruce (*Picea mariana*), which is typically found along poorly-drained north-facing slopes and valley bottoms. Aspen (*Populus tremuloides*), birch (*Betula papyrifera*), alder (*Alnus crispa*), and sporadic white spruce (*Picea glauca*) are found on the well-drained, south-facing soils [*Haugen et al.*, 1982]. Tussock tundra (*Carex aquatilis*), feather moss (*Hylocomium spp.*), and sphagnum mosses (*Sphagnum sp.*) are also found along the valley bottoms.

3.3 Determination of components

The generalized water balance equation used in this study is,

$$(P_{snow_max} + P_{rain}) - Q - ET - \Delta S = 0 \tag{3.1}$$

where P_{snow_max} is the maximum snow water equivalent just prior to spring melt, P_{rain} is the summer precipitation, Q is stream flow runoff, ET is evapotranspiration, and ΔS is the change in storage, for example aufeis, active layer, groundwater, and surface storage.

Woo [1990] makes a case that year-to-year changes in storage may be significant in permafrost basins. In the boreal forest, many of the storage processes, such as interception storage, stream icings (aufeis), and differences in subsurface storage (due to presence or absence of permafrost) are not well quantified. As we are unable to accurately measure these storage processes, the storage term is calculated as the residual in water balance equation. All water balance components are determined from the time of maximum snow water equivalent (late March to early April) through the fall freeze-up period (late September to early October).

3.3.1 Precipitation

Snow

Beginning in 1970, the United States National Resource Conservation Service (NRCS, formerly US Soil Conservation Service) has been compiling monthly snow water equivalent and snow depth measurements from three 'snow course' sites in the Caribou Creek basin: Haystack Mtn., Caribou Creek, and Snow Pillow (Figure 3.1, Sites 1, 3, and 13). Beginning in 1998, extensive snow surveys throughout CPCRW have been collected in mid-March (to determine the maximum cumulative snow water equivalent and snow depth), followed by periodic measurements through the ablation period. At each measurement site, a double sampling method [*Rovansek et al.*, 1993] is used to determine the snow water equivalent. The maximum snow water equivalents measured during the basin-wide snow surveys (1998-2003) display little orographic effect (Figure 3.2). Maximum snow pack is usually observed from mid-March to early April as snow typically accumulates all winter, and mid-winter thaw events are uncommon. Ablation measurements at the Wyoming gage (Figure 3.1, Site 10) indicate snowmelt usually occurs over a 2-3 week period, beginning in mid-April. Rapid ablation of the snow pack occurs over the final 4-7 days when the air temperature remains above 0°C throughout the day and night and the albedo of the snowpack decreases. No significant redistribution of the snow pack has been observed in CPCRW, except along exposed ridge tops, which occupy a small proportion of the watershed area. The maximum snow water equivalent was determined by averaging the maximum snow water equivalents measured at the three NRCS Snow Course sites (1978-1997) and the basin wide snow surveys, which include the NRCS sites (1998-2003). A high correlation (r^2 = 0.99, slope = 0.93, SD = 0.37) exists between snow surveys conducted at the NRCS sites and the basin wide snow surveys conducted during the 1998-2003 period, indicating that historic measurements conducted at these index sites do provide a valid proxy for the estimation of the total watershed snowpack (Figure 3.3).

Rain

Liquid precipitation has been monitored at Helmer's Ridge, Caribou Peak, CT 1600, and CT 2100 meteorological stations located in CPCRW (Figure 3.1, Sites 4, 5, 6, and 7) since

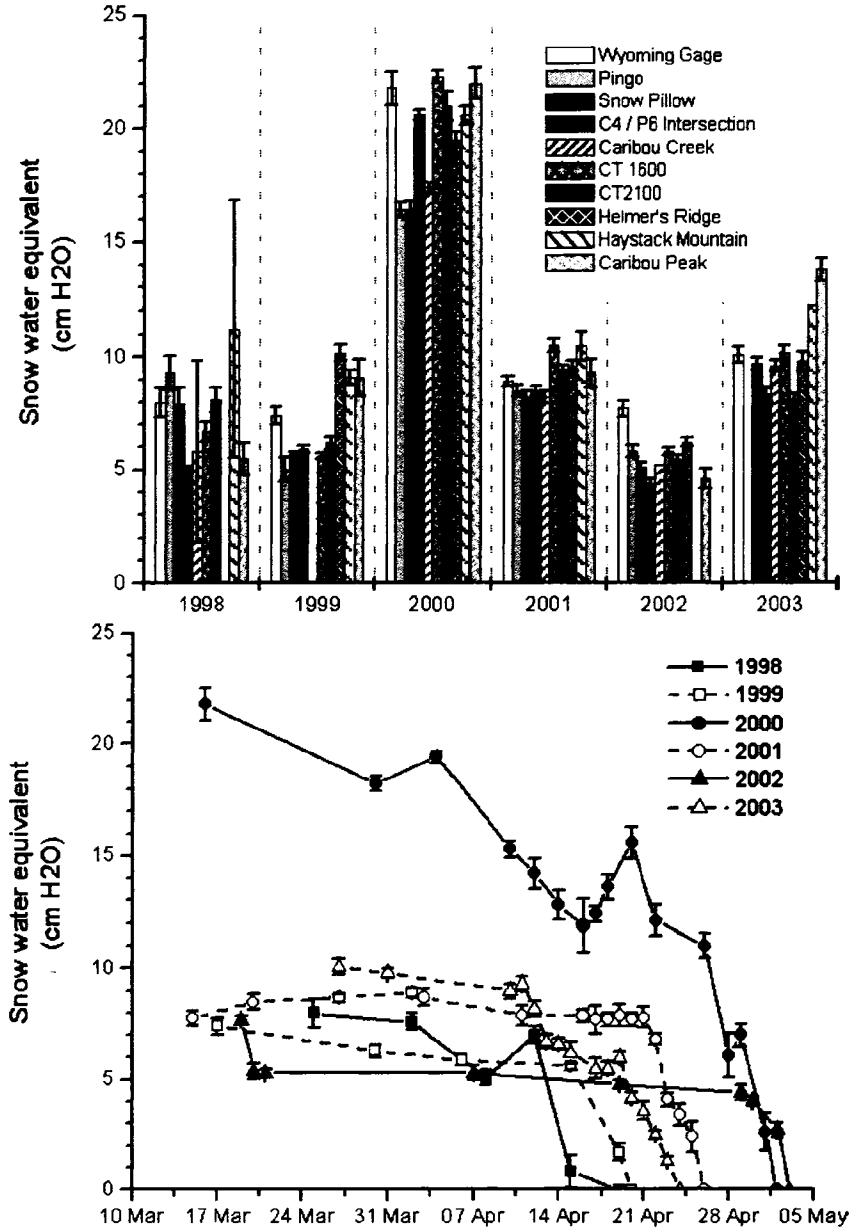

Figure 3.2: (a) Maximum snow water equivalent measured during the mid-March basin-wide sampling event. The sites in the legend are in ascending order of elevation. (b) Snow ablation (1998-2003) near the confluence of Caribou and Poker Creeks. Error bars represent one standard deviation.

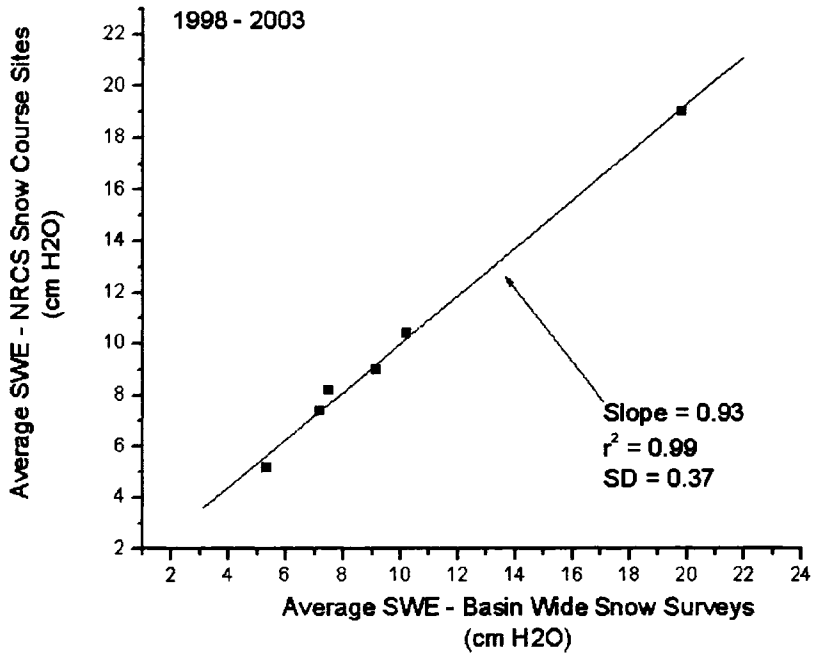

Figure 3.3: Comparisons of the average snow water equivalent at the NRCS sites to the basin wide snow survey sites, 1998-2003.

1976, with continuous measurements beginning in 1988. Prior to 1988, monthly precipitation data are estimated based upon comparisons with Fairbanks records. As with the maximum snow water equivalent, comparisons of the seasonal cumulative precipitation display little, albeit inconsistent, orographic effects. The rainfall total for each month is determined by averaging the monthly total precipitation for each site in which continuous data are available. The total yearly rainfall is the summation of the monthly averages.

3.3.2 Evapotranspiration

For years 2000-03, calculation of the evapotranspiration (ET) is based upon a modified Priestley-Taylor equation [*Priestley and Taylor*, 1972]. For each sub-basin, the Priestley-Taylor coefficient (α), defined here as the ratio of actual evapotranspiration to equilibrium evapotranspiration, is determined by multiplying the percentage of each vegetation type (estimated from *Haugen et al.* [1982]) with the appropriate α-value for that vegetation (estimated from *Baldocchi et al.* [2000]). The area ratios of black spruce (α = 0.4) to deciduous

vegetation (predominately birch/aspen, $\alpha = 0.9$) are estimated to be 1:3, 4:1, and 1:2 in the C2, C3, and C4 sub-basins. For the C2, C3, and C4 sub-basins, α is assumed to be 0.78, 0.5, and 0.74, respectively. Meteorological data from the CRREL Met. Stn. (Figure 3.1, Site 11) were used in calculating ET. Energy conducted into the ground was calculated using soil temperatures at 2 and 11.5 cm, with a thermal conductivity of 0.3 W m^{-1} $^oC^{-1}$ [*Yoshikawa et al.*, 2003]. Although thermal conductivity of the organic soils changes with moisture content (0.1 to 0.7 W m^{-1} $^oC^{-1}$ for 5 to 90% soil moisture (by volume), [*Yoshikawa et al.*, 2002]), it should be noted that this thermal conductivity value is probably typical for most periods of the thawed season.

For years prior to 2000, ET is estimated by relating the total daily ET calculated by the modified Priestley-Taylor Method from 2000-02 to the daily maximum (T_{max}), daily minimum (T_{min}), daily average air temperature (T_{ave}), and Julian day (JD) using linear regression. The equations used to estimate ET for the C2, C3, and C4 sub-basins are:

$$DailyET(mm)C2 = 1.506 + 0.09878(T_{max}) - 0.00991(JD) - 0.07632(T_{min}) + 0.0686(T_{ave}), r^2 = 0.81 \quad (3.2)$$

$$DailyET(mm)C3 = 0.971 + 0.06373(T_{max}) - 0.00639(JD) - 0.04924(T_{min}) + 0.04426(T_{ave}), r^2 = 0.81 \quad (3.3)$$

$$DailyET(mm)C4 = 1.428 + 0.09369(T_{max}) - 0.00940(JD) - 0.07230(T_{min}) + 0.06506(T_{ave}), r^2 = 0.81 \quad (3.4)$$

Figure 3.4 shows daily ET for 2003 as calculated by the Priestley-Taylor method and estimated by equations 3.2, 3.3, and 3.4. Temperature data from CPCRW were used when possible. Missing temperature data were estimated using the Fairbanks temperature records by the function (based upon 2000-03 field data):

$$T_{max}[CPCRW] = -0.60736 + 1.08345 * T_{max}[Fairbanks], r^2 = 0.94 \quad (3.5)$$

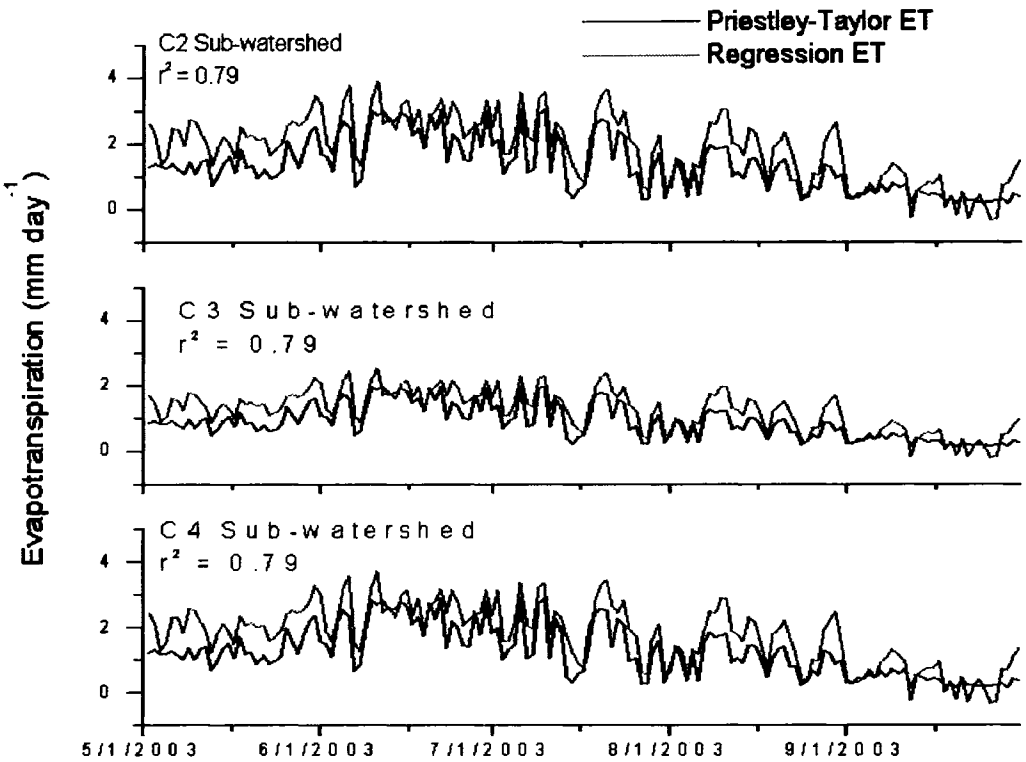

Figure 3.4: Evapotranspiration in the C2, C3, and C4 sub-basins for the 2003 summer. ET calculations were made using the Priestley-Taylor method from 2000-03. Differences in ET reflect varying proportions of vegetation type in each sub-basin.

$$T_{min}[CPCRW] = -5.12049 + 0.89691 * T_{min}[Fairbanks], r^2 = 0.70 \quad (3.6)$$

$$T_{ave}[CPCRW] = -1.82356 + 0.96183 * T_{ave}[Fairbanks], r^2 = 0.92 \quad (3.7)$$

In 1983, evapotranspiration at Ester Creek, located approximately 50 km southwest of CPCRW, was reported to be 229 mm [*Gieck*, 1986], which compares well to the 192-299 mm range estimated for CPCRW.

3.3.3 Runoff

Calibrated Parshall flumes were installed in the C2, C3, and C4 sub-basins in 1977, 1978, and 1979, respectively [*Slaughter*, 1981]. Stage measurements were recorded at regular intervals, which in turn were used to generate a continuous stage-discharge record. Periodic manual discharge measurements have been made at various stage levels to verify the calculated discharge data. Stream flow measurements were conducted from the initiation of spring snowmelt until late fall when freeze-up occurs.

Spring snowmelt is usually the major hydrologic event of the year. However, discharge measurements during this period have been difficult to obtain to due to extensive aufeis (icing) formations at the gauging stations, which often disperse the flow outside the main stream channel. As a result, continuous discharge measurements usually begin after the main snowmelt pulse. Although the snowmelt period is the major hydrologic event of the year, the record peak stream flow usually occurs during summer rainstorm events. This is due to the fact that the highest rainfall intensities are greater than the maximum snowmelt rate on a daily time scale [*Kane and Hinzman*, 2004].

Differences in stream flow among watersheds are dramatic and are dependent upon the amount of permafrost underlying each sub-basin. Comparison of the basins show that as the areal extent of permafrost increases, peak specific discharge increases, specific baseflow decreases, and the time to peak discharge to precipitation events increase (Figure 3.5)[*Haugen et al.*, 1982; *Bolton et al.*, 2000]. Comparison of total summer runoff ratios (Q/P) displays little difference between the sub-basins (Table 3.2). In years in which daily streamflow is available before 15 May, the Q/P ratios average 0.24, 0.27, and 0.27 for the C2, C3, and C4 sub-basins, respectively. Although higher permafrost basins have a greater runoff ratios during precipitation events, the lower permafrost basins make up the difference through a higher baseflow between precipitation events. Large amounts of aufeis have been observed in these sub-basins (such as 1992 and 2000). Surface water, generated by melting aufeis increases the Q/P ratio by increasing the runoff with no corresponding increase in the precipitation. This demonstrates the importance of aufeis in northern watersheds and in some cases may explain the some of the observed year-to-year variability in the runoff ratio.

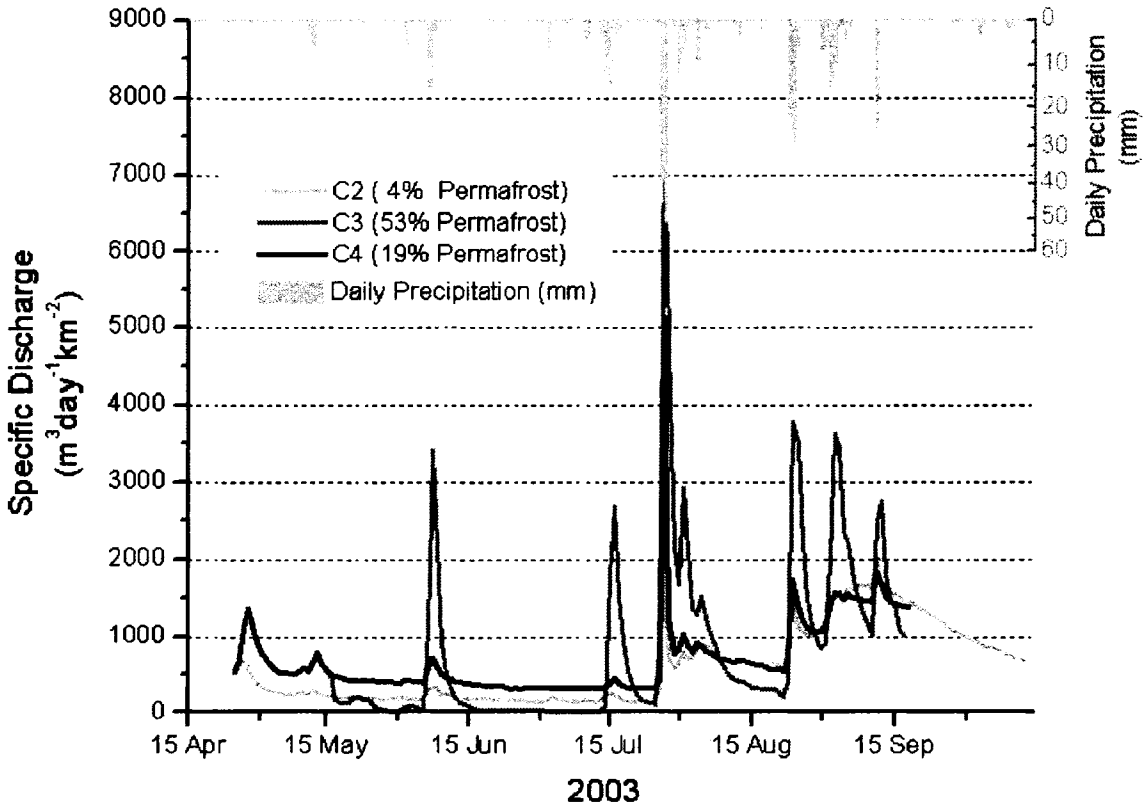

Figure 3.5. Specific discharge of the C2, C3, and C4 sub-watersheds of CPCRW.

Table 3.2: Summer (1 May – 1 October) evapotranspiration and runoff ratios for the C2, C3, and C4 sub-basins, Caribou-Poker Creeks Research Watershed, Interior Alaska, 1978-2003.

	C2 Sub-basin		C3 Sub-basin		C4 Sub-basin	
Year	ET/P_{rain}	Q/P_{rain}	ET/P_{rain}	Q/P_{rain}	ET/P_{rain}	Q/P_{rain}
1978	1.36	–	0.88	–	1.29	–
1979	1.31	–	0.84	–	1.24	–
1980	1.31	–	0.85	–	1.24	–
1981	1.07	–	0.69	–	1.01	–
1982	1.09	–	0.70	–	1.03	–
1983	1.15	–	0.74	–	1.09	–
1984	1.26	–	0.81	–	1.20	–
1985	0.99	–	0.64	–	0.94	–
1986	1.23	–	0.79	–	1.16	–
1987	1.43	–	0.92	–	1.36	–
1988	1.09	–	0.70	–	1.03	–
1989	1.37	–	0.89	–	1.30	–
1990	1.01	–	0.65	–	0.96	–
1991	2.24	–	1.44	–	2.12	–
1992	0.85	–	0.55	–	0.80	–
1993	1.09	–	0.70	–	1.03	–
1994	1.04	0.30	0.67	0.27	0.99	0.31
1995	1.10	0.24	0.71	–	1.05	0.21
1996	1.01	–	0.65	–	0.95	–
1997	1.65	–	1.07	–	1.57	–
1998	0.85	–	0.55	–	0.81	–
1999	1.29	–	0.83	–	1.22	0.29
2000	0.87	–	0.56	–	0.82	0.29
2001	1.11	0.24	0.72	0.26	1.05	–
2002	0.96	–	0.62	–	0.91	–
2003	0.54	0.21	0.35	0.28	0.51	0.25
Mean	1.16	0.25	0.75	0.27	1.10	0.27
Max	2.24	0.30	1.44	0.28	2.12	0.31
Min	0.54	0.21	0.35	0.26	0.51	0.21
SD	0.31	0.04	0.20	0.01	0.30	0.04

P_{rain}: Rain preciptiation; Q C2, C3, C4: Summer streamflow runoff for the C2, C3, and C4 sub-basins; –:< 85% Continuous data. Note: Q/P_{rain} ratios are only presented for years in which daily meteorological and streamflow data area available before 15 May. ET/P_{rain} ratios greater than 1.0 are possible as soil moisture derived from snowmelt is not included in these calculations.

3.4 Results and discussion

The Sub-arctic represents an important transitional region from temperate to arctic environments. Spring and summer runoff appears to be increasing in many Siberian rivers [*Yang et al.*, 2002; *Peterson et al.*, 2002]. It has been suggested the increased discharge may be due to a reduction in permafrost or, more likely, to an increase in precipitation [*Berezovskaya et al.*, 2005]. The presence or absence of permafrost significantly impacts many of the hydrologic processes in the Sub-arctic. Ice-rich conditions at the permafrost table inhibit percolation of surfaces waters to deeper subsurface soils, resulting in a decreased groundwater recharge and an increased runoff generation compared to permafrost free areas. During precipitation events, enhanced saturated conditions above the permafrost table allow surface waters to move relatively quickly downslope through the organic mat and active layer to the stream. In contrast, areas free of permafrost are relatively well drained, allowing infiltration to deeper subsurface systems. In these areas, the infiltration capacity of these non-permafrost soils must be exceeded before runoff generation can take place. Comparison of the C2 and C3 sub-basins (3 and 53% permafrost extent, respectively), in the years of similar discharge records (1978, 1983, 1987, 1994, 2000, and 2001), show that stream flow in C2 is consistently lower than that in C3 (Table 3.3), with the exception of 1994 - which is the only year measurements include snowmelt. In general, the ratio of summer runoff to summer precipitation varies little between the sub-basins (Table 3.2). In the C2 and C4 sub-basins, evapotranspiration accounts for the loss of at least one-half to nearly all summer precipitation. In the C3 sub-basin, evapotranspiration only accounts for one-third to three-quarters summer precipitation. Differences between the C2 and C3 sub-basin summer runoff are offset by a higher winter discharge (from a larger groundwater storage reservoir) from the C2 sub-basin.

In the sub-arctic environment, the storage processes are critically important in calculation of the water balance, but are the least well quantified. If the northern climate continues to warm as expected, we should expect a gradual shift in the water balance. In basins with substantial permafrost now, one should expect a decrease in summer runoff and an increase in winter baseflow as permafrost extent decreases. These results may be unique to watersheds with discontinuous permafrost, perhaps representing an interim between watersheds with no permafrost and those with continuous permafrost. The degree of sim-

ilarity to basins in more arctic or more temperate regions is dictated by the percentage of permafrost. As the percentage of frozen ground decreases, base flow increases and the specific peak flow decreases. As the summer proceeds and the active layer increases in thickness, the available storage increases, the rates of recession or recession constants decrease (longer recession periods) as water moves more slowly through deeper soil layers toward the stream. Similarly, as the active layer increases in thickness, streams become somewhat less flashy as the peak flows decrease due to greater attenuation of surface runoff in the deeper soil layers.

3.5 Acknowledgements

Support for this research was provided by the U.S. National Science Foundation Division of Environmental Biology under the Long Term Ecological Research Program (Grant Number DEB-9211769), NSF Arctic System Science Program (OPP-0229705), a grant from the Center of Global Change - University of Alaska Fairbanks, and a fellowship from the Inland Northwest Research Alliance (U.S. Department of Energy contract DE-FG07-02ID14277).

Table 3.3: Water balance data for the C2, C3, and C4 sub-basins, Caribou-Poker Creeks Research Watershed, Interior Alaska, 1978 – 2003. (mm over basin).

				C2 Sub-basin				C3 Sub-basin				C4 Sub-basin			
Year	Snow	Rain	P_{Total}	Q	Q_{Dates}	ET	ΔS	Q	Q_{Dates}	ET	ΔS	Q	Q_{Dates}	ET	ΔS
1978	81.3	229.3	310.5	30.5	172–275	231.3	-32.3	42.9	172–274	201.5	66.1	–	–	296.1	–
1979	117.7	251.9	369.6	–	–	329.0	–	27.1	116–273	212.3	130.2	–	–	311.9	–
1980	93.1	227.6	320.7	24.6	169–267	298.2	-2.1	–	–	192.4	–	32.8	142–267	282.7	5.2
1981	95.7	271.1	370.8	108.0	140–280	293.4	-30.6	102.4	156–266	189.3	79.1	81.0	160–280	278.2	11.6
1982	84.7	288.8	373.5	86.3	146–279	313.8	-26.6	77.6	159–279	202.5	93.4	71.2	133–279	297.5	4.8
1983	143.9	260.3	404.2	123.5	130–266	298.7	-18.0	137.1	130–267	192.8	74.3	81.8	131–273	283.2	39.2
1984	100.8	240.7	341.5	145.1	138–284	303.7	-107.3	–	–	195.9	–	114.7	138–274	287.9	-61.1
1985	188.0	292.2	480.2	171.6	151–288	288.8	19.8	61.9	170–266	186.3	232.0	91.4	151–255	273.8	115.0
1986	97.4	257.2	354.6	70.6	175–269	315.7	-31.7	–	–	203.7	–	101.1	141–290	299.3	-45.8
1987	88.1	229.0	317.1	27.7	147–286	327.7	-38.3	40.1	147–279	211.4	65.6	54.0	134–286	310.7	-47.6
1988	67.7	300.4	368.2	–	–	326.4	–	–	–	210.6	–	64.4	133–272	309.5	-5.7
1989	171.0	239.6	410.6	–	–	329.3	–	–	–	212.5	–	–	–	312.3	–
1990	161.7	333.5	495.2	41.9	142–268	336.1	117.2	–	–	216.9	–	44.5	136–269	318.7	132.0
1991	342.1	150.4	492.4	74.8	155–218	336.7	80.9	115.8	136–268	217.2	159.4	100.5	151–265	319.2	72.7
1992	153.2	346.3	499.6	79.0	155–291	293.5	127.1	64.0	155–273	189.4	246.2	–	–	278.3	–
1993	331.6	323.5	635.1	–	–	352.4	–	–	–	227.4	–	–	–	334.1	–
1994	102.4	339.3	441.7	115.3	97–278	352.9	-26.5	99.9	95–278	227.7	114.1	111.7	89–277	334.6	-4.6
1995	163.4	325.9	489.3	89.1	101–271	359.7	40.5	–	–	232.1	–	36.4	108–205	341.0	111.9
1996	110.9	313.4	424.3	–	–	315.4	–	46.5	142–268	203.5	174.3	21.4	191–270	299.1	103.8
1997	131.2	212.3	343.5	37.2	155–279	351.3	-45.0	–	–	226.7	–	–	–	331.1	–
1998	75.2	345.4	420.7	–	–	293.7	–	–	–	189.5	–	72.3	141–269	278.5	69.9
1999	71.6	242.1	313.6	34.2	145–275	311.7	-32.3	–	–	201.1	–	64.6	103–253	295.6	-46.6
2000	197.9	319.5	517.4	116.7	145–276	276.7**	124.0	152.8	144–276	178.5**	186.1	95.0	101–254	262.4**	160.0
2001	91.6	271.4	363.0	76.2	113–278	301.2*	-14.4	83.1	113–278	194.4*	85.5	–	–	285.7*	–
2002	53.2	307.2	360.4	53.0	188–294	295.8*	11.6	69.4	183–295	190.8*	100.2	20.5	183–289	280.5*	59.4
2003	102.1	381.6	483.7	95.3	114–287	204.9*	183.5	105.6	133–260	132.2*	245.9	103.7	114–262	194.3*	185.7
Mean	130.7	280.9	411.6	80.0		312.3	15.0	83.8		201.5	136.8	68.1		296.1	45.2
Max	342.1	381.6	635.1	171.6		359.7	183.5	152.8		232.1	246.2	114.7		341.0	185.7
Min	53.2	150.4	310.5	24.6		204.9	-107.3	27.1		132.2	65.6	20.5		194.3	-61.1
SD	69.5	52.6	80.3	41.5		31.3	74.0	36.8		20.2	66.0	30.1		29.7	74.9

P_{Total}: total precipitation (= snow + rain); ET: evapotranspiration; Q: streamflow runoff; Q_{Dates}: Julian dates of continuous measurement of streamflow runoff; ΔS: change in storage; –: < 85% continuous data; *: ET calculated using Priestley-Taylor Method; **: ET calculated using simulated ET for days 121–146 and Priestley-Taylor Method for remaining days.

References

Baldocchi, D., F. M. Kelliher, T. Black, and P. Jarvis (2000), Climate and vegetation controls on boreal zone energy exchange, *Global Change Biology*, *6*(Supplement 1), 69–83.

Berezovskaya, S., D. Yang, and L. Hinzman (2005), Long-term annual water balance analysis of the Lena River, *Global and Planetary Change*, *48*, 1-3, doi:10.1016/j.gloplacha.2004.12.006.

Bolton, W., L. Hinzman, and K. Yoshikawa (2000), Stream flow studies in a watershed underlain by discontinuous permafrost, in *Proceedings Water Resources in Extreme Environments*, edited by D. Kane, pp. 31–36.

Chapman, W., and J. Walsh (1993), Recent variations in sea ice and air temperature in high latitudes, *Bulletin American Meteorology Society*, *74*, 33–47.

Gieck, R. E. (1986), A water resource evaluation of two subarctic watersheds, MS thesis, University of Alaska Fairbanks.

Haugen, R., C. Slaughter, K. Howe, and S. Dingman (1982), Hydrology and climatology of the Caribou-Poker Creeks Research Watershed, Alaska, *CRREL Report 82-26*, US Army Corps of Engineers Cold Regions Research and Engineering Laboratory.

IPCC (2001), Climate change 2001: Synthesis report. summary for policymakers., *Tech. rep.*, Intergovernmental Panel on Climate Change.

Kane, D., and L. Hinzman (2004), Monitoring extreme environments: Arctic hydrology in transition, *Water Resources Impact*, *6*(1), 24–27.

Peterson, B., R. Holmes, J. McClelland, C. Vörösmarty, R. Lammers, A. Shiklomanov, I. Skiklomanov, and S. Rahmstort (2002), Increasing river discharge to the Arctic Ocean, *Science*, *298*, 2171–2173.

Priestley, C., and R. Taylor (1972), On the assessment of surface heat flux and evaporation using large scale parameters., *Monthly Weather Review*, *100*(2), 81–92.

Rovansek, R., D. Kane, and L. Hinzman (1993), Improving estimates of snowpack water equivalent using double sampling, in *Proceedings of the 50th Eastern Western Snow Conference*, edited by M. Ferrick and T. Pangburn, pp. 157–163.

Slaughter, C. (1981), Streamflow measurement with pre-fabricated partial flumes in a permafrost dominated watershed., *Research Note 382*, USDA Forest Service PNW Forest and Range Experiment Station.

Woo, M. K. (1990), Permafrost hydrology, in *Northern Hydrology, Canadian Perspectives. Proceedings of the Northern Hydrology Symposium*, edited by T. Prowse, C. Ommanney, and M. Woo, no. 1 in Canadian National Hydrology Research Institute Science Report, pp. 63–76.

Yang, D., D. Kane, L. Hinzman, X. Zhang, T. Zhang, and H. Ye (2002), Siberian Lena River hydrologic regime and recent change, *Journal Geophysical Research, 107*(D23), 4694, doi:10.1029/2002JD002,542.

Yoshikawa, K., L. Hinzman, N. Ishikawa, C. Collins, and V. Lunardini (1998), Air and ground temperature models at Caribou-Poker Creeks Research Watershed, in *Proceedings of the 49th AAAS Arctic Science Conference*, Fairbanks, Alaska.

Yoshikawa, K., W. Bolton, V. Romanovsky, M. Fukuda, and L. Hinzman (2002), Impacts of wildfire on the permafrost in the boreal forest of interior Alaska, *Journal of Geophysical Research, 107*(8148: doe:10.1029/2001JD000438), printed 108(D1), 2003.

Yoshikawa, K., D. White, L. Hinzman, D. Goering, K. Petrone, W. Bolton, and N. Ishikawa (2003), Water in permafrost: Case study of aufeis and pingo hydrology in discontinuous permafrost, in *International Conference on Permafrost, Proceedings 8*, vol. 2, edited by M. Phillips, S. Springman, and L. Arenson, pp. 1259–1264.

Chapter 4

Toward an understanding of the hydrologic processes in a watershed dominated by discontinuous permafrost *

Abstract

The sub-arctic environment can be characterized by being located in the zone of discontinuous permafrost. Discontinuous permafrost introduces very distinct changes in soil hydraulic properties, which then introduce sharp discontinuities in hydrological processes and ecosystem characteristics. Hydraulic properties vary over all time scales as the active layer develops over the course of a summer or as permafrost degrades in response to a changing climate. Although the distribution of permafrost is site-specific, it impacts most of the hydrologic processes, including stream flow, soil moisture dynamics, evapotranspiration, groundwater flow, and water storage processes. It is essential to develop a model that can incorporate such temporal and spatial dynamics, both to model watersheds currently situated in discontinuous permafrost and to project future changes in regions underlain by continuous permafrost. This paper describes a spatially-distributed, process-based hydrologic model, TopoFlow, designed to simulate and predict soil moisture dynamics and most other hydrologic processes throughout a sub-arctic watershed. All of the major water balance processes are simulated, including precipitation, snowmelt, evapotranspiration, infiltration, groundwater flow, and overland/channel flow. For every process simulated, a user-specified method and time-step are selected. Each input variable can be a scalar, time-series, grid, or grid sequence. The modular structure of TopoFlow permits implementation of additional processes and methods without altering the functionality of the model. The design and structure of TopoFlow is intended to promote a community-based evolution and serve the broad hydrologic community.

KEY WORDS: Permafrost; Active layer; Modeling; Computational hydrology; Hydrologic processes, Sub-arctic.

*W.R. Bolton, S. D. Peckham, and L.D. Hinzman, In Preparation to be submitted to the *Journal of Geophysical Research – Biogeosciences*

4.1 Introduction

The Köppen Climate Classification System defines the sub-arctic as the region where the mean monthly air temperature is at least 10°C between one and three months of the year. However, the sub-arctic environment can also be characterized as the region located in the zone of discontinuous permafrost (Figure 4.1). Permafrost underlies approximately 24% of the exposed land area in the Northern Hemisphere [*Romanovsky et al.*, 2002], of which approximately 22% (or 5.6 X 10^6 km^2) is located in the discontinuous zone [*Anisimov and Nelson*, 1997]. Permafrost in this region can be very warm and unstable [*Yoshikawa et al.*, 2002]. Although the distribution of permafrost in this region is site-specific, it dominates the response of many hydrologic processes in this region, including stream flow, soil moisture dynamics [*Haugen et al.*, 1982; *Bolton et al.*, 2000], infiltration and percolation [*Kane and Stein*, 1983a,b], evapotranspiration [*Dingman and Koutz*, 1974; *Baldocchi et al.*, 2000; *Hinzman et al.*, 2006], nutrient transport [*Jones et al.*, 2005], sediment transport [*Slaughter et al.*, 1983], and water storage processes.

4.1.1 System response to a warming climate

Temperatures in the western portion of the high northern latitudes are rising at an unprecedented rate [*Chapman and Walsh*, 1993; *Serreze et al.*, 2000]. The permafrost conditions in Interior Alaska are warm and unstable, with temperatures often $-1°C$ or warmer [*Yoshikawa et al.*, 2002]. Recent studies indicate permafrost temperatures in this region are warming [*Osterkamp and Romanovsky*, 1999; *Osterkamp*, 2003]. The warmer climate in combination with an unstable permafrost regime has led to gradual shrinking permafrost coverage and more rapid increases in active layer depth [*Jorgenson et al.*, 2001; *Serreze et al.*, 2002; *Zhang*, 2005]. These changes to the permafrost regime and increased atmospheric temperatures have led to observed changes in the hydrologic regime, including later freeze-up and earlier break-up dates of rivers [*Magnuson et al.*, 2000], increased arctic river runoff [*Peterson et al.*, 2002], shrinking lakes [*Smith et al.*, 2005], and thermokarst development [*Osterkamp and Romanovsky*, 1999; *Osterkamp et al.*, 2000; *Jorgenson et al.*, 2001]. As the sub-arctic thermal and hydrologic systems are fully coupled, it is not surprising that changes in the permafrost regime have led to these observed changes in the hydrologic system [*Hinzman et al.*, 2005; *Walsh et al.*, 2005].

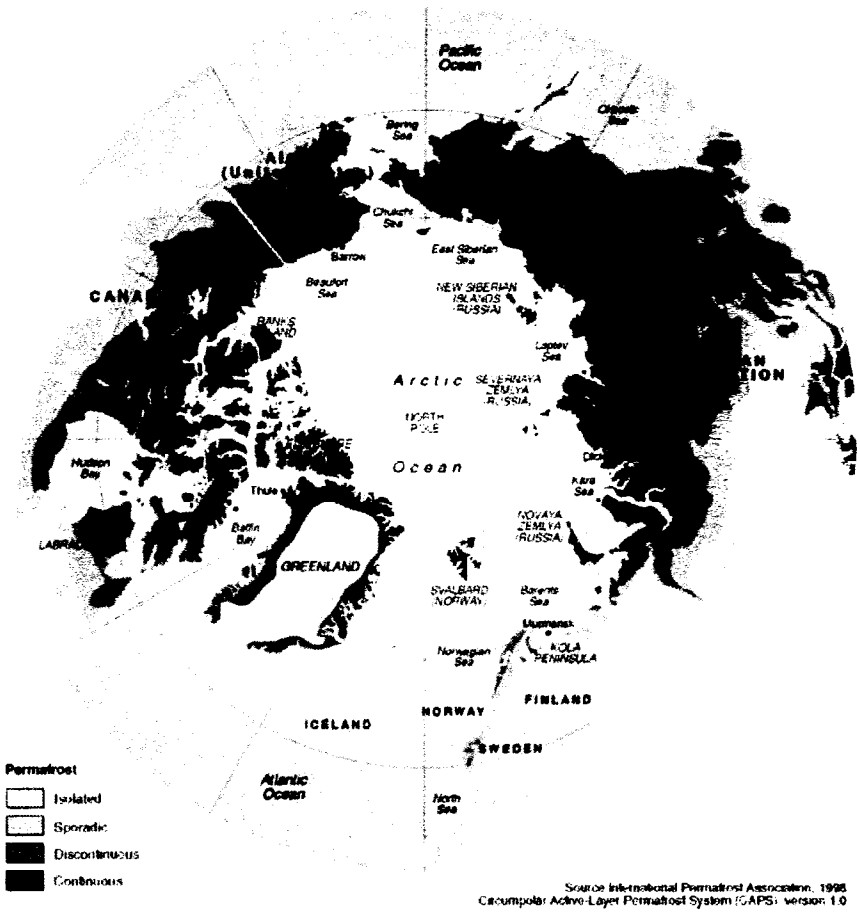

Figure 4.1: Panarctic permafrost distribution. Source: International Permafrost Association, 1998. Circumpolar Active-Layer Permafrost System (CAPS), version 1.0.

Increases in air temperature (particularly winter) and precipitation (both summer and winter) are expected to continue into the future [*IPCC*, 2001]. If the northern environment continues to warm as predicted, one should expect a shifting change in the water balance corresponding to a thinner and spatially reduced permafrost condition. In watersheds with significant permafrost coverage, it is likely that a decreasing summer and an increasing winter discharge will be observed [*Bolton et al.*, 2004; *Hinzman et al.*, 2005]. Changes in the quantity and timing of relatively warm freshwater inflow into the Arctic Ocean may have profound impacts on the thermohaline circulation pattern, potentially changing the regional climate system [*ACIA*, 2005; *Arnell*, 2005].

In the arctic and sub-arctic environment, soil respiration is typically slow due to low ground temperatures [*French et al.*, 1997]. Currently, the boreal forest accounts for about one-third of the carbon sequestered in terrestrial ecosystems [*McGuire et al.*, 1995]. Projected increases in the surface temperature may lead to enhanced degradation of this stored organic matter to either carbon dioxide (CO_2) or methane (CH_4), dependent upon a lowering (aerobic condition) or rising (anaerobic condition) of the water table [*Callaghan and Jonasson*, 1996; *Moore et al.*, 1998; *Friborg et al.*, 2003]. An increase in the input rate of either CO_2 or CH_4, both strong greenhouse gases, into the atmosphere would serve as a positive feedback to further warming of the atmosphere.

4.1.2 Modeling need

In light of these predicted changes and potential feedbacks, it is important to be able to understand and predict the feedback mechanisms of the water cycle [*Kane and Hinzman*, 2004]. At this point, a good understanding of many of the arctic and sub-arctic hydrologic processes exists at the plot and hillslope scales. However, the understanding we have gained from these plot-scale studies has not been adequately or systematically incorporated into process- based meso-scale hydrologic models [*Vörösmarty et al.*, 1993]. Furthermore, the land-surface parameterizations used in global climate models do not adequately resolve the soil conditions [*Walsh et al.*, 2005], which often rely on either point measurements or on information derived from satellite data. It is clear that a meso-scale physically-based hydrologic model is needed to bridge the gap between our plot-scale understanding and regional- (or global-) scale climate models by capturing the hydrologic behavior and

variation of individual watersheds. Currently, there is a lack of process-based hydrologic models that adequately simulate the soil moisture dynamics at the watershed scale and also include a realistic land-atmosphere exchange in permafrost-dominated regions.

Several hydrologic models have been developed to simulate the spatial distribution and temporal variation of physical processes. The approach and design of these models varies with the problem being studied, with each emphasizing a specific process, hydrologic regime, or spatial/temporal scale. The TOPMODEL (TOPography based hydrological MODEL, *Bevin and Kirkby* [1979]) and its variants (e.g. STOPMODEL [*Walter et al.*, 2002], Dynamic TOPMODEL [*Bevin and Freer*, 2001]) rely on a statistical method of hydrologic similarity, based upon a topography index. The topographic index is defined as $\ln(a/\tan\beta)$, where a is the area draining through a point upslope and β is the local slope angle. All points with the same index value are assumed to respond in a hydrologically similar way, requiring calculations only for different index values. Similarly, lumped parameter models such as the PRMS (Precipitation-Runoff Modeling System, [*Leavesley et al.*, 1983]), HSPF (Hydrologic Simulation Program - Fortan, [*Bicknell et al.*, 1997]), SWAT (Soil and Water Assessment Tool, [*Arnold et al.*, 1993]), VIC (Variable Infiltration Capacity, [*Liang et al.*, 1994]), and the SLURP (Simple Lumped Reservoir Parametric Model [*Kite*, 1978, 1989]) rely on sub-dividing watersheds based upon similar soil, hydrologic, and land use properties, called hydrologic response units (HRUs), reducing the number of variables and and calculations required during simulations. The SHE (Systéme Hydrologique Européen, [*Jonch-Clausen*, 1979; *Abbott et al.*, 1986]) and MIKE-SHE [*DHI*, 1998] models are spatially-distributed, physically-based models that simulate many of the hydrologic processes, including precipitation, evapotranspiration, overland flow, channel flow, vadose zone flow, and groundwater flow. The physically-based process models require a substantial set of high quality data, often not available in the arctic and sub-arctic environments. The KINEROS2 (Kinematic Runoff and Erosion Model [*Goodrich et al.*, 2000]), DR_3M (Distributed Routing Rainfall-Runoff Model, [*Alley and Smith*, 1982]), and the CASC2D (CASCade 2-Dimensional, [*Julian and Saghafian*, 1991]) are single event based models, emphasizing a specific process. *Wigmosta et al.* [1994] presents a model (Distributed Hydrology Vegetation Model, DHVM) that focuses on vegetation - hydrology relationships with the inclusion of a two-layer canopy model for evapotranspiration and a two-layer rooting zone

model. The models described above generally developed for specific applications particular to a specific hydrologic regime. None of these models is suited to handle the rapidly changing thermal (permafrost versus non-permafrost and active layer development) and hydraulic (hydraulic conductivity and storage capacity) conditions in the x-, y-, and z-directions typical of the sub-arctic hydrologic regime. *Fox* [1992] presents an algorithm to estimate the soil freeze-thaw depth in permafrost and non-permafrost areas to investigate the effects of soil freezing and thawing in a water balance model. While not presented in a spatially-explicit manner, the algorithm described by *Fox* [1992] was designed to be implemented into a spatially-distributed model called HYFOR-FT (Hydrology of Forests with Freezing and Thawing) [*Fox*, 1976].

4.1.3 Objective

The main purpose of the model we are developing, TopoFlow, is to describe, simulate, and predict all arctic and sub-arctic hydrologic processes at the meso-scale using energy and climate forcings. The main objective of this paper is to describe and document the TopoFlow numerical model, which is able to reproduce most hydrological processes while reflecting the spatially and temporally varying properties that are ubiquitous in both the arctic and sub-arctic environments.

4.2 Model development

4.2.1 TopoFlow overview

TopoFlow is a process-based, spatially-distributed hydrologic model based upon the ARHYTHM (ARctic HYdrologic and THermal Model, (*Hinzman et al.* [1995]; *Zhang et al.* [2000])). TopoFlow utilizes an user friendly graphical user interface (GUI), incorporating point-and-click functionality and context-specific help dialogs. TopoFlow is designed to evolve into a hydrologic model that is utilized and enhanced by all disciplines within the hydrologic community. Well documented open-source code (available for download from the TopoFlow website (http://instaar.colorado.edu/topoflow/) is structured in a modular fashion. Members of the hydrologic community are able (and encouraged) to develop and incorporate new hydrologic methods without altering the overall structure or functional-

ity of TopoFlow. Other features of TopoFlow include pre- and post-processing tools which aid in the preparation of spatially-distributed input files and rapid visualization and analysis of output files. Written in IDL (Interface Data Language), TopoFlow is portable across the Windows, MacIntosh, and Unix computing environments.

Numerically, TopoFlow is based upon the conservation of mass principle,

$$Inputs - Outputs \pm \Delta Storage = 0 \tag{4.1}$$

where: *Inputs*, *Outputs*, and $\Delta Storage$ are the amount of water over a time period, Δt. Using the continuity principle, the water balance is calculated for each element in the model domain for each time step,

$$P_T + GW_{in} - (Q_{CH} + ET + GW_{out}) = \Delta Storage \tag{4.2}$$

where: P_T is precipitation (rain and snowmelt), $GW_{in,out}$ is groundwater inflow and outflow, Q_{CH} is overland and channel flow, ET is evapotranspiration, and $\Delta Storage$ is the change in storage (all forms of water storage).

The structure of TopoFlow is divided into three components: model input, process simulation, and model output. Each of these components are described below.

4.2.2 Model input

The model input component of TopoFlow consists of two parts: 1) digital elevation model (DEM) analysis, and 2) determination of the model time step. Both the DEM analysis and determination of the model time-step must be completed before the process simulation can begin. However, once the DEM analysis has been completed for the model domain, it does not need to be repeated.

DEM analysis and flow routing

In order to run TopoFlow, input files that define the model domain, the topography, the direction of lateral water movement, the Horton-Strahler order number, and an information file, describing the structure of the model domain, must be generated. Although not

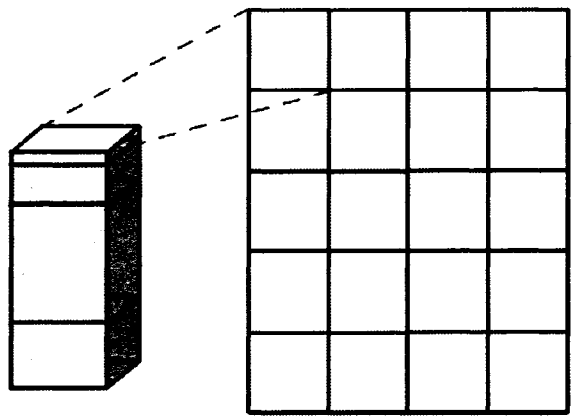

Figure 4.2: Rectangular elements used in TopoFlow. The dimensions of each element corresponds to the DEM pixel resolution in the x- & y-directions. Up to 10 user defined layers of variable thickness represent the z-direction. Elements are labeled sequentially in calendar fashion (by rows) from the upper left (NW corner) to the lower right (SE corner).

necessary to complete this step, commercial software such as RiverTools^{TM}are able to efficiently generate each of these files. An example of the required information file can be found on the TopoFlow website (http://instaar.colorado.edu/topoflow).

Implementation of DEMs to aid in hydrologic analysis has become commonplace due to the increased availability and quality of DEMs, and rapid growth in computing power. In hydrologic analysis, the most common form of the DEM is the square-grid network. The square-grid network is computationally simple to setup and efficient, and overlying other spatial information is relatively simple compared to other networks such as those created using contours or triangular irregular network (TINs) [*Moore et al.*, 1993; *Grayson and Blöschel*, 2000]. For each TopoFlow simulation, the model domain and topography are defined by a square-grid network DEM, which encompasses the catchment area. Each TopoFlow element has dimensions of the DEM pixel resolution (x- & y-directions) with up to ten user specified layers of variable thickness in the z-direction (Figure 4.2).

The slope between two TopoFlow elements is defined as the difference in the land surface elevation between two elements divided by the straight-line distance between the centers of the elements [dimensionless value]. Each TopoFlow element is assigned a 'local slope', which is defined as the steepest (largest positive value) slope between an element and its eight neighboring elements (Figure 4.3b).

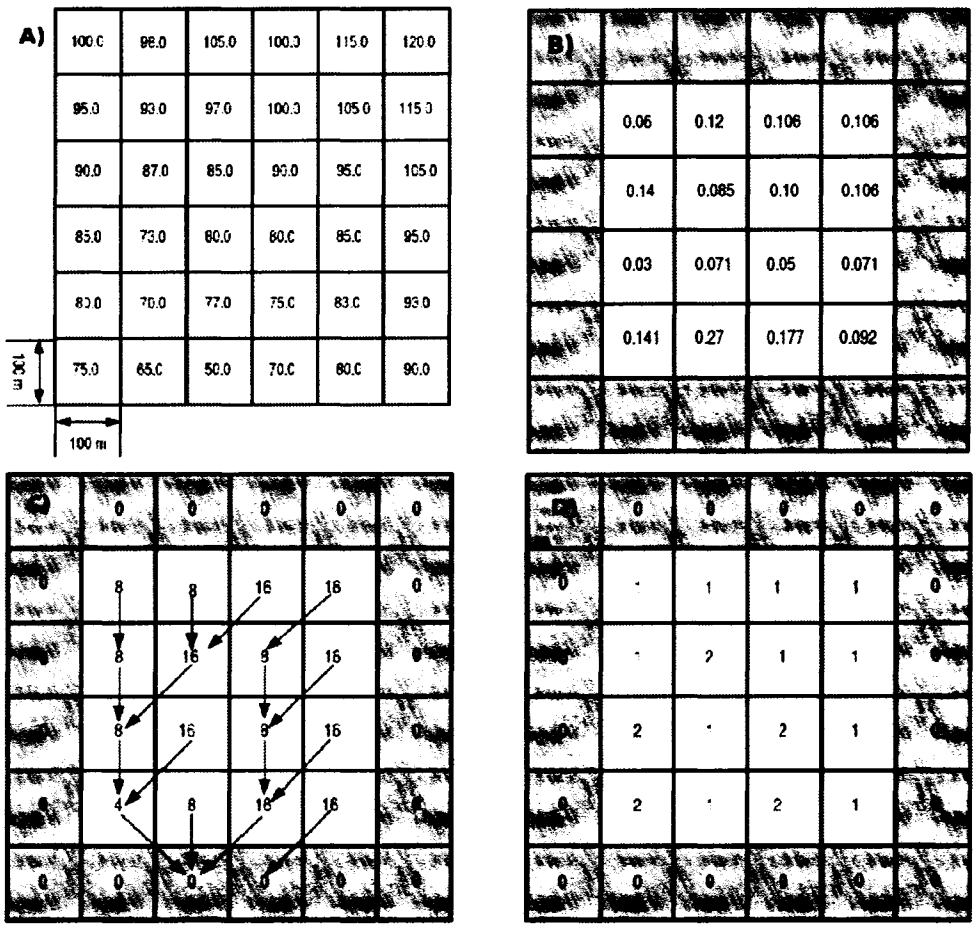

Figure 4.3: Digital elevation analysis. A) An example of a 100-meter DEM. Numerical values in each element represent the land surface elevation. B) The 'local slope' of each interior element. The 'local slope' is defined as the steepest (largest positive value) slope between an element and its eight neighboring elements. C) Flow routing. Each element is assigned a numerical value which designates the direction in which water from one element flows one of the adjacent eight elements. Arrows indicate direction of flow determined by the direction of the local slope. D) Order number. Each of these four files (DEM, Local Slope, Flow Direction, and Order Number) and an Information file must be generated prior to running TopoFlow. Note: Elements on the edge of the DEM (shaded elements) are not considered part of the model domain.

The horizontal water direction for each TopoFlow element is based upon the D8 method [*O'Callaghan and Mark*, 1984]. Flow directions are defined as moving from one element to an adjacent element in the direction of the 'local slope.' In the case of flat areas, where the steepest slope is equal to zero, the flow direction is forced in the direction from higher surrounding topography to lower topography [*Garbrecht and Martz*, 1997]. Each element within the model domain is assigned a flow direction based on one of the eight primary compass directions [NE, E, SE, S, SW, W, NW, N] corresponding to the eight surrounding neighbor elements. Flow directions for each element are coded with corresponding values of [1, 2, 4, 8, 16, 32, 64, 128]. Flow directions for edge elements of the DEM are not assigned a flow direction (Figure 4.3c). The decision to move from the triangular elements used in ARHYTHM [*Hinzman et al.*, 1995; *Zhang et al.*, 2000] model to rectangular elements was in part due to difficulties in routing flow through flat regions, such as those found on the North Slope of Alaska. Although the triangular elements are the most efficient method of representing topographic features [*Grayson and Blöschel*, 2000], the ability to efficiently route water through these flat regions was determined to be more critical.

Each TopoFlow element is assigned an order number based upon the Horton-Strahler classification [*Horton*, 1945; *Strahler*, 1957]. Each 'headwater' element is designated as first-order. An element in which the flow direction of two first-order elements join together form a second-order element. An element in which the flow directions of two second-order elements meet forms a third-order element, and so on (Figure 4.3d). Only when two elements of the same order flow into another element, does the flow order increase, meaning that numerous lower-order elements can flow into a larger-order element without changing the order number of the larger-order element. *Peckham* [1995] observed that by 'pruning' (or removing) lower-order elements from the flow network tree, the remaining 'un-pruned' branches closely resemble the natural channel pattern of the drainage network. Conceptually, the 'pruned' lower-order element represent elements in which overland flow would occur (if either the water table elevation exceeds the land surface elevation or if the infiltration capacity of the soils is exceeded by either the snowmelt or precipitation rate). Higher-order, 'non-pruned' branches are elements in which channel flow occurs.

Model timestep

In order to maintain numerical stability, the maximum distance traveled by a parcel of water in one time step must be less than one pixel width, i.e. the Courant condition:

$$(vmax \cdot \Delta t) \leq dx \tag{4.3}$$

where: $vmax$ is the estimated maximum velocity a particle of water can travel, [m/s]; Δt is the model time step, [s]; and dx is the width of an element, [m]. In order to satisfy the Courant condition, the time step used in the channel flow process must be $\leq dx/vmax_{chan}$, where $vmax_{chan}$ is the maximum velocity a particle of water travels within a channel segment. This is the maximum model time-step possible for simulations.

TopoFlow input tools

TopoFlow has a number of features to aid in the model input and simulation process. TopoFlow features an user friendly point-and-click GUI (Figure 4.4). The wizard-style GUI is designed to ensure all required files or variables are inputted correctly. For each process, the formulas used for each selected method are available with a click of a button. Additionally, context specific 'Help' dialogs are also available with a click of a button.

A number of pre-processing tools are available to aid in the creation of spatially distributed input files. Three of the pre-processing tools relate to the creation of spatially and temporally distributed meterological data. Using the Inverse Distance Method, the first tool creates spatial and temporal meteorologic data (grid sequence file) from point measurements. The second tool calculates the clear sky short-wave radiation flux (grid sequence file) for a specified period (Day A to Day B) and interval (i.e. hour, minute, day). Direct, diffuse, and backscatter radiation components are calculated based upon topographic/surface features, such as slope and aspect angle and albedo, and atmospheric properties, such as air temperature and relative humidity. The third pre-processing tool creates a grid sequence file for fractal rain events. Fractal rain events are localized rain events which follow power-law distributions derived from several decades of data [*Dickman*, 2004]. Tools which create the channel geometry grids (based upon either the order or area grids), a profile smoothed DEM, and a steady state initial flow depth grid are also

available.

4.2.3 Process simulation

The sub-Arctic lies in the transition zone between the continuous permafrost region of the arctic and the sporadic/non-permafrost region of the temperate environment. As a result, the thermal and hydrologic characteristics of both the Arctic and temperate region occur in the sub-Arctic, and are reflected with permafrost distribution. Many of the sub-arctic hydrologic processes are highly variable in both space and time. For example, groundwater flow in this region occurs in the deep subsurface system (in permafrost free areas, sub-permafrost groundwater) or in the shallow surface soils within the active layer (in permafrost areas, supra-permafrost groundwater). The supra-permafrost groundwater flow is also strongly influenced by the active layer depth, which is in a continuous state of change (either thawing or freezing). Other hydrologic processes such as evapotranspiration (reflected in vegetation distribution and surface energy balance), infiltration, percolation, overland and channel flow, as well as soil moisture dynamics (all reflected in permafrost distribution) exhibit a high spatial and temporal variability. Additionally, many of the hydrologic processes take place on different time scales - channel flow in seconds, infiltration and percolation in minutes to hours, groundwater flow and snowmelt in hours to days.

In the high latitudes, data collection stations (stream discharge, meteorological stations) are sparse for a number of reasons (lack of funding, harsh and remote environment, etc.) [*Shiklomanov et al.*, 2002]. As a result, spatial and/or temporal data sets may not be available as model input. TopoFlow addresses this issue by allowing the user to select a specific data type for nearly every input variable. The format for each input variable can take one of the following forms: 'scalar' - constant value in both time and space; 'time series' - spatially constant data, variable in time; 'grid' - spatially variable data, constant with time; and 'grid sequence' - both spatial and temporally variable data.

The structure of TopoFlow is such that a method is specified for each hydrologic process. For each process, the option of 'None' exists, meaning that specific process will not be used in the simulation. For those hydrologic processes simulated, a physically-based method of simulation is available. However, many of these physically-based methods are

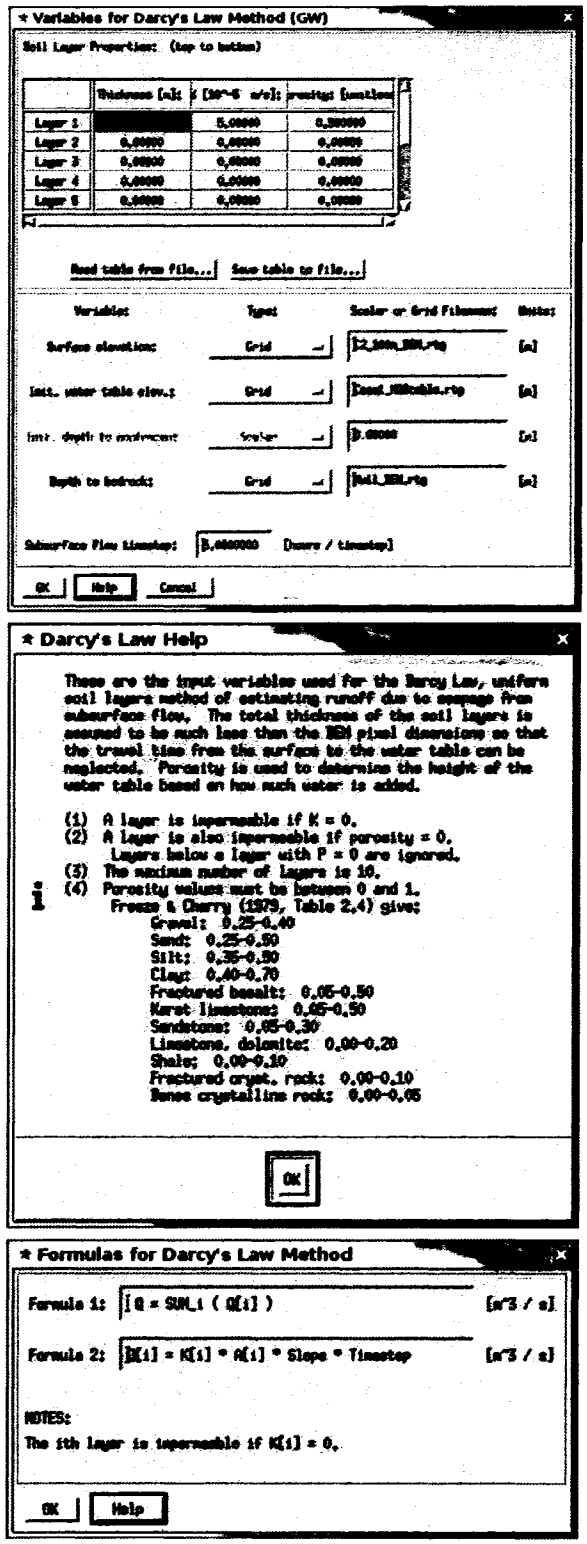

Figure 4.4: TopoFlow graphical user interface. TopoFlow features an user friendly point-and-click GUI with method specific Help and Formulae dialogs.

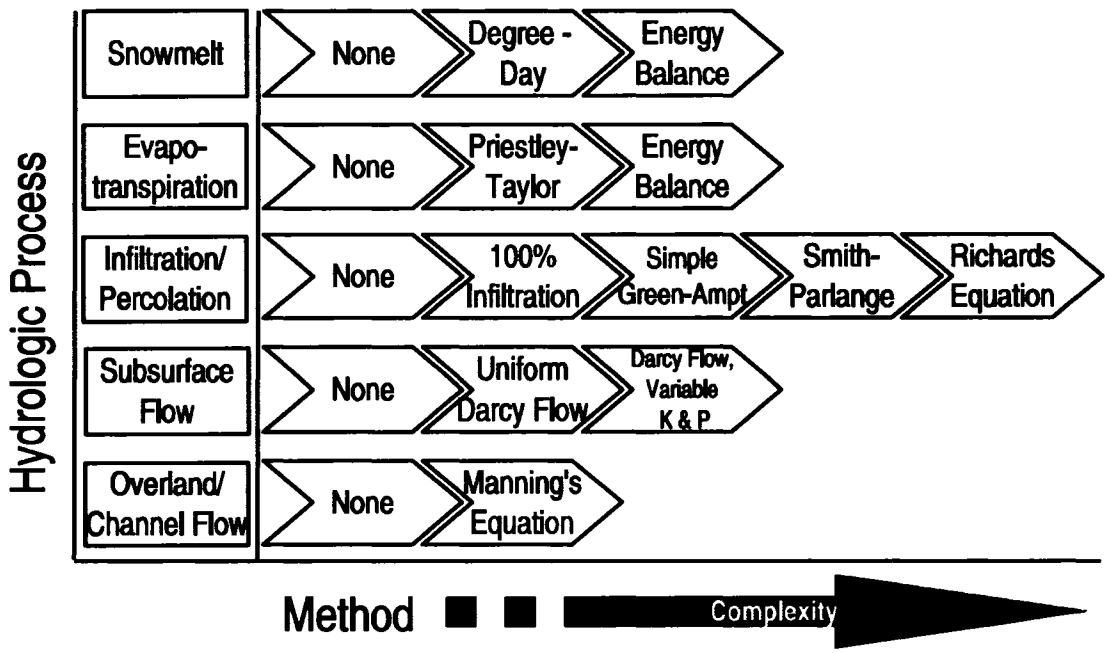

Figure 4.5: Hydrologic processes and methods simulated in TopoFlow. For each model simulation, any combination of processes (including 'None') maybe employed.

extremely data intensive. Given the overall lack (and declining number) of meteorologic stations [*Shiklomanov et al.*, 2002] located in the northern regions, process simulations using (semi-)empirical methods, having fewer data requirements, are also available (Figure 4.5). As the complexity of the method used to simulate processes increases, the data and computational requirements increase proportionately (Section 4.2.4). The time step used for each process simulated is user specified and is independent of the other processes simulated.

The TopoFlow model is a modification (second generation) of the ARHYTHM model. As such, many of the hydrologic processes simulated are formulated in the exact manner as ARHYTHM and are documented in *Zhang et al.* [2000]. The hydrologic processes currently supported include precipitation, snowmelt, evapotranspiration, infiltration, overland/channel flow, and groundwater flow. The governing equations for all the hydro-

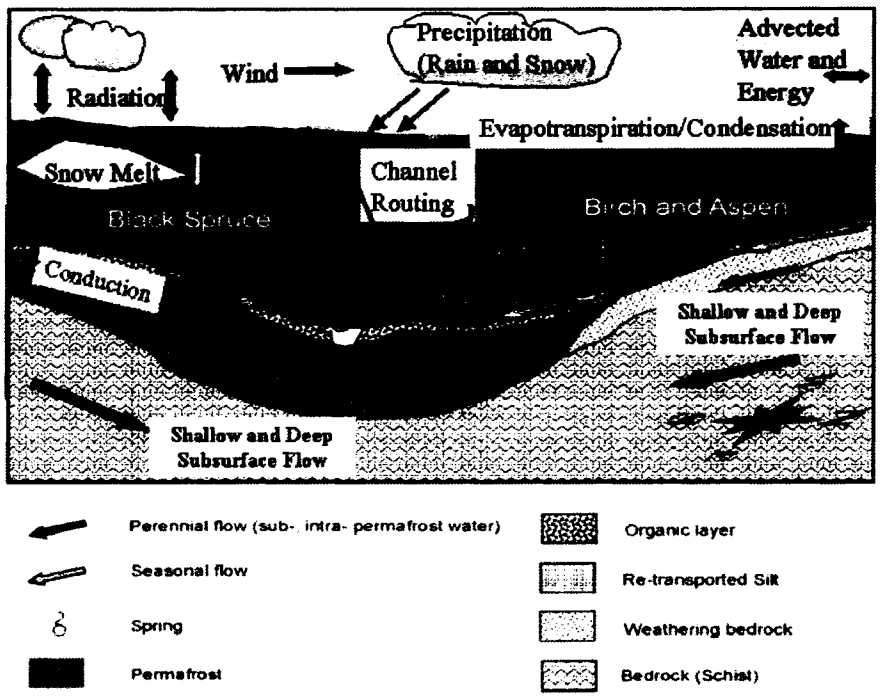

Figure 4.6: Energy and hydrologic processes simulated in TopoFlow. Figure modified from *Hinzman et al.* [2006].

logic processes and methods currently used in TopoFlow are listed in the Appendix of this chapter (Table 4.4). Significant changes in the infiltration and overland and channel flow processes have been made in TopoFlow and are described in detail below. The energy and hydrologic processes considered in the model development are shown in Figure 4.6.

Infiltration and percolation

There is a high degree of spatial and temporal variability in the infiltration and percolation processes in the sub-arctic environment. In the sub-Arctic, the presence or absence of permafrost significantly controls the pathways of groundwater flow, either limiting it to the near surface active layer (in areas underlain with permafrost) or allowing percolation to a deep (sub-permafrost) groundwater system [*Hinzman et al.*, 2000]. As a result, runoff patterns between permafrost and permafrost-free slopes are markedly different [*Slaughter and Kane*, 1979; *Bolton et al.*, 2000] (Section 5.2). The distribution of water in the soil col-

umn is an important factor in determination of the runoff response to precipitation events. As near surface moisture content increases, the amount of water storage available in the soils is reduced. A number of studies (e.g. *Dingman* [1973], *Roulet and Woo* [1988], *Kane et al.* [1989], and *Quinton and Marsh* [1999]) have suggested that the wetter the watershed prior to a rainfall event, the higher the percentage of runoff that would occur (compared to similar magnitude rainfall events). Percolation of surface waters to the deep groundwater system is not only dependent upon the distribution of permafrost, but also the time of year. The snowmelt period in most high-latitude regions is typically the major hydrologic event of the year [*Kane and Yang*, 2004; *Bolton et al.*, 2004] as 6-8 months of precipitation, held in storage as the winter snowpack, is released into the system over a relatively short 2-3 week period. *Kane and Stein* [1983a,b] have indicated the snowmelt period is of particular importance as most groundwater recharge occurs during this period, as evapotranspiration demands are typically very low. Groundwater recharge occasionally occurs during prolonged precipitation events [*Kane and Stein*, 1983b] following the snowmelt period.

TopoFlow currently uses four different methods to simulate the infiltration and percolation processes. Three of the methods are primarily based upon Darcy's Law and the principle of conservation of mass: 1) Finite-Difference Solution of the Richards Equation; 2) Green-Ampt, Single Event; and 3) Smith-Parlange, Single Event. A fourth method, Instantaneous Infiltration, was used in the ARHYTHM model and can be used in areas of continuous permafrost. As with the other processes, the amount of input data and computational resources required is proportional to the complexity of the method used. Discussion of the four different methods used to simulate the infiltration and percolation processes follows below.

Finite-Difference Solution of the Richards Equation. The Richards Equation [*Richards*, 1931] for infiltration is:

$$\frac{\partial \theta}{\partial t} = \frac{\partial}{\partial x}\left[K\frac{\partial \psi}{\partial x} - K\right] \tag{4.4}$$

where θ is the soil water content [by volume]; z is vertical depth into the soil, positive downward from the surface, [m]; K is the hydraulic conductivity of the soil, [m/s]; ψ is the soil water capillary head, [m]; and t is time, [sec]. The Richards equation is solved using

the finite difference solution as described in *Smith* [2002]. The finite difference formulation of the Richards Equation (Equation 4.4) can be rewritten (following *Smith* [2002]) as:

$$\frac{[\theta^j - \theta^{j-1}]}{\Delta t} = \frac{-2}{(x_{\iota+1} - x_{\iota-1})} \left\{ \begin{array}{l} \omega \left[\overline{K}_{\iota,\iota+1} \left(\frac{(\psi_{\iota+1} - \psi_\iota)}{\Delta x_{\iota,\iota+1}} - p_g \right) - \overline{K}_{\iota,\iota-1} \left(\frac{(\psi_\iota - \psi_{\iota-1})}{\Delta x_{\iota,\iota-1}} - p_g \right) \right]^j + \\ (1-\omega) \left[\overline{K}_{\iota,\iota+1} \left(\frac{(\psi_{\iota+1} - \psi_\iota)}{\Delta x_{\iota,\iota+1}} - p_g \right) - \overline{K}_{\iota,\iota-1} \left(\frac{(\psi_\iota - \psi_{\iota-1})}{\Delta x_{\iota,\iota-1}} - p_g \right) \right]^{j-1} \end{array} \right\} \quad (4.5)$$

where ι are individual points (or nodes) that represent a soil layer (conceptually at the center of the soil layer); p is the gravitational term (=1 for vertical infiltration); ω is a weighing factor (when ω = 1.0, the equation is fully implicit requiring an iterative solution, when ω=0.0, an explicit solution at time step j is allowed, dependent only on known values from the previous time step,$j-1$); $\overline{K}$ is the mean hydraulic conductivity of the soil layer; and Δx is the spatial distance between the specified nodes. Assuming vertical infiltration and ω=0.0 (explicit solution), Equation 4.5 reduces to:

$$\frac{\theta^j - \theta^{j-1}}{\Delta t} = \frac{-2}{(x_{\iota+1} - x_{\iota-1})} \left[\overline{K}_{\iota,\iota+1} \left(\frac{\psi_{\iota+1} - \psi_\iota}{\Delta x_{\iota,\iota+1}} - 1.0 \right) - \overline{K}_{\iota,\iota-1} \left(\frac{\psi_\iota - \psi_{\iota-1}}{\Delta x_{\iota,\iota-1}} - 1.0 \right)^{j-1} \right] \quad (4.6)$$

A complication with this formulation is that the left side of Equation 4.6 has the unknown value θ^j and the right side has unknown terms ψ at ι, $\iota-1$, and $\iota+1$. Using the Brooks-Corey [1964] relation, the pressure head, ψ can be found as a function of soil moisture, θ:

$$\psi(\theta) = \psi_b \cdot \theta_e^{-1.0/\lambda} \quad (4.7)$$

where ψ_b is the air entry tention, θ_e is the effective saturation, and λ is the pore size distribution coefficient. The effective saturation is determined using transitional Brooks and Corey (TB-C) relationship [*Smith*, 1990; *Smith et al.*, 1993]:

$$\theta_e = \left[1 + \left(\frac{\psi + \psi_a}{\psi_b} \right)^c \right]^{-\frac{\lambda}{c}} \quad (4.8)$$

Here, c is a curvature parameter and ψ_a is a small shift parameter to approximate the hysteresis. Similarly, the unsaturated hydraulic conductivity of the soil can be found as a function of the pressure head,

$$K(\psi) = K_{sat} \cdot K_r \tag{4.9}$$

where K_{sat} and K_r are the saturated and relative hydraulic conductivities of the soil, respectively. The relative hydraulic conductivity is defined as:

$$K_r \equiv \frac{K}{K_s} = \left(\frac{\psi}{\psi_b}\right) \tag{4.10}$$

Combining Equations 4.8 and 4.10 results in,

$$K_r(\psi) = \left[1 + \left(\frac{\psi + \psi_a}{\psi_b}\right)^c\right]^{-\frac{\eta}{c}} \tag{4.11}$$

where η, the conductivity exponent parameter, is related to λ, the pore-size distribution parameter.

$$\eta = 2.0 + (3.0 \cdot \lambda) \tag{4.12}$$

Typical values of λ for a number of soils are listed in Table 4.1. Given the established relationships between soil moisture, pressure head, and hydraulic conductivity, the kinematic wave approximation can be used to determine the rate of the moisture wave front through the vadose zone.

$$u_s(\theta_u, \theta_l) = \frac{K(\theta_u) - K(\theta_l)}{\theta_u - \theta_l} \tag{4.13}$$

where u_s is the kinematic shock velocity and the subscripts u and l indicate the upper and lower boundaries of the soil layer.

Green-Ampt, Single Event. The Green-Ampt equation [*Green and Ampt*, 1911] was the first physically-based attempt to simulate the infiltration process. Based upon Darcy's Law and the principle of conservation of mass, the Green-Ampt model assumes idealized conditions - a single homogeneous soil layer of infinite depth, a horizontal surface, constant

Table 4.1: Representative values of parameters used in the finite difference solution of the Richards equation and Green-Ampt equation for a variety of soils. Values of porosity, saturated hydraulic conductivity, air entry tension, and pore size distribution indexes are shown. Values in parentheses are standard deviations. Table modified from *Dingman* [2002] and *Williams et al.* [1998]. Data from *Clapp and Hornberger* [1978]; *Brakensiek et al.* [1981]; *Panian* [1987]; *Carsel and Parrish* [1988].

Soil Texture	Porosity	K_{sat} $[m/s]$	$\lvert\psi_b\rvert$ $[cm]$	b	λ
Sand	0.395 (0.056)	1.76E-4	12.1 (14.3)	4.05 (1.78)	0.4 - 1.68
Loamy Sand	0.410 (0.068)	1.56E-4	9.0 (12.4)	4.38 (1.47)	0.46 -1.28
Sandy Loam	0.435 (0.086)	3.47E-5	21.8 (31.0)	4.90 (1.75)	0.40 - 0.89
Silt Loam	0.485 (0.059)	7.20E-6	78.6 (51.2)	5.30 (1.96)	0.22 - 0.42
Loam	0.451 (0.078)	6.95E-6	47.8 (51.2)	5.39 (1.87)	0.26 -0.56
Sandy clay loam	0.420 (0.059)	6.30E-6	29.9 (37.8)	7.12 (2.43)	0.37 - 0.48
Silty clay loam	0.477 (0.057)	1.70E-6	35.6 (37.8)	7.75 (2.77)	0.18 - 0.36
Clay loam	0.476 (0.053)	2.45E-6	63.0 (51.0)	8.52 (3.44)	0.28 -0.4
Sandy clay	0.426 (0.057)	2.17E-6	15.3 (17.3)	10.4 (1.64)	–
Silty clay	0.492 (0.064)	1.03E-6	49.0 (62.1)	10.4 (4.45)	0.09 - 0.38
Clay	0.482 (0.050)	1.28E-6	40.5 (39.7)	11.4 (3.70)	0.09 - 0.41

K_{sat}: Saturated hydraulic conductivity; ψ_b: Air entry tension; b: Pore size distribution index
λ: Brooks-Corey pore size distribution coefficient.

surface ponding depth, uniform antecedent soil moisture content, and no that evapotranspiration occurs during the rain event. The Green-Ampt method assumes a piston-type water content profile, meaning the soil profile is assumed saturated down to the wetting front, where it abruptly drops to the antecedent moisture conditions. As the model formulation assumes a sharp wetting front, the actual distribution of soil moisture cannot be realistically simulated [*Ravi and Williams*, 1998]. The TopoFlow formulation of the Green-Ampt equation is only valid for simulations of a single precipitation event. The infiltration rate using the Green-Ampt equation is as follows:

$$IN = \frac{(K_{sat} - K_i) \cdot (G \cdot (\theta_s - \theta_i) + I')}{I'} + K_i \tag{4.14}$$

where K_{sat} and K_i are the saturated and initial hydraulic conductivities of the soil, $[m/s]$; and θ_s and θ_i are the saturated and initial soil moisture content, [*unitless*].

Rawls et al. [1992] estimated the capillary drive parameter, G, as:

$$G = \frac{2 \cdot b + 3}{2 \cdot b + 6} \cdot \psi_b \tag{4.15}$$

where b is the pore size distribution index, [*unitless*], and ψ_b is the air entry tension, $[m]$. Estimates of b and ψ_b for different soil types are listed in Table 4.1.

The incremented infiltration depth, I' $[m]$, is defined as:

$$I' = I - K_i t \tag{4.16}$$

where I is the cumulative infiltration depth, $[m]$, and t is time, [*sec*].

$$I = \frac{(K_s - K_i) \cdot (\theta_s - \theta_i) \cdot G}{IN} \tag{4.17}$$

Smith-Parlange 3-parameter infiltration. Based upon Darcy's Law and conservation of mass principle, a two-branch model for ponding time and infiltration is based on two extreme and opposite assumptions regarding the behavior of the unsaturated hydraulic conductivity near saturation. The first assumption is that unsaturated hydraulic conductivity varies slowly near saturation. The second assumption is the unsaturated hydraulic conductivity varies exponentially near saturation and includes an estimate of ponding time

[*Smith and Parlange*, 1978]. As with the Green-Ampt formulation, a number of simplifying assumptions are made - uniform, homogeneous soil of infinite depth, horizontal surface, and a uniform antecedent soil moisture profile. The TopoFlow formulation of the Smith-Parlange infiltration model describes the total infiltrated depth of the soil profile, but does not provide the actual soil moisture distribution. Like the Green-Ampt formulation, the Smith-Parlange 3-parameter infiltration model is valid only for simulating the infiltration of a single precipitation event. The Smith-Parlange 3-parameter [*Smith and Parlange*, 1978] infiltration model is:

$$IN = K_s + \frac{\zeta \cdot (K_s - K_i)}{exp\left(\frac{\zeta \cdot I'}{G \cdot (\theta_s - \theta_i)}\right)} \tag{4.18}$$

where ζ is a weighting factor, ranging between 0 - 1. The ζ-value of most soils ranges between 0.8 and 0.85 [*Smith*, 2002].

Instantaneous Infiltration. In the Arctic, ice-rich permafrost restricts hydrologic processes to the shallow depth of the active layer. Near surface arctic organic soils are typically very porous and have a large hydraulic conductivity, readily absorbing and releasing snowmelt and summer precipitation waters. Underlying these organic soils, a lower conductivity mineral soil is present. The vertical flow rate of snowmelt or rain water to reach the near surface groundwater table is significantly faster than the lateral flow through the mineral soils [*Zhang et al.*, 2000]. As a result the assumption is made that in the area of continuous permafrost, surface waters (derived from either snowmelt or rainfall) instantaneously percolate to the near-surface supra-permafrost water table upon reaching the ground surface. In using this method of infiltration, overland flow only occurs once the groundwater table rises above the surface elevation. The formulation for this process is as follows:

$$IN = (SM + P) \tag{4.19}$$

where IN is the infiltration rate, $[m/s]$; SM is the snowmelt rate $[m/s]$; and P is the rainfall rate $[m/s]$.

Overland and channel flow

The integral form of the mass balance for surface flows can be written as:

$$\frac{\partial}{\partial t}\int_{\Omega}\rho_w R dA_c = \int_{\Omega}\rho_w dA_c - \int_{\partial\Omega}(\hat{n}\cdot\rho_w\langle\underline{v}\rangle d)d(wb) \tag{4.20}$$

where ρ_w is the density of water, A_c is the cross-sectional area, $\langle v\rangle$ denotes the vertically-averaged downstream velocity, d is the flow depth, wb is the characteristic channel width, and R is the effective rainrate. The effective rainrate is the net sum of all vertical hydrologic processes to an element:

$$R = (P+S)-(ET+I) \tag{4.21}$$

where, P, S, ET, and I are respectively, the precipitation (rain and liquid water), subsurface flow, evapotranspiration, and infiltration rates, $[m/s]$. Applying a discretized version of Equation 4.20 to element i in a TopoFlow flow grid (Figure 4.3c) yeilds the following results:

$$\frac{\Delta d(i,t)}{\Delta t}(\Delta x\Delta y) = R(i,t)(\Delta x\Delta y) + \sum_{k\in N} Q(k,t) - Q(i,t) \tag{4.22}$$

where Δx and Δy are the element dimensions, Δt is the time step, and N is the set of elements that have element i as their parent.

$$Q(i,t) = v(i,t)d(i,t)\Delta w(i) \tag{4.23}$$

is the discharge from element i to its "parent" element just downstream, v is the fluid velocity, and $\Delta w(i)$ is the "differential" width of flow away from element i, which may be approximated with Δx or Δy. Solving for Δd yields:

$$\Delta d(i,t) = \Delta t\left\{\left[\frac{\sum_{k\in N} Q(k,t) - Q(i,t)}{\Delta x\Delta y}\right] + R(i,t)\right\} \tag{4.24}$$

For a vertically-integrated hydrostatic flow, the momentum balance can be written:

$$\frac{\partial}{\partial t}\int_{\Omega}\rho_w\langle v\rangle d\, dA_c = \int_{\Omega} -\rho_w g d\nabla h dA_c + \int_{\Omega}\tau_b(1+\nabla b\cdot\nabla b)^{1/2}dA_c - \int_{\partial\Omega} d\langle v\rangle(\hat{n}\cdot\rho_w\langle v\rangle)d(wb) \quad (4.25)$$

where $\langle v\rangle$ is the vertically-integrated horizontal velocity, d is the depth, b is the height of the bed above an arbitrary datum, and $h = (d+b)$ is the free-surface height. The quantity τ_b is the horizontal component of the (total) shear stress of the bed, which include all of the momentum loss mechanisms in the problem, including skin friction due to grain roughness, and form (or pressure) drag due to bedforms, bars, and any other topographic elements. The factor $(1+\nabla b\cdot\nabla b)^{1/2}dA_c$ is the differential surface area of the bed, b, which can be appreciably greater than dA_c near the banks of the channel.

Applying a discretized (and channel-fitted) version of equation 4.25 to an element, i, in a TopoFlow flow grid, we get:

$$\left[\frac{\Delta v(i,t)}{\Delta t}d(i,t) + \frac{\Delta d(i,t)}{\Delta t}v(i,t)\right](\Delta x\Delta y) = \sum_{k\in N} v(k,t)Q(k,t) - v(i,t)Q(i,t) + gd(i,t)S_{FS}(i,t)(\Delta x\Delta y) - f(i,t)v^2(i,t)(\Delta x\Delta y) \quad (4.26)$$

where $S_{FS}(i,t)$ is strictly the free-surface slope between element i and its parent element. The drag coefficient, f, is given by:

$$f = \left[\frac{\kappa}{\ln(\varpi d/z_0)}\right]^2 \quad (4.27)$$

where z_0 is the roughness parameter, $(z_0/\varpi d)$ is the relative roughness, $\kappa \approx 0.408$ is von Karman's constant, and ϖ is an integration constant equal to 0.476.

Solving Equation 4.26 for $\Delta v(i,t)$ we get:

$$\Delta v(i,t) = -\left[\frac{v(i,t)}{d(i,t)}\right] + \left(\frac{\Delta t}{d(i,t)}\right)\left\{\left[\frac{\sum_{k\in N} v(k,t)Q(k,t) - v(i,t)Q(i,t)}{\Delta x \Delta y}\right] + gd(i,t)S(i,t) - f(i,t)v^2(i,t)\right\} \quad (4.28)$$

Substituting $\Delta d(i,t)$ from Equation 4.24, Equation 4.28 simplifies to:

$$\Delta v(i,t) = \left(\frac{\Delta t}{d(i,t)}\right)\left\{\frac{\sum_{k\in N}[v(k,t) - v(i,t)]Q(k,t)}{\Delta x \Delta y}\right\} + \left(\frac{\Delta t}{d(i,t)}\right)[-R(i,t)v(i,t) + gd(i,t)S_{FS}(i,t) - f(i,t)v^2(i,t)] \quad (4.29)$$

Using Equation 4.23, $Q(i,t)$ can be eliminated from Equations 4.24 and 4.29 resulting in the flow depth and downstream velocity change for each element in a time increment, Δt, as a function of the velocity and depth at time, t.

$$v(i,t+\Delta t) = v(i,t) + \Delta v(i,t) \quad (4.30)$$

$$d(i,t+\Delta t) = d(i,t) + \Delta d(i,t) \quad (4.31)$$

Given the flow depth, the kinematic wave solution is used to calculate both channel and overland flow when flow depth, d, in an element is positive. A positive flow depth occurs when either the water table exceeds the land surface elevation or when the infiltration capacity of the soils is exceeded by the precipitation rate. Using the kinematic wave assumption, the friction slope (S_f) and the bed slope (S_o) are equal. The Manning equation can then be used to express the relationship between flow and depth:

$$q = v \cdot A_c = \frac{A_c}{N} R_H^{2/3} \sqrt{S_f} \quad (4.32)$$

where q is the rate of lateral flow per unit length $[m^3/s/m]$; v is the fluid velocity, $[m/s]$; R_H =

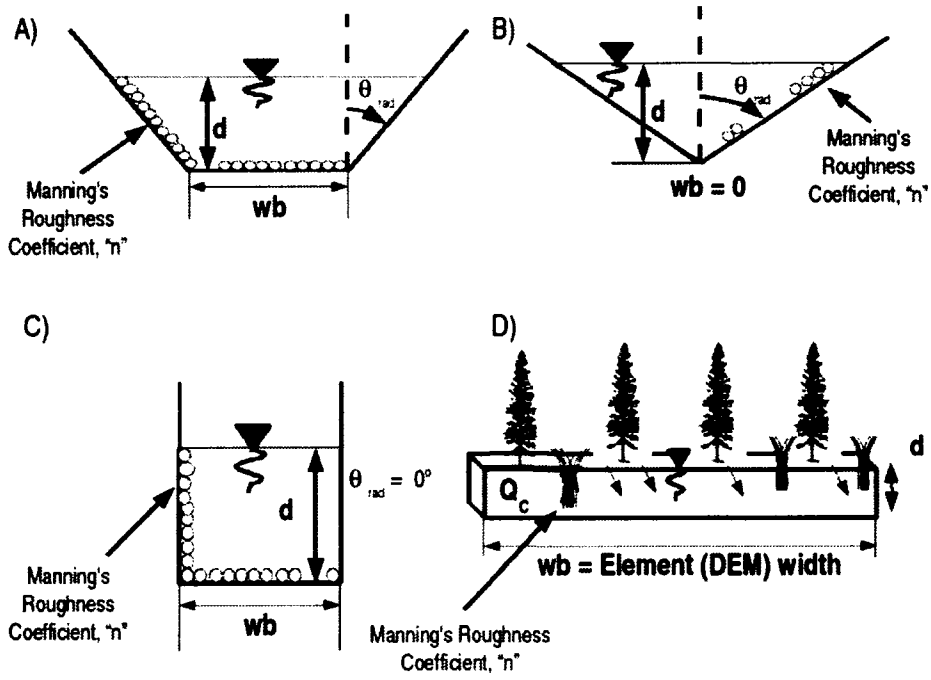

Figure 4.7. Overland and channel flow components.

A_c/PW is the hydraulic radius, $[m]$; PW is the wetted perimeter, $[m]$; N is the Manning's roughness coefficient, [unitless]; and A_c is the cross-section area, $wb \cdot d$, $[m^2]$.

A characteristic channel width (wb), bank angle (θ_{rad}), and Manning's roughness coefficient (n) are assigned for each Horton-Strahler Order number (or rank) number (see Section 4.2.2). A characteristic channel cross-section is defined for each stream segment having a specific order number. A channel cross section can be defined as a trapezoid, a triangle, or a rectangle (Figures 4.7a-c). We further assume that overland flow occurs as a sheet flow. Using this assumption, $R_H \approx d$. For elements in which overland flow will occur (i.e. lower-order Horton-Strahler elements which have been 'pruned' from the channel network tree), the characteristic channel width is set to the width of the element (the DEM dimension) (Figure 4.7d).

4.2.4 Model performance

A process simulation analysis was conducted to compare the model performance characteristics when the process time interval, process methods, and input data types are varied. The analysis was performed on a 64-bit Linux work station equipped with an Advanced Micro Devices (AMD) Opteron 250 CPU and 2 gigabytes RAM. The model domain used in this analysis has dimensions of 29 columns by 38 rows by 3 soil layers. For each test, the following processes were simulated: overland/channel flow, snowmelt, evapotranspiration, infiltration, soil moisture content (derived from soil characteristic curves, see Section 4.2.5), and groundwater flow.

Results from process time interval test are shown in Figure 4.8a. The time interval used in Test 1 are user specified for every process. For overland/channel flow, the time interval is 20 seconds (the model time step). The time step used for the snow melt, evapotranspiration, infiltration, and soil moisture content processes is 60 minutes. Finally, the time step for the ground water flow process is set at 24 hours. For Test 2, a 20 second time step is used for each process. In order to maintain numerical stability, the model time step is limited by the Courant condition. Results from this comparison display the advantage of an independent time step for each hydrologic process simulated. Comparison of the total simulation time between Test 1 and 2 show that utilization of process specific time steps results in approximately a factor of 9 reduction in computational time. The computational efficiency of process specific time steps would be higher for either a longer simulation period or a larger model domain.

The effect of method complexity of model performance was tested varying the snowmelt and evapotranspiration processes (Figure 4.8b). In Test 2 the relatively complex Energy Balance method of snowmelt and evapotranspiration were simulated. In Tests 3 the relatively less complex methods of Degree-day method for snowmelt and the Priestley-Taylor method for evapotranspiration were simulated. Comparison of Tests 2 and 3 demonstrate the complexity of the process simulated is proportional to computational time. This is particularly evident when comparing the simulation time for the snow melt process. The computational difference between the Energy Balance (Test 2), requiring seven function calls, and the Degree-Day (Test 3), requiring a single function call, snow melt methods is approximately 72%.

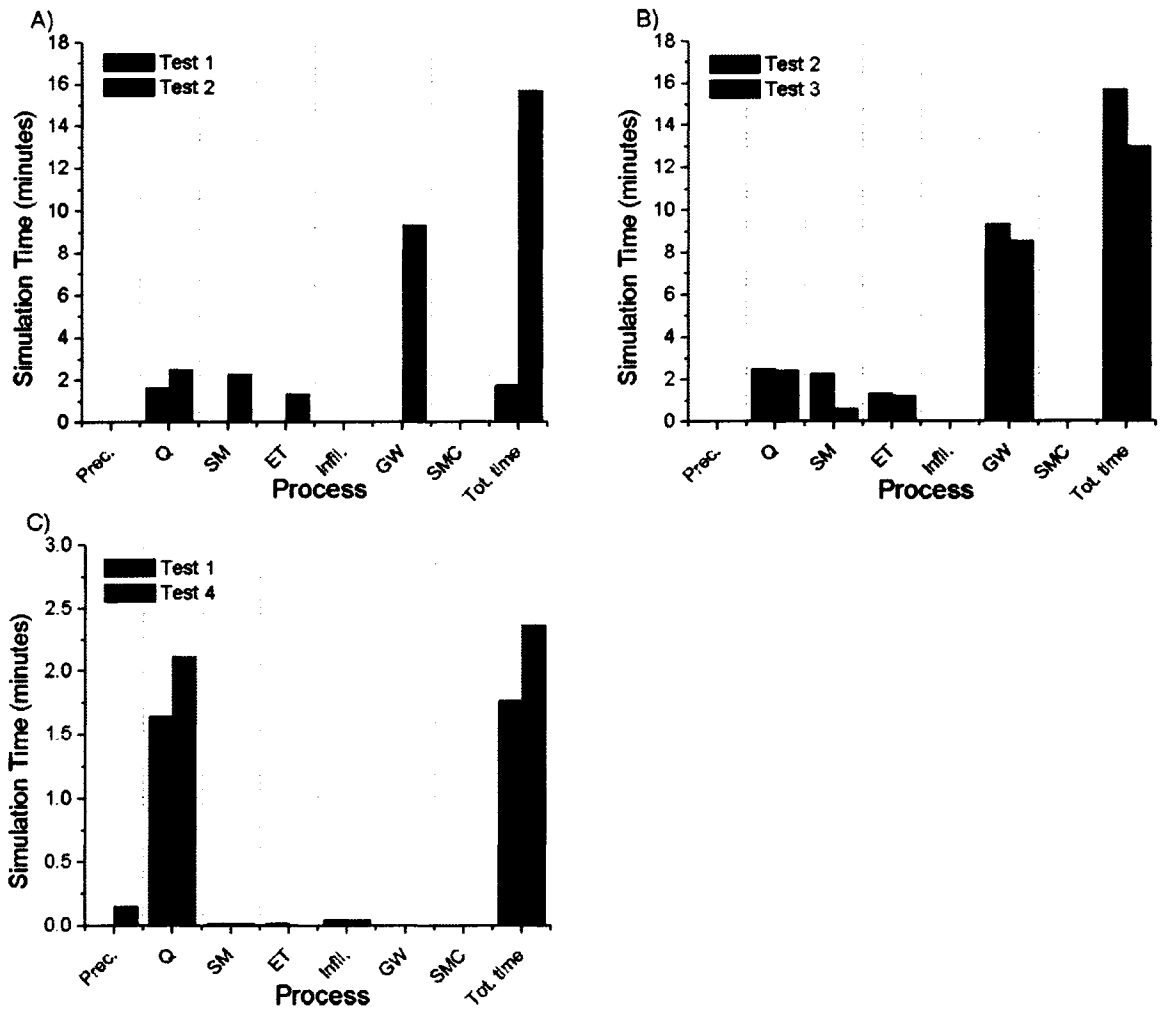

Figure 4.8: TopoFlow performance analysis. A) Comparison of process time interval. B) Comparison of process complexity. C) Comparison of input data type. Note: Prec.: Precipitation; Q: Channel/Overland flow; SM: Snow melt; Infil.: Infiltration; GW: Ground water flow; SMC: Soil moisture content; Tot. Time: Cumulative time for process simulation.

The model performance using different types of input data was explored (Figure 4.8c). In Tests 1, data input consisted of grid sequences – binary files that vary in both time and space. For Test 4, input data consisted of time series files – ASCII files that are only temporally variable. Uniform soil properties are used for the groundwater flow process, with values read from an input table. The format of the input data results in a slight difference in the total computational time, with the time series data format (Test 4), slightly higher than the grid sequence format. The difference in computational time is most dramatic in the precipitation and stream flow processes. The input variables used in the stream flow process are identical for Tests 1 and 4, meaning the format of the precipitation data has a direct impact on the computational efficiency on the stream flow process. This is in part due to the fact that variable precipitation durations are allowed in the time series input method. In using this method, a precipitation function call occurs at each model time step to check for changes in the precipitation rate. Conversion of ASCII data to binary format and spatial distribution of point data may also account for a lower computational efficiency.

4.2.5 Model output

For each simulation, TopoFlow is able to output a number of parameters calculated during the simulation. TopoFlow has two types of output. The first type of output is a time series at a specified element(s). The second is spatially distributed values for each element within the model domain. The time interval for both types of output is user specified for each hydrologic process. Table 4.2 shows the calculations available for output.

Soil moisture content from soil moisture characteristic curves

The volumetric soil moisture content may be obtained from the position of the water table and a soil moisture characteristic curve for each soil layer. A first-order exponential decay equation (with the form $Y = y0 + A1 \cdot \exp(-X/t1)$, is used to fit the soil moisture characteristic curve data (Figure 4.9). For each soil layer, the coefficients $y0$, $A1$, and $t1$, are input into TopoFlow. The soil moisture content is calculated, at the specified time interval, based on the distance between the top of each soil layer and the position of either the near-surface

Table 4.2. TopoFlow calculations available for output.

Hydrologic Process	Output Available
Snowmelt	Snowdepth
	Snow water equivalent
	Snowmelt rate
Evapotranspiration	Evapotranspiration rate
Infiltration	Infiltration rate
	Total infiltrated depth
Subsurface flow	Water table elevation
	Volumetric soil moisture content
Surface flow	Discharge
	Flow velocity
	Flow depth
	Drag coefficient

water table in permafrost regions or the deeper groundwater table in the non-permafrost upland areas. In order to reduce the computational time, the soil moisture content is only calculated for soil layers which output is specified.

Near surface soil moisture dynamics for rapid wetting and drying events are not captured using this method. However, this appears to be a viable and efficient method of determining the long-term moisture content of deeper soil layers or in areas of continuous permafrost, as the water table typically is located at or near the land surface.

TopoFlow output tools

TopoFlow has two post-processing tools that provide immediate graphical feedback of simulation output files. The first tool displays the time series output from a single specified element. The upper panel of Figure 4.10 shows an example of this tool. The second tool displays, in animation form, spatially distributed output for the entire model domain. The lower series of images in Figure 4.10 display example screenshots from a grid sequence of an output file for water velocity. The color scheme of the animation tool is defined such that low output values correspond to 'cool' or darker colors, while high output values correspond to 'hot' lighter colors. Particle tracking is also possible as red pixels are randomly placed in the animation track the position throughout the duration of the animation. The

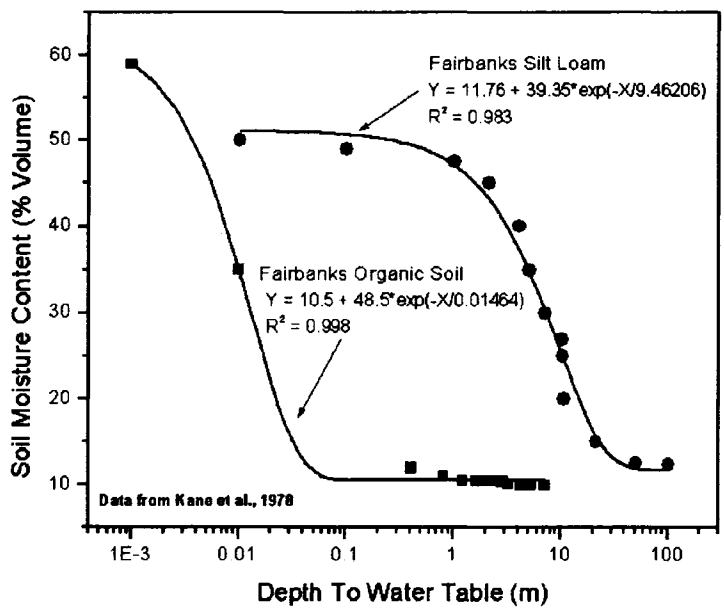

Figure 4.9: Soil moisture characteristic curves for Fairbanks Organic Soil and Fairbanks Silt Loam. A first-order exponential decay equation (with the form $Y = y0 + A1exp(-X/t1)$)) is used to fit the soil moisture characteristic curve data. Soil data from *Kane et al.* [1978].

particle tracking feature is most useful for output variables where lateral exchange of water from element to element take place (overland/channel flow volume, overland/channel velocity, groundwater flow, etc.) The TopoFlow dialog box provides additional information including the largest and smallest values displayed in the animation. With these tools, rapid visualization and analysis of simulation results is possible without the use of external programs.

4.3 Model discussion and conclusions

The sub-Arctic ecosystem represents an important transitional region between the temperate and arctic environments. Many of the observed and predicted changes in the arctic hydrologic system will occur in this region first, as the permafrost conditions are very warm and unstable. Soil moisture is an important variable in most hydrologic and thermal processes in the (sub-)Arctic including permafrost distribution, stream flow, carbon flux, and energy balance processes. Soil moisture is also the common link between the terrestrial and atmospheric systems. In this environment, accurate prediction of the soil moisture and streamflow regimes, at the watershed scale, is essential in developing a more complete understanding of local and regional scale climatic processes.

In every environment, accurate prediction of hydrologic processes requires addressing a number of challenges distinct to the system. The sub-arctic environment is no exception. In this paper, a number of challenges to hydrologic modeling in the sub-arctic environment are identified. They include the discontinuous distribution of permafrost resulting in an environment where the hydraulic conductivity and storage capacity of the soil can vary greatly over short distances and short and long time scales. Additional challenges include multiple, distinct groundwater systems, hydrologic processes which operate on different time scales, and a limited number of meteorologic data collection stations. The hydrologic model described in this paper, TopoFlow, is designed to address each of these challenges.

TopoFlow simulates the major components of water balance (precipitation, snowmelt, evapotranspiration, groundwater flow, and overland/channel flow) and some storage processes. Significant improvements in the model design and processes simulated have been made since the release of the ARHYTHM model. The overland/channel flow process has significantly improved by defining characteristic channel properties by order number and

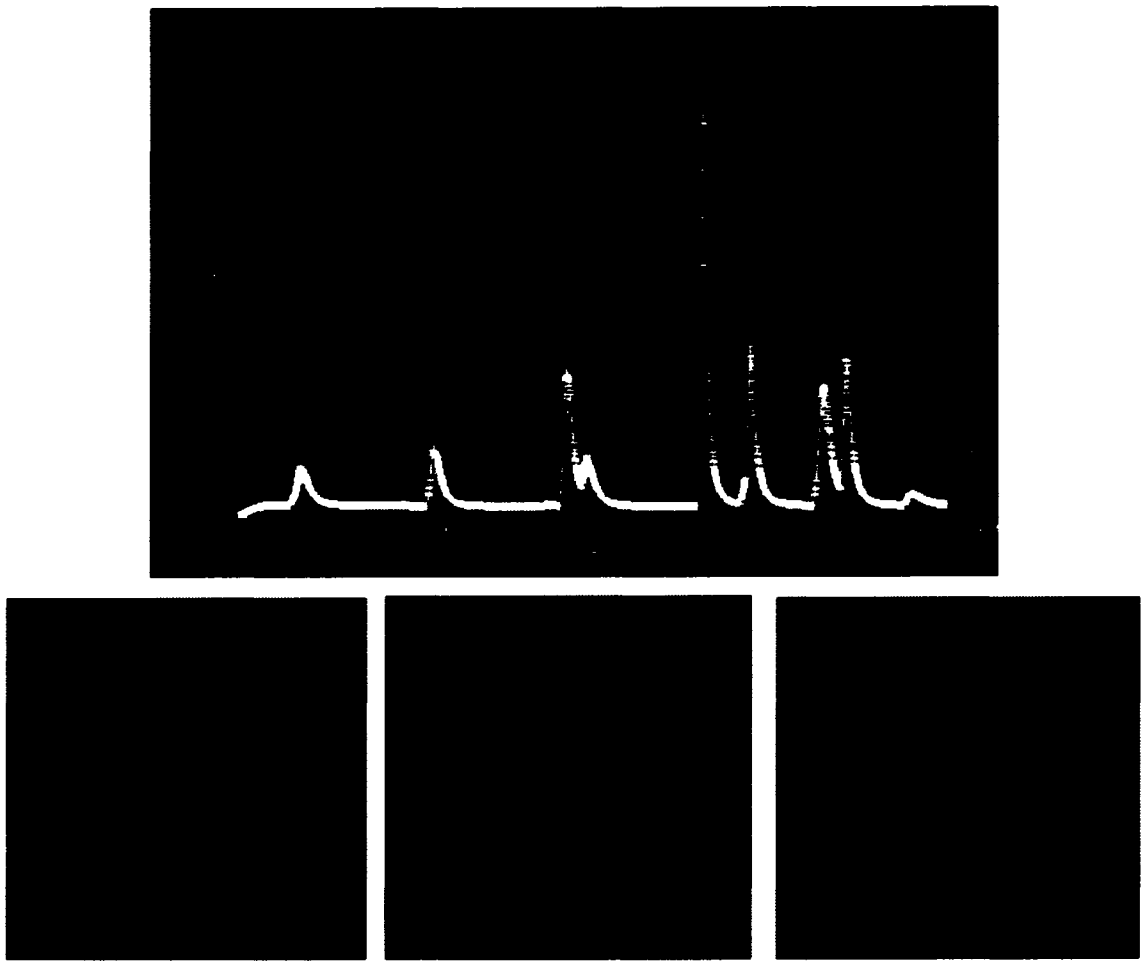

Figure 4.10: TopoFlow output tools. TopoFlow has two tools providing immediate graphical feedback of simulation output files. The upper panel shows an example, in this case discharge, of simulated output from a single specified element at a specified interval. The lower series of images are screen captures from an TopoFlow animation tool which displays spatially distributed output. The animation utility displays 'high' values with 'warm' light colors and 'low' values with 'cold' darker colors. Particle tracking is also possible with red pixels that are randomly placed in the animation. The TopoFlow dialog box provides additional information including the range of values displayed throughout the animation.

incorporating a robust flow routing mechanism.

The performance of TopoFlow is dependent upon a number of factors such as the size of the model domain and duration of the simulation period. Additional factors include method complexity, process time-step, and format of the input data. The complexity of the hydrologic method simulated is proportional to the simulation time. As the time-step used by TopoFlow is limited by the Courant condition, it is important that for each hydrologic processes simulated, an appropriate time-step is used. The availability of meteorologic data may or may not warrant creating spatial and temporal input data sets. However, the computational efficiency of TopoFlow increases if grid sequence files are utilized. Creating grid sequence files is a simple task using the available pre-processing tools.

TopoFlow simulates the major components of water balance (precipitation, snowmelt, evapotranspiration, groundwater flow, and overland/channel flow) and some storage processes (snow accumulation and Richards Equation soil moisture). Significant improvements in the model design and processes simulated have been made since the release of the ARHYTHM model. The overland/channel flow process has significantly improved by defining characteristic channel properties by order number and incorporating a robust flow routing mechanism. Process specific time-steps and multiple data formats make possible a hydrologic model flexible enough to handle spatial and temporal created by the discontinuous permafrost condition.

A number of storage processes, important in the sub-arctic environment, are not currently incorporated into TopoFlow. Storage processes such as aufeis accumulation and melt, precipitation interception, and surface storage (lakes or ponds), have not been addressed. Future plans for TopoFlow development include enhancements to both the model structure and incorporation of additional hydrologic processes. The basic structure of TopoFlow will be examined and modified to allow simulations from a 'batch' file (multiple simulations completed using one instruction file) and to run on multiple computer processors (high performance computing platform). Additional hydrologic processes such as nutrient, contaminant, and sediment transport, landform evolution, and lake storage are also being planned for future releases of TopoFlow.

4.4 Acknowledgments

Support for this research was provided by the U.S. National Science Foundation Arctic System Science Program (OPP-0229705), the U.S. National Science Foundation Division of Environmental Biology under the Long Term Ecological Research Program (Grant number DEB-9211769), a fellowship from the Inland Northwest Research Alliance (U.S. Dept. of Energy contract DE-FG07-021D14277), and a grant from the Center of Global Change - University of Alaska Fairbanks.

The TopoFlow source code and executables may be downloaded from http:// instaar. colorado.edu/topoflow. TopoFlow maybe used for free but is subject to the GNU license agreement (found on the TopoFlow website). You are permitted to use, study or modify it for your own needs but you may not publish, sell or distribute it in any form without the written permission of the authors. You may not remove the copyright notices or use the TopoFlow name for another program. It you use results from TopoFlow for a publication, the authors would greatly appreciate an acknowledgment and a reprint. The purpose of freely sharing this source code is to encourage further developments and code sharing by a user community of hydrologists.

4.5 Appendix

Table 4.3. List of symbols used.

Symbol	Meaning	Unit
A_c	Cross sectional area of stream channel	m^2
a	Area draining through a point upslope	m^2
b	Pore size distribution index	
c	Curvature parameter	
C_o	Degree-day melt factor	$mm/^oCday$
C_p	Heat capacity of snow	J/kg^oC
C_{pa}	Specific heat of air	$J/kg/^oC$
D_e	Bulk exchange coefficient for vapor	m/s
D_h	Bulk exchange coefficient for heat	m/s
d	Channel flow depth	m
dx	Element width	m
ET	Evapotranspiration rate	m/s
e_a	Air vapor pressure	$mbar$
e_s	Surface vapor pressure	$mbar$
f	Drag coefficient	
G	Capillary drive parameter	m
GW	Ground water flow rate	m/s
g	Gravitational constant	m/s
h	Free surface height	m
h_{sn}	Snow depth	m
I	Cumulative infiltration depth	m
IN	Infiltration rate	m/s
i	Element in TopoFlow flow grid	
I'	Incremented infiltration depth	m
j	Reference time step	
K	Hydraulic conductivity	m/s
$\overline{K}$	Mean hydraulic conductivity	m/s
K_e	Eddy diffusivity for water vapor	m^2/s
K_h	Eddy diffusivity for heat	m^2/s
K_i	Initial hydraulic conductivity	m/s
K_r	Relative hydraulic conductivity	m/s
K_s	Thermal conductivity of soil	W/m^oC
K_{sat}	Saturated hydraulic conductivity	m/s
k	Reference to 'kid' element	
L_f	Latent heat of fusion	J/kg
L_v	Latent heat of vaporization	J/kg
l	Subscript to indicate lower boundary of soil layer	
M	Snow water equivalent	m
M_{ET}	Water loss through evapotranspiration	m

Continued on next page...

Table 4.3 - Continued

Symbol	Meaning	Unit
N	Set of elements that have element 'i' as their parent	
n	Manning roughness coefficient	
P	Rainfall rate	m/s
P_T	Precipitation (rain and/or snow) rate	m/s
PW	Wetted perimeter of channel	m
p	Atmospheric pressure	$mbar$
p_g	Gravitational coefficient	
Q_{CH}	Overland or stream flow	m^3/s
Q_a	Advective heat flux	W/m^2
Q_c	Conductive heat flux	W/m^2
Q_{cc}	Cold content of the snowpack	W/m^2
Q_{ET}	Energy utilized to evaporate water	W/m^2
Q_e	Latent heat flux	W/m^2
Q_h	Sensible heat flux	W/m^2
Q_m	Energy utilized to melt snow	W/m^2
Q_{net}	Net radiation	W/m^2
q	Rate of lateral flow per unit length	m^2/s
R	Effective rainrate	m/s
R_H	Hydraulic radius	m
R_i	Richardson number	
S	Number of time-steps per day	
Sh	Slope of the groundwater surface in an element	
SM	Snowmelt rate	m/s
s	Slope of the specific humidity and temperature curve	$^oC^{-1}$
S_f	Friction slope	
S_{FS}	Free-surface slope between elements	
S_o	Bed slope	
T	Average snow temperature	^oC
T_a	Air temperature	^oC
T_o	Temperature when snow reaches isothermal condition for melting	^oC
T_s	Surface temperature	^oC
T_sn	Snow temperature	^oC
T_x	Soil temperature at depth x	^oC
t	Time	sec
u	Subscript to indicate upper boundary of soil layer	
u_s	Kinematic shock velocity	m/s
$u_{1,2}$	Wind speed at height $z_{1,2}$	m/s
$\langle u \rangle$	Vertically-averaged downstream velocity	m/s
v	Fluid velocity	m/s

Continued on next page...

Table 4.3 - Continued

Symbol	Meaning	Unit
$vmax$	Estimated maximum velocity a particle of water can travel	m/s
$vmax_{chan}$	Maximum velocity of a particle of water travels within a channel segment	m/s
wb	Characteristic bed width	m
x	Vertical depth into soil	m
y	Saturated depth of an element	m
z	Vertical height above ground surface	m
z_o	Roughness parameter or length	m
α	Modified Priestley-Taylor coefficient	
β	Local slope angle	*radians*
η	Conductivity exponent parameter	
$\Delta Storage$	Change in water storage (all forms)	m^3
Δt	Model time step	*sec*
$\Delta w(i)$	'Differential' width of flow away from an element	m
Δx	Spatial distance between nodes	m
Δx	Element dimension in x-direction	m
Δy	Element dimension in y-direction	m
Δx	Spatial distance between nodes	m
γ	Psychrometric constant in terms of specific humidity	$^oC^{-1}$
ι	Reference location used in Richard Equation	
κ	von Karmon's constant	0.408
λ	Pore-size distribution coefficient	
μ	Kinematic velocity of soil moisture wave	m/s
ω	Weighting factor	
ϖ	Integration constant	0.476
ψ	Soil water capillary head	m
ψ_a	Small shift parameter used to approximate hysteresis	m
ψ_b	Air entry or 'bubbling' tension	m
ρ_a	Density of air	kg/m^3
ρ_s	Density of snow	kg/m^3
ρ_w	Density of water	kg/m^3
τ_b	Shear stress of the channel bed	N/m^2
θ	Volumetric soil water content	
θ_e	Effective saturation	
θ_i	Initial soil moisture content	
θ_r	Retained soil moisture content	
θ_s	Saturated soil moisture content	
θ_{rad}	Characteristic channel bank angle	*degrees*
ξ	Weighting factor	
ζ	Weighting factor using in Smith-Parlange Infiltration	0.8 -0.85

Table 4.4: Simulated processes and formulation used in TopoFlow. A listing of the symbols used in this table are found in Table 4.3.

Process	Method	Formula	Equation
Snowmelt	Energy Balance	Energy Balance of the Snowpack	$Q_m = Q_{net} + Q_h + Q_e + Q_a + Q_c - Q_{cc}$
		Sensible Heat Flux	$Q_h = \rho_a \cdot C_{pa} \cdot K_h \cdot dT/dz$ $= \rho_a \cdot C_{pa} \cdot D_h \cdot (T_a - T_s)$
		Latent Heat Flux	$Q_e = \rho_a \cdot L_v \cdot K_e \cdot dq/dz$ $= \rho_a \cdot L_v \cdot D_e \cdot (0.622/p) \cdot (e_a - e_s)$
		Bulk Exchange Coefficient for Atmospheric Stability ($T_a = T_s$)	$D_n = \kappa^2(u_z)/[\ln((z-h)/z_0)]^2$
		Bulk Exchange Coefficient for Unstable Atmosphere ($T_a < T_s$)	$D_{(u)} = D_n/(1 + 10 \cdot R_i)$
		Richardson Number	$R_i = \frac{gz \cdot (T_a - T_s)}{u_z^2 \cdot (T_a + 273.15)}$
		Roughness Length	$z_0 = exp\left[\frac{u_2 \ln(z_1) - u_1 \ln(z_2)}{u_2 - u_1}\right]$
		Cold Content	$Q_{cc} = h_{sn} \cdot \rho_s \cdot C_p \cdot (T_0 - T_{sn})$
		Snowmelt rate	$M = (1000 \cdot Q_m)/(\rho_w \cdot L_f)$
	Degree-Day	Degree-Day Melt Rate	$M = C_0(T_a - T_0)/S$
Evapotranspiration	Energy Balance	Energy Balance ET	$Q_{ET} = Q_{net} + Q_h + Q_c$
		Conductive Heat Flux	$Q_c = K_s \cdot \frac{T_x - T_s}{x}$
		Evapotranspiration Rate	$M_{ET} = \frac{1000 \cdot Q_{ET}}{\rho_w \cdot L_v}$
	Priestley-Taylor Method	Priestley-Taylor equation	$Q_{ET} = \alpha \cdot \left(\frac{s}{s+\gamma}\right)(Q_{net} - Q_c)$
		Stewart & Rouse Approximation	$\frac{s}{s+\gamma} = 0.406 + 0.011 T_a$

Continued on next page...

Table 4.4 – Continued

Process	Method	Formula	Equation
Infiltration & Percolation	Richards Equation	Richards Infiltration Rate	$\frac{\partial\theta}{\partial t} = \frac{\partial}{\partial z}\left[K\frac{\partial\psi}{\partial z} - K\right]$
		Finite Difference Solution Richard Equation	$\frac{\theta^j-\theta^{j-1}}{\Delta t} = \frac{-2}{(z_{i+1}-z_{i-1})}\cdot \left[\overline{K}_{i,i+1}\left(\frac{\psi_{i+1}-\psi_i}{\Delta z_{i,i+1}} - 1.0\right) - \overline{K}_{i,i+1}\left(\frac{\psi_i-\psi_{i-1}}{\Delta z_{i,i-1}-1.0}\right)^{j-1}\right]$
		Brooks - Corey Relationship	$\psi(\theta) = \psi_b \cdot \theta_e^{1.0/\lambda}$
		Transitional Brooks-Corey Relationship	$\theta_e = \left[1 + \left(\frac{\psi+\psi_a}{\psi_b}\right)^c\right]^{-\frac{\lambda}{c}}$
		Unsaturated Hydraulic Conductivity	$K(\psi) = K_s \cdot K_r$
		Relative Hydraulic Conductivity	$K_r = \left[1 + \left(\frac{\psi+\psi_a}{\psi_b}\right)^c\right]^{-\frac{\eta}{c}}$
		Conductivity exponent Parameter	$\eta = 2.0 + (3.0 \cdot \lambda)$
		Wetting Front Velocity	$u_s(\theta_u, \theta_l) = \frac{K(\theta_u)-K(\theta_l)}{\theta_u-\theta_l}$
	Green-Ampt, Single Event	Green-Apmt Infiltration Rate	$IN = \frac{(K_s-K_i)(G\cdot(\theta_s-\theta_i)+I')}{I'} + K_i$
		Capillary Drive Parameter	$G = \frac{2\cdot b+3}{2\cdot b+6}\cdot\psi_b$

Continued on next page...

Table 4.4 – Continued

Process	Method	Formula	Equation
		Incremented Soil Moisture Depth	$I' = \frac{G \cdot (\theta_s - \theta_i) \cdot (K_s - K_i)}{IN - K_s}$
	Smith-Parlange 3-Parameter Infiltration	Smith-Parlange Infiltration Rate	$IN = K_s + \frac{\gamma \cdot (K_s - K - i)}{exp\left(\frac{\gamma \cdot I'}{G \cdot (\theta_s - \theta_i)}\right)}$
	Instantaneous Infiltration	Instantaneous Rate	$IN = (P + SM)$
Subsurface Flow	Darcy's Law	Darcy Flow	$Q = K \cdot Sh \cdot dw \cdot y$
		Total Darcy Flow	$Q_T = \sum_{i=1}^{n} (K_i \cdot Sh_i \cdot dw_i \cdot y_i)$
Overland & Channel Flow	Manning's Equation	Manning Formula	$Q_c = R^{2/3} \cdot A_c \cdot \sqrt{S}/N$
		Hyrdaulic Radius	$R_H = A_C/PW$
		Cross-Sectional Area	$A_C = d \cdot (wb + (d \cdot tan(\theta_{rad})))$
		Wetted Perimeter	$PW = wb + (2.0 \cdot d/cos(\theta_{rad})$

References

Abbott, M., J. Bathurst, J. Counge, P. O'Connell, and J. Rasmussen (1986), An introduction to the European Hydrological System - Systéme Hydrologique Européen 'SHE', 2: Structure of the physically based, distributed modeling system., *Journal of Hydrology, 87*, 61–77.

ACIA (2005), *Impacts of a warming Arctic: Arctic Climate Impact Assessment*, 1046 pp., Cambridge University Press.

Alley, W., and P. Smith (1982), Distributed Routing Rainfall-Runoff Model - Version II, *Open File Report 82-344*, United States Geological Survey.

Anisimov, O., and F. E. Nelson (1997), Permafrost zonation and climate change: Results from transient general circulation models, *Climatic Change, 35*, 241–258.

Arnell, N. (2005), Implications of climate change for freshwater inflows to the Arctic Ocean, *Journal of Geophysical Research, 110*, D07105, doi:10.1029/2004JD005348.

Arnold, J., P. Allen, and G. Bernhardt (1993), A comprehensive surface-groundwater flow model, *Journal of Hydrology, 142*, 47–69.

Baldocchi, D., F. M. Kelliher, T. Black, and P. Jarvis (2000), Climate and vegetation controls on boreal zone energy exchange, *Global Change Biology, 6*(Supplement 1), 69–83.

Bevin, K., and J. Freer (2001), Dynamic TOPMODEL, *Hydrologic Processes, 15*(10), 1993–2011.

Bevin, K., and M. Kirkby (1979), A physically based variable contributing area model of catchment hydrology, *Hydrologic Science Bulletin, 24*, 43–69.

Bicknell, B., J. Imhoff, J. Kittle, A. Donigian, and R. Johanson (1997), Hydrological simulation program - Fortan, Users manual for Version 11, *Tech. Rep. EPA/600/R-97/090*, United States Environmental Protection Agency.

Bolton, W., L. Hinzman, and K. Yoshikawa (2000), Stream flow studies in a watershed underlain by discontinuous permafrost, in *Proceedings Water Resources in Extreme Environments*, edited by D. Kane, pp. 31–36.

Bolton, W., L. Hinzman, and K. Yoshikawa (2004), Water balance dynamics of three small catchments in a sub-arctic boreal forest, in *Northern Research Basins Water Balance (Proceedings of a workshop held at Victoria, Canada, March 2004)*, edited by D. L. Kane and D. Yang, IAHS Series of Proceedings and Reports Number 290, pp. 213 – 223.

Brakensiek, D., R. Engelman, and W. Rawls (1981), Variation within texture classes of soil water parameters, *Transaction of the American Society of Agricultural Engineers, 24*, 335–339.

Brooks, R., and A. Corey (1964), Hydraulic properties of porous media, *Hydrology Paper 3*, Civil Engineering Department, Colorado State University.

Callaghan, T., and S. Jonasson (1996), Arctic terrestrial ecosystems and environmental change, in *The Arctic and Environmental Change*, edited by P. Wadhams, J. Dowdeswell, and A. Schofield, pp. 59–76, Gordon and Breach.

Carsel, R., and R. Parrish (1988), Developing joint probability distributions of soil water retention characteristics, *Water Resources Research, 24*, 755–769.

Chapman, W., and J. Walsh (1993), Recent variations in sea ice and air temperature in high latitudes, *Bulletin American Meteorology Society, 74*, 33–47.

Clapp, R., and G. Hornberger (1978), Empirical equations for some soil hydraulic properties, *Water Resources Research, 14*, 601–604.

DHI (1998), MIKE-SHE water movement - User guide and technical reference, *Tech. Rep. 1.1*, Danish Hydraulic Institute.

Dickman, R. (2004), Fractal rain distributions and chaotic advection, *Brazilian Journal of Physics, 34*(2), 337–345, doi:10.1590/S0103-97332004000300002.

Dingman, S. (1973), Effects of permafrost on stream flow characteristics in the discontinuous permafrost zone of central Alaska., in *Permafrost: North American Contribution to the Second International Conference*, pp. 447–453, National Academy of Sciences, Washington D.C.

Dingman, S. L. (2002), *Physical Hydrology*, 2 ed., 646 pp., Prentice Hall, New Jersey.

Dingman, S. L., and F. R. Koutz (1974), Relations among vegetation, permafrost, and potential insolation in central Alaska, *Arctic and Alpine Research, 6*(1), 37–42.

Fox, J. D. (1976), A forest hydrology model of vegetation-streamflow relations, PhD Dissertation, 275 pp. University of Washington.

Fox, J. D. (1992), Incorporating freeze-thaw calculations into a water balance model, *Water Resources Research, 28*, 2229–2244.

French, N., E. Kasischke, J. Michalek, and L. Bourgeau-Chavez (1997), Monitoring the effects of fire on soil temperature and moisture in boreal forest ecosystems using satellite imagery, in *Proceedings of the International Symposium on Physics, Chemistry, and Ecology in Seasonally Frozen Soils*, edited by I. Iskandar, E. Wright, J. Radke, B. Sharratt, P. Groenevelt, and L. Hinzman, pp. 551–557, Fairbanks, Alaska.

Friborg, T., H. Soegaard, T. Christensen, C. Lloyd, and N. Panikov (2003), Siberian wetlands: Where a sink is a source, *Geophysical Research Letters, 30*(21), 2129.

Garbrecht, J., and L. Martz (1997), The assignment of drainage direction over flat surfaces in raster digital elevation models, *Journal of Hydrology, 193*, 204–213.

Goodrich, D., C. Unkrich, R. Smith, and D. Woolhiser (2000), KINEROSC - a distributed runoff and erosion model, in *Proceedings of the 2nd Federal Interagency Hydrologic Modeling Conference*, p. 14.

Grayson, R., and G. Blöschel (2000), *Spatial Patterns in Catchment Hydrology*, chap. Spatial Modelling of Catchment Dynamics, pp. 51–81, Cambridge University Press.

Green, W., and G. Ampt (1911), Studies on soil physics: 1. the flow of air and water through soils, *Journal of Agricultural Science, 4*, 1–24.

Haugen, R., C. Slaughter, K. Howe, and S. Dingman (1982), Hydrology and climatology of the Caribou-Poker Creeks Research Watershed, Alaska, *CRREL Report 82-26*, US Army Corps of Engineers Cold Regions Research and Engineering Laboratory.

Hinzman, L., D. Kane, and Z. Zhang (1995), A spatially distributed hydrologic model for arctic regions, in *International GEWEX Workshop on Cold-Season/Region Hydrometeorology. Summary Report and Proceedings*, no. 15 in Int. GEWEX Project Office Publication, pp. 236–239.

Hinzman, L., R. Johnson, D. Kane, A. Farris, and G. Light (2000), *Contaminant Hydrology: Cold Regions Modeling*, chap. Measurements and modeling of benzene transport in a discontinuous permafrost region, pp. 175–237, Lews Publishers.

Hinzman, L., W. Bolton, K. Petrone, J. Jones, and P. Adams (2006), Watershed hydrology and chemistry in Alaska's boreal forest: The central role of permafrost, in *Alaska's Changing Boreal Forest*, edited by F. C. III, M. Oswood, K. V. Cleve, L. Viereck, and D. Verbyla, Oxford University Press, Oxford.

Hinzman, L., N.D. Bettez, W.R. Bolton, F.S. Chapin, M.B. Dyurgerov, C.L. Fastie, B. Griffith, R.D. Hollister, A. Hope, H.P. Huntington, A.M. Jensen, G.J. Jia, T. Jorgenson, D.L. Kane, D.R. Klein, G. Kofinas, A.H. Lynch, A.H. Lloyd, A.D. McGuire, F.E. Nelson, W.C. Oechel, T.E. Osterkamp, C.H. Racine, V.E. Romanovsky, R.S. Stone, D.A. Stow, M. Sturm, C.E. Tweedie, G.L. Vourlitis, M.D. Walker, D.A. Walker, P.J. Webber, J.M. Welker, K.S. Winker, and K. Yoshikawa. (2005), Evidence and implications of recent climatic change in northern Alaska and other arctic regions, *Climatic Change*, *72*, 251–298.

Horton, R. (1945), Erosional development of streams and their drainage basins: hydrophysical approach to quantitative morphology, *Geologic Society of American Bulletin*, *56*, 275–370.

IPCC (2001), Climate change 2001: Synthesis report. Summary for policymakers., *Tech. rep.*, Intergovernmental Panel on Climate Change.

Jonch-Clausen, T. (1979), SHE, Systéme Hydrologique Européen, a short description, *Tech. rep.*, Danish Hydraulic Institute, Hørsholm, Denmark.

Jones, J., K. Petrone, J. Finlay, L. Hinzman, and W. Bolton (2005), Nitrogen loss from watersheds of interior Alaska underlain with discontinuous permafrost, *Geophysical Research Letters*, *32*(10.1029/2004GL021734), L02,401.

Jorgenson, M., C. Racine, J. Walters, and T. Osterkamp (2001), Permafrost degradation and ecological changes associated with a warming climate in central Alaska, *Climate Change, 48*, 551–571.

Julian, P., and B. Saghafian (1991), CASC2D: A two-dimensional watershed rainfall-runoff model, CASC2D user's manual, *Report CER90-91PYJ-BJ-12*, Colorado State University, Colorado State University, Fort Collins, Colorado.

Kane, D., and L. Hinzman (2004), Monitoring extreme environments: Arctic hydrology in transition, *Water Resources Impact, 6*(1), 24–27.

Kane, D., and J. Stein (1983a), Water movement into seasonally frozen soils, *Water Resources Research*, (6), 1547–1557.

Kane, D., and J. Stein (1983b), Field evidence of groundwater recharge in interior Alaska, in *Proceedings of the Fourth International Conference on Permafrost*, pp. 572–577, National Academy Press.

Kane, D. L., and D. Yang (2004), Overview of water balance determinations for high latitude watersheds, in *Northern Research Basins Water Balance*, edited by D. L. Kane and D. Yang, 290, pp. 1–12, International Association of Hydrologic Sciences.

Kane, D. L., R. D. Seifert, and G. S. Taylor (1978), Hydrologic properties of subarctic organic soils, *Tech. Rep. IWR-88*, Institute of Water Resources, University of Alaska Fairbanks.

Kane, D. L., L. D. Hinzman, C. .S. Benson, and K. R. Everett (1989), Hydrology of Imnavait Creek, an arctic watershed, *Holarctic Ecology, 12*, 262–269.

Kite, G. (1978), Development of a hydrologic model for a Canadian watershed, *Canadian Journal of Civil Engineering, 5*, 126–134.

Kite, G. (1989), Hydrologic modelling with remotely sensed data, in *Proceedings of the 5th Annual Western Snow Conference*, pp. 1–8, Fort Collins, Colorado.

Leavesley, G., R. Lichty, B. Troutman, and L. Saindon (1983), Precipitation-runoff modeling system, *Water Resources Investigations Report 83-4238*, United States Geological Survey.

Liang, X., D. Lettenmair, E. Wood, and S. Burges (1994), A simple hydrologically based model of land surface water, energy, fluxes for general circulation models, *Journal of Geophysical Research, 99*(D7), 14,415–14,428.

Magnuson, J., D. Robertson, B. Benson, R. Wynne, D. Livingstone, T. Arai, R. Assel, R. Barry, V. Card, E. Kuusisto, N. Granin, T Prowse, K. Steward, and V. Vuglinski. (2000), Historical trends in lake and river ice cover in the northern hemisphere, *Science, 289*, 1743–1746.

McGuire, A., J. Melillo, D. Kicklighter, and L. Joyce (1995), Equilibrium responses of soil carbon to climate change: Empirical and process-based estimates, *Journal of Biogeography, 22*, 785–796.

Moore, I., R. Grayson, and A. Ladson (1993), Digital terrain modelling: A review of hydrological, geomorphological, and biological applications, in *Terrain Analysis and Distributed Modelling in Hydrology*, edited by K. Beven and I. Moore, pp. 7–34.

Moore, T., N. Roulet, and J. Waddington (1998), Uncertainty in predicting the effect of climatic change on the carbon cycling of Canadian peatlands, *Climatic Change, 40*, 229–245.

O'Callaghan, J., and D. Mark (1984), The extraction of drainage networks from digital elevation data, *Computer Vision, Graphics, and Image Processing, 28*(3), 323–344.

Osterkamp, T. (2003), A thermal history of permafrost in Alaska, in *Proceedings of the Eighth International Conference on Permafrost, 21-25 July 2003*, pp. 863–868, Balkema Publishers.

Osterkamp, T., and V. Romanovsky (1999), Evidence for warming and thawing of discontinuous permafrost in Alaska, *Permafrost and Periglacial Processes, 10*, 17–37.

Osterkamp, T., L. Viereck, Y. Shur, M. Jorgenson, C. Racine, A. Doyle, and R. Boone (2000), Observations of thermokarst and its impact on boreal forests in Alaska, USA, *Arctic, Antarctic and Alpine Research, 32*, 303 – 315.

Panian, T. (1987), Unsaturated flow properties data catalog, volume ii, *DOE/NV/10384-20 45061*, Water Resources Center, Desert Research Institute.

Peckham, S. D. (1995), New results for self-similar trees with applications to river networks, *Water Resources Research*, *31*(4), 1023–1029.

Peterson, B., R. Holmes, J. McClelland, C. Vörösmarty, R. Lammers, A. Shiklomanov, I. Skiklomanov, and S. Rahmstort (2002), Increasing river discharge to the Arctic Ocean, *Science*, *298*, 2171–2173.

Quinton, W.L. and P. Marsh (1999), A conceptual framework for runoff generation in a permafrost environment, *Hydrologic Processes*, *13*, 2563–2581.

Ravi, V., and J. R. Williams (1998), Estimation of infiltration rate in the vadose zone: *Tech. Rep. EPA/600/R-97/128a*, U.S. Environmental Protection Agency.

Rawls, W., L. Ahuja, D. Brakensiek, and A. Shirmohammadi (1992), Infiltration and soil water movement, in *Handbook of Hydrology*, edited by D. Maidment, McGraw-Hill, New York.

Richards, L. (1931), Capillary conduction of liquids through porous media, *Physics*, *1*, 316–333.

Romanovsky, V., M. Burgess, S. Smith, K. Yoshikawa, and J. Brown (2002), Permafrost temperature records: Indicators of climate change, *EOS Transactions of the American Geophysical Union*, *83*(50), 589–594.

Roulet, N.T. and M.-K. Woo (1988), Runoff generation in a low arctic drainage basin, *Journal of Hydrology*, *101*, 213–226.

Serreze, M., D. Bromwich, M. Clark, A. Etringer, T. Zhang, and R. Lammers (2002), Large-scale hydro-climatology of the terrestrial arctic drainage system, *Journal Geophysical Research*, *108*(D2), D01,108.

Serreze, M., J. Walsh, F. Chapin, T. Osterkamp, M. Dyurgerov, V. Romanovsky, W. Oechel, J. Morison, T. Zhang, and R. Barry (2000), Observational evidence of recent change in the northern high latitude environment, *Climatic Change*, *46*, 159–207.

Shiklomanov, A., R. Lammers, and C. Vörösmarty (2002), Widespread decline in hydrological monitoring threatens pan-arctic research, *EOS, Transactions, American Geophysical Union*, *83*(2), 13–17.

Slaughter, C., and D. Kane (1979), Hydrologic role of shallow organic soils in cold climates, in *Canadian Hydrology Symposium: Proceedings, 79-Cold Climate Hydrology*, pp. 380–389.

Slaughter, C., J. Hilgert, and E. Culp (1983), Summer streamflow and sediment yield from discontinuous-permafrost headwater catchments, in *Proceedings of the Fourth International Permafrost Conference*, pp. 1172–1177, National Academy Press.

Smith, L., Y. Sheng, G. MacDonald, and L. Hinzman (2005), Disappearing arctic lakes, *Science*, *308*, 1429.

Smith, R. (1990), Analysis of infiltration through a two-layer soil profile, *Soil Science Society*, *54*(5), 1219–1227.

Smith, R., and J.-Y. Parlange (1978), A parameter-efficient hydrologic infiltration model, *Water Resources Research*, *14*(3), 533–538.

Smith, R., C. Corradini, and F. Melone (1993), Modeling infiltration for multistorm runoff events, *Water Resources Research*, *29*(1), 133–144.

Smith, R. E. (2002), *Infiltration Theory for Hydrologic Applications*, Water Resources Monograph 15, American Geophysical Union.

Strahler, A. (1957), Quantitative analysis of watershed geomorphology, *American Geophysical Union Transactions*, *38*(6), 913–920.

Vörösmarty, C., W. Gutowski, M. Person, T.-C. Chen, and D. Case (1993), Linked atmosphere-hydrology models at the macroscale, in *Macroscale Modeling of the Hydrosphere*, edited by W. Wilkinson, no. 214 in International Association of Hydrological Sciences, pp. 3–27.

Walsh, J. E., O. Anisimov, J.O.M. Hagen, T. Jakobsson, J. Oerlemans, T.D. Prowse, V. Romanovsky, N. Savelieva, M. Serreze, A. Shiklomanov, I. Shiklomanov, S. Solomon, A. Arendt, D. Atkinson, M.N. Demuth, J. Dowdeswell, M. Dyurerov, A. Glazovsky, R.M. Koerner, M. Meier, N. Reeh, O. Sigurosson, K. Steffen, and M. Truffer (2005), Cryosphere and hydrology, in *Arctic Climate Impact Assessment*, edited by C. Symon, L. Arris, and B. Heal, chap. 6, pp. 184–242, Cambridge University Press.

Walter, M. T., T. S. Steenhuis, V. K. Mehta, D. Thongs, M. Zion, and E. Schneiderman (2002), Refined conceptualization of TOPMODEL for shallow subsurface flows, *Hydrological Processes, 16*, 2041–2045.

Wigmosta, M. S., L. W. Vail, and D. Lettenmair (1994), A distributed hydrology - vegetation model for complex terrain, *Water Resources Research, 30*(6), 1665–1679.

Williams, J. R., Y. Ouyang, and J.-S. Chen (1998), Estimation of infiltration rate in vadoze zone: Application of selected mathematical models, Volume II, *Tech. Rep. EPA/600/R-97/128b*, U.S. Environmental Protection Agency.

Yoshikawa, K., W. Bolton, V. Romanovsky, M. Fukuda, and L. Hinzman (2002), Impacts of wildfire on the permafrost in the boreal forest of interior Alaska, *Journal of Geophysical Research, 107*(8148: doe:10.1029/2001JD000438), printed 108(D1), 2003.

Zhang, T. (2005), Spatial and temporal variability in active layer thickness over the Russian arctic drainage basin, *Journal of Geophysical Research, 110*, D16,101.

Zhang, Z., D. Kane, and L. Hinzman (2000), Development and application of a spatially-distributed arctic hydrological and thermal process model (ARHYTHM), *Hydrological Processes, 14*, 1017–1044.

Chapter 5

Evaluating the hydrologic response to changing watershed characteristics and climate in the subarctic*

Abstract

The Arctic region is currently experiencing rapid environmental change, with increases in both air temperature and precipitation. These changes in the climate system are expected to continue well into the current century. Simulation of the hydrologic processes in the sub-arctic environment is challenging due to rapidly changing thermal regime (permafrost versus non-permafrost, thaw depth development) and hydrology (hydraulic conductivity and storage capacity), both temporally and spatially. By spatial and temporal variation of the hydraulic conductivity (proxy for permafrost distribution) and porosity (proxy for storage capacity) with active layer thaw depth, the sub-arctic hydrologic environment can be adequately represented. A sensitivity analysis of the TopoFlow hydrologic model, as measured by simulated stream flow, was conducted. Sensitivity results indicate that TopoFlow is most sensitive to changes in precipitation. TopoFlow is also sensitive to changes in permafrost distribution, having a strong control on both the contributing area and storage processes. Simulation results indicate the only changes in simulated stream flow occur with changes within the contributing area of the watershed. If the expected changes in the permafrost regime are realized (decrease in areal extent of permafrost and an increase in active layer depth), the contributing area of the watershed will decrease, reducing the area of influence in the watershed to which runoff processes respond.

KEY WORDS: Permafrost; Active layer; Hydrologic Modeling; Computational hydrology; Climate Impacts; Hydrologic Processes; Environmental Change.

5.1 Introduction

The Arctic, including Alaska, is currently experiencing an unprecedented degree of environmental change [*Chapman and Walsh*, 1993; *Serreze et al.*, 2000; *IPCC*, 2001; *ACIA*, 2005; *Hinzman et al.*, 2005]. Increases in both the mean annual surface temperature (2-3^{o}C from

*W.R. Bolton, L.D. Hinzman, and D.L. Kane, in Preparation to be submitted to the *Journal of Geophysical Research – Biogeosciences*.

1954-2003) and annual precipitation have been observed [*Chapman and Walsh*, 1993; *Serreze et al.*, 2000; *ACIA*, 2005; *Hinzman et al.*, 2005]. In Interior Alaska, the combination of the recent increase in air temperature and an unstable permafrost condition [*Yoshikawa et al.*, 2002] has resulted in a reduction in areal extent of permafrost and an increase in active layer depth [*Jorgenson et al.*, 2001; *Yoshikawa et al.*, 2003]. Recent studies have documented a variety of hydrologic responses associated with the shifting climatic and permafrost regimes, including later freeze-up and earlier break-up dates of rivers [*Magnuson et al.*, 2000], increased arctic river discharge [*Peterson et al.*, 2002], shrinking lakes [*Smith et al.*, 2005], and thermokarst development [*Osterkamp and Romanovsky*, 1999; *Osterkamp et al.*, 2000; *Jorgenson et al.*, 2001].

The observed climatic changes are expected to continue into the next century [*IPCC*, 2001; *ACIA*, 2005]. The sub-arctic environment can be characterized as being located in the zone of discontinuous permafrost. As such, most of the current or expected changes (such as increased temperature and precipitation, decreased permafrost extent, increased active layer depth, tree line expansion and vegetation composition), will be experienced first in this region. In light of the observed and expected changes, it is important to understand the feedback mechanisms of the water cycle [*Kane and Hinzman*, 2004], where small changes in the natural system may result in dramatic, threshold changes in the hydrology, ecology, and surface energy balance, with subsequent climatological impacts on local, regional, and even global scales.

The objectives of this study were to (1) examine the viability of representing the hydrology in a zone of discontinuous permafrost through spatial and temporal variation of the hydraulic conductivity and porosity within a spatially-distributed, process-based hydrologic model; and (2) assess the sensitivity of a spatially-distributed, process-based hydrologic model to changes in the permafrost regime (permafrost distribution and active layer depth), climate conditions (temperature and precipitation), and vegetation distribution.

5.2 Influence of permafrost on the stream flow regime

In the sub-arctic environment, the presence or absence of permafrost is generally controlled by physiographic features such as aspect, slope, and elevation. Other factors such as soil types, soil moisture, vegetation cover, and disturbance - either anthropogenic or natural

(such as wildfire) can also influence the distribution of permafrost [*Haugen et al.*, 1982; *Yoshikawa et al.*, 2002]. In Interior Alaska, permafrost is generally located on north-facing slopes and valley bottoms, while areas free of permafrost are generally located on south to southwest facing slopes [*Nelson*, 1978; *Haugen et al.*, 1982]. Hydrologically speaking, the sub-arctic environment is unique in that the thermal and hydrologic regime of the soil (permafrost versus non-permafrost) can vary greatly over short horizontal spatial scales (x- and y-direction), and with depth (z-direction), and over time (short- and long-term). It is well documented that the hydraulic conductivity of ice-rich permafrost soils can be several orders of magnitude lower than their unfrozen counterpart (e.g. *Kane and Stein* [1983]; *Burt and Williams* [1976]; *Freeze and Cherry* [1979]). Ice-rich soils are common at the permafrost table as surface water, which percolates to the permafrost, refreezes [*Woo*, 1986]. The ice-rich condition at the permafrost table significantly reduces the permeability of the soil, effectively creating an aquitard, dividing the groundwater system into a sub- and supra-permafrost components [*Dingman*, 1975; *Woo*, 1990].

In areas underlain with permafrost, the active layer, the thin layer of soil above the permafrost, which annually thaws and freezes, is the zone where most hydrologic, biologic, ecologic, and geomorphic processes occur [*Kane et al.*, 1991; *Hinzman et al.*, 1998; *Woo*, 2000]. The thawing of the active layer begins immediately upon the completion of snowmelt [*Boike et al.*, 1998] and is dependent upon a number of factors including soil material (thermal conductivity), duration of snow cover, soil moisture and ice-content, and convection of heat by ground water [*Woo*, 1986]. As a result, the depth of the active layer is spatially and temporally quite variable. In Interior Alaska, the active layer depth is thinner on north-facing slopes than south-facing slopes due to differences in vegetative cover and a late lying snow cover [*Brown*, 1973; *Washburn*, 1979]. The active layer zone is hydrologically dynamic where both the hydraulic conductivity and storage capacity increase throughout the summer. As the position of the active layer is both spatially and temporally variable, the storage capacity and hydraulic conductivity of these near surface soils are also variable in both space and time [*Woo and Steer*, 1983].

The difference in hydraulic properties between areas underlain with permafrost and non-permafrost areas result in markedly different runoff patterns [*Slaughter and Kane*, 1979]. In permafrost areas, ice-rich soil pores inhibit percolation of surface waters (either snow-

melt or rainfall) at the permafrost table. This results in lateral movement of surface waters relatively quickly downslope through the shallow organic mat and near surface mineral soils. In contrast, the relatively well-drained non-permafrost soils allow percolation of surface waters to a deep subsurface groundwater system without significant lateral flow [*Slaughter and Kane*, 1979]. Movement of water through this deep groundwater system is relatively slow compared to the water movement through the near surface soils in permafrost regions [?*Bolton et al.*, 2004]. Stream flow in permafrost-dominated watersheds can be characterized by a larger contributing area, higher specific discharge (discharge normalized by basin area), rapid rise to peak flow (often described as 'flashy'), rapid decline following peak flow with prolonged recession, and a lower specific baseflow compared to catchments of lesser permafrost coverage (Figure 2.3) [*Dingman*, 1973; *Slaughter and Kane*, 1979; *Haugen et al.*, 1982; *Chacho and Bredthauer*, 1983; *McNamara et al.*, 1998; *Bolton et al.*, 2000; *Petrone et al.*, 2000]. Over the course of a summer season, the thawing of the active layer increases the potential water holding capacity of the soil, resulting in a decreasing surface water contribution during precipitation events and a steadily increasing baseflow contribution [*Hinzman and Kane*, 1991; *Bolton et al.*, 2000].

5.3 Conceptual model

A number of studies have focused on runoff generation mechanisms in the sub-arctic. *Dingman* [1973] used the variable source area concept to describe the runoff generation as originating from the valley bottoms. In this study, *Dingman* [1973] noted the size of the source area (or contributing area) during precipitation events is dictated by the the position of the water table in the valley bottoms, which in turn depends on the antecedent conditions of the watershed. *Carey and Woo* [2001] expanded upon the variable source concept by including a two-layer flow system, described by *Kane et al.* [1978], due to the sharp change in hydraulic conductivity between the organic and mineral soils.

The conceptual model used in this study incorporates the above concepts. In areas underlain with permafrost, a relatively thick organic layer (of high hydraulic conductivity and porosity) overlies an ice-rich mineral soil (of very low hydraulic conductivity and porosity). A near-surface ground water table is located above the permafrost table generally near the interface of the organic and mineral soils, due to the impermeable nature of

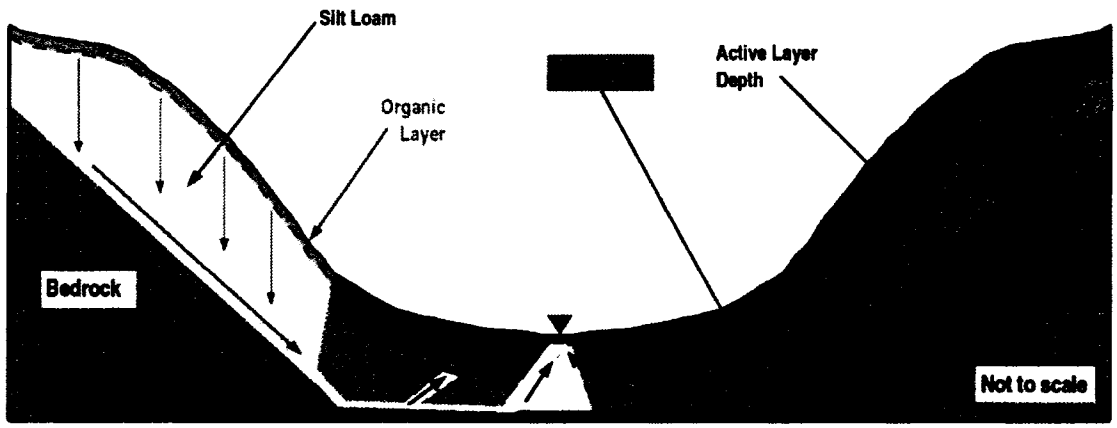

Figure 5.1: Conceptual model the water flow paths in areas of discontinuous permafrost. The direction and magnitude of flow paths are indicated by the arrows.

the ice-rich mineral soil. During precipitation events, the ice-rich conditions inhibit percolation to the deeper subsurface and result in rapid rise of the shallow water table (often up into the organic soils), allowing surface waters to travel relatively quickly through the organic mat and active layer to the stream (Figure 5.1).

Permafrost-free areas consist of a relatively thin organic layer (of high hydraulic conductivity and porosity) overlying a well-drained mineral soil (with relatively high hydraulic conductivity and porosity due to a lack of pore-ice). The ground water table is located in the deeper sub-surface. During precipitation events, surface waters are allowed to rapidly percolate to the deep groundwater system. In these non-permafrost areas, the infiltration capacity of the soils must be exceeded before near-surface runoff generation can occur. The deeper groundwater system contributes a steady source of base flow to stream.

5.4 Choice of model

The process-based, spatially-distributed hydrologic model, TopoFlow, is selected for use in this study. The TopoFlow structure is described in *Zhang et al.* [2000] and *Bolton et al.* [This issue]. This model has been successfully applied in an arctic environment [*Schramm*, 2005]. TopoFlow is well suited to the sub-arctic environment as input variables are allowed to change through both time and space. This feature is particularly important in the sub-

arctic environment where the thermal and hydraulic properties of the soils vary rapidly (generally due to phase change) in both the spatial and temporal dimensions.

5.5 Adaptation of TopoFlow

Hydrologically speaking, the main difference between frozen (permafrost) soils and thawed (non-permafrost) soils is the difference in hydraulic conductivity [*Burt and Williams*, 1976; *Kane et al.*, 1978; *Freeze and Cherry*, 1979; *Kane and Stein*, 1983] and storage capacity; both a function of the amount of ice in the pores [*Woo*, 1986]. In our conceptualization of the sub-arctic hydrologic regime, permafrost soils are represented with a very low hydraulic conductivity and a low porosity. Non-permafrost soils (or thawed soils in the active layer) are represented by appropriately larger soil hydraulic conductivity and porosity.

Development of the thaw depth begins immediately at conclusion of snowmelt [*Boike et al.*, 1998] and progresses throughout the summer season. The thaw depth is approximated by a step function (Equation 5.1) that is proportional to the square root of time since the beginning of the thaw depth development [*Terzaghi*, 1952; *Woo*, 1986].

$$X[t] = \Gamma\sqrt{t} \tag{5.1}$$

where X is the depth of thaw from the surface, Γ is the characteristic thaw coefficient, and t is the time from the completion of snowmelt . The relationship between X and $\sqrt{t}$ is given by Equation 5.2:

$$\Gamma = \left(\frac{2k_u T_s}{L}\right)^{1/2} \tag{5.2}$$

where k_u is the unfrozen soil thermal conductivity; T_s is the applied constant surface temperature; and L is the volumetric latent heat of the soil [*Nixon and McRoberts*, 1973]. This solution assumes a linear temperature distribution in the thawed zone of the soil and a frozen ground temperature of approximately 0^oC.

For each layer, the frozen and thawed hydraulic conductivity and porosity of the soil are defined. In permafrost areas, the location of the thaw depth (Equation 5.1) is determined relative to the soil layers following the completion of snowmelt (Figure 5.2). Prior to the completion of snowmelt, the frozen hydraulic conductivity and porosity are used

for each soil layer. If an entire soil layer(s) is in the area above the thaw depth, the thawed hydraulic conductivity and porosity values are used for that time step. If the entire soil layer(s) is below the thaw depth, the frozen hydraulic conductivity and porosity values are used for that time step. If the thaw depth is located within a soil layer, the hydraulic conductivity and porosity are determined using simple weighting functions:

$$K_X = \frac{K_F d_F + K_T d_T}{D} \tag{5.3}$$

and

$$P_X = \frac{P_F d_F + P_T d_T}{D} \tag{5.4}$$

where $K_{F,T}$ are the frozen and thawed hydraulic conductivity; $P_{F,T}$ are the frozen and thawed porosity; $d_{F,T}$ are the thickness of the frozen and thawed portion of the soil layer in question; and D is the total depth of the soil layer, X (note: $D = d_F + d_T$).

In the model formulation, the hydraulic conductivity and porosity of the non-permafrost surface soil layers are prescribed based upon the presence or absence of snow. In the time steps prior to the completion of snowmelt, the frozen hydraulic conductivity and porosity are defined for all soil layers. Following the completion of snowmelt, the simplifying assumption is made that the soils are well-drained and the ground thaws instantaneously and the corresponding thawed hydraulic conductivity and porosity are used for all soil layers. This assumption is based upon observed field measurements showing relatively rapid warming of the seasonal ground frost layer following the completion of snowmelt. At the Wolf Creek Basin, Yukon Territories, Canada, *Carey and Woo* [1998] report the time required to completely thaw the seasonal ground frost layer following the completion of snow melt on a south-facing (permafrost free) slope ranged from 0 to 14 days. The rapid temperature rise in the frost layer is attributed to the release of latent heat by the re-freezing of infiltrated snowmelt water during the melt period, and two-sided thawing of the frost layer from the ground surface and below the frost layer [*Carey and Woo*, 1998]. *Kane and Stein* [1983] report the hydraulic conductivity of a well-drained, seasonally frozen silt loam soil is only a factor of two lower than its thawed counterpart, due mainly to the change in water viscosity with temperature.

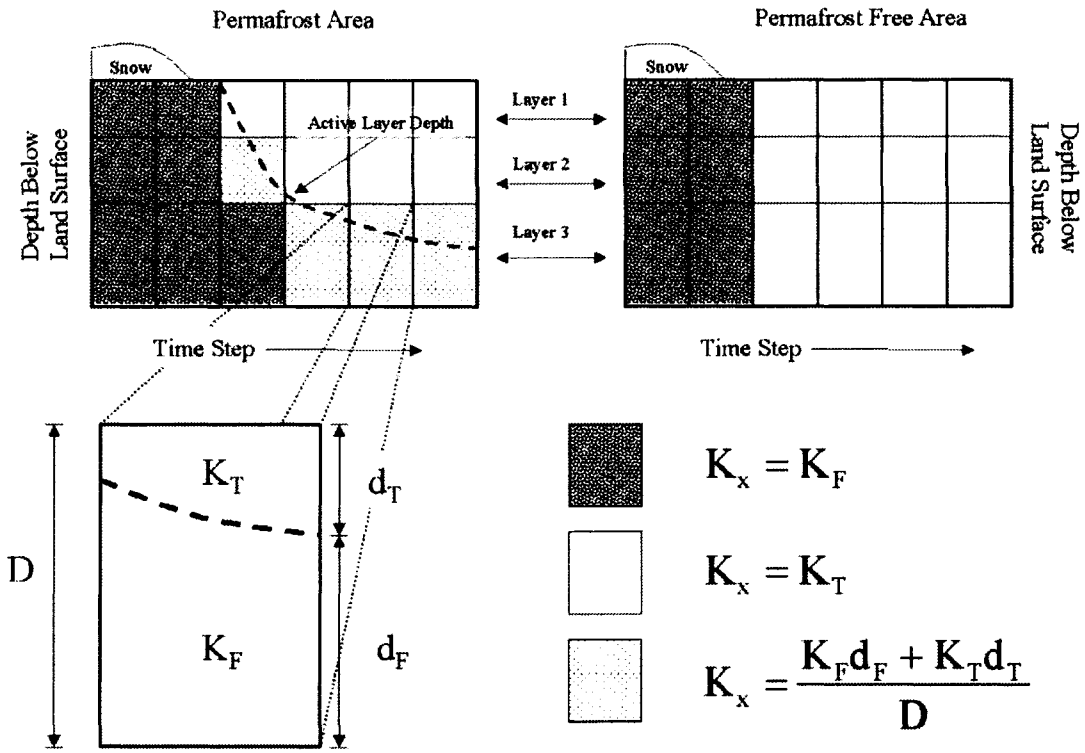

Figure 5.2: Mathematical representation of discontinuous permafrost regime and thaw depth development. The porosity of each soil layer is determined in the same manner.

The mathematical representation of the discontinuous permafrost regime was tested. In this test, the areal extent of permafrost within the model domain was set at 17, 50, and 80%. Each soil layer is assumed to have the same frozen and thawed hydraulic properties (and varies only with permafrost extent). Simulations last 120 days, with a large (uniform) precipitation event lasting 1 day occurring at Days 0, 30, 60, and 90. The thaw depth is initialized at 0.0 meters and begins to develop at the beginning of the simulations. The thaw depth at the end of the 120 days is 0.5 meters ($\Gamma = 0.046\ m \cdot day^{-1/2}$). The snowmelt and evaporation processes were not represented in these simulations.

Comparison of the simulated hydrographs show that increasing permafrost extent results in a larger peak discharge, a lower base flow between precipitation events, and a longer recession period following each precipitation event (Figure 5.3). These patterns are similar to field observations and give us confidence in the mathematical conceptualization of the sub-arctic hydrologic system.

5.6 Sensitivity analysis

A number of scenarios are used in order to assess the sensitivity, determined by simulated discharge, of the TopoFlow model through the use of the 'virtual control watershed' concept [*Andreassian et al.*, 2003]. The scenarios explored include changes in permafrost extent, active layer depth, distribution of vegetation, equilibrium evapotranspiration rates, precipitation, and temperature (air, ground, and soil). Simulation scenarios used in this analysis are listed in Table 5.1.

The reference scenario (Control, Table 5.1) is as follows: 1) The areal extent of permafrost is 64% (Figure 5.4); 2) the maximum active layer depth at the end of the simulation is 0.54 meters ($\Gamma = 0.05\ m \cdot day^{-1/2}$); 3) vegetation is distributed by permafrost distribution, with coniferous vegetation (40% equilibrium evapotranspiration rate) occupying the permafrost region and deciduous vegetation (100% equilibrium evapotranspiration rate) in the permafrost free region; 4) with the exception of precipitation, the model simulation is driven by climatic data measured in the Caribou-Poker Creeks Research Watershed (CPCRW), beginning on 1 May 2000 for a period of 120 days; and 5) realistic soil and channel properties, obtained from field measurements within CPCRW, are used. Soil properties fall within the range of values listed in *Kane et al.* [1978]; *Beringer et al.* [2001]; *Mölders et al.*

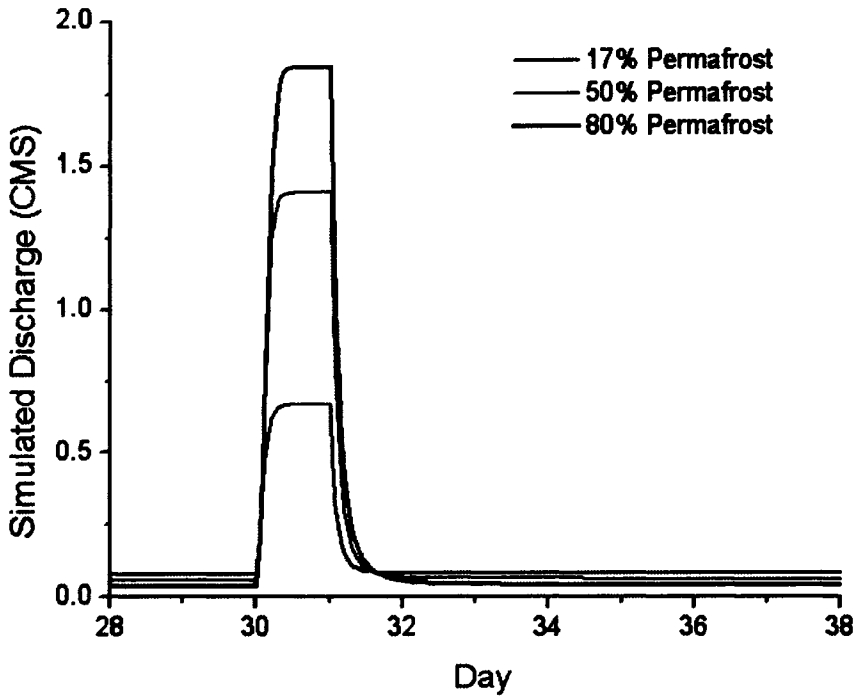

Figure 5.3: Comparison of simulated hydrographs for varying representation of permafrost extent. As permafrost extent increases, higher peak flows during precipitation events, a longer recession period following precipitation events, and a lower base flow between precipitation events are simulated.

Table 5.1. Test scenarios used in the sensitivity analysis

Test #:	Scenario	Permafrost Distribution	Active Layer Depth	Conifer Distribution	Equilibrium Evapotrans-piration	Average Temp-erature	Precip-piration
			Reference Simulation				
Control	Reference	64%	0.545 meters	64%	0.4 C, 1.0 D	10.1°C Air 4.8°C Surface 0.9°C Ground	6.25 mm
			Change (%) from Reference Simulation				
1	Permafrost	-100, -63 +57	NC	NC	NC	NC	NC
2a, 2b	Active Layer Depth	NC	-100, -66 +60, +100	NC	NC	NC	NC
3a, 3b	Conifer Distribution	NC NC	NC NC	-100, -63 +57	NC NC	NC NC	NC NC
4	Equilibrium ET Rate	NC	NC	NC	-100, -66 +60, +100	NC NC	NC NC
5a	Temperature	NC	NC	NC	NC	-66, +60	NC
5b	Temperature	NC	NC	NC	NC	-60, -30 +30, +60	NC
6	Precipitation	NC	NC	NC	NC	NC	-100, -66 +60, +100

Symbols Used: C: Conifer Vegetation; D: Deciduous Vegetation; NC: No change from the reference conditions. Notes: The initial ground water is from Test 2a outputted data. The distribution of vegetation is reversed in Tests 3a and 3b. The Priestley-Taylor and Energy Balance methods of evapotranspiration are used in Tests 5a and 5b, respectively. The percent change in temperature in Test 5b is in reference to air temperature.

Table 5.2: Soil and channel variables used in the model simulations. Soil properties from *Kane et al.* [1978], *Beringer et al.* [2001] and *Mölders et al.* [2005]. Order 1 and 2 elements are assumed to contribute to streamflow only through the overland flow process. The channel width for these elements is set to the width of the DEM.

Soil Properties					
		Permafrost			
Layer	Thickness [m]	K_T [m/s]	K_F [m/s]	P_T	P_F
1	0.10	1.5e-4	1.5e-5	0.9	0.7
2	0.15	2.0e-5	2.0e-7	0.9	0.3
3	5.0	2.83e-7	2.83e-9	0.48	0.25
4	0.50	1.0e-10	1.0e-10	0.5	0.5
		Non-Permafrost			
Layer	Thickness [m]	K_T [m/s]	K_F [m/s]	P_T	P_F
1	0.10	1.5e-4	1.5e-5	0.9	0.7
2	0.15	2.83e-7	2.83e-10	0.5	0.5
3	5.0	2.83e-7	2.83e-9	0.5	0.5
4	0.50	5.0e-6	5.0e-6	0.5	0.5
		Channel Properties			
		Order	Manning's 'N'	Width [m]	Bank Angle [Degrees]
		1	0.3	100	89
		2	0.3	100	89
		3	0.16	0.15	33
		4	0.16	0.30	33
		5	0.16	0.48	33

[2005]. Table 5.2 shows the soil and channel properties used for each simulation.

5.6.1 Changes in permafrost condition

The ground water process in TopoFlow is very sensitive to the location of the water table [*Schramm*, 2005]. The large differences in hydraulic properties between the organic and mineral soil amplify this sensitivity. In these simulations, the water table is set at a depth of 0.15 meters below land surface in permafrost regions and 3.5 meters in non-permafrost regions. Each scenario is run twice. In the first simulation, the water table location is outputted every 2 days. The last outputted water table data from the first simulation is used as the initial water table condition for the second simulation.

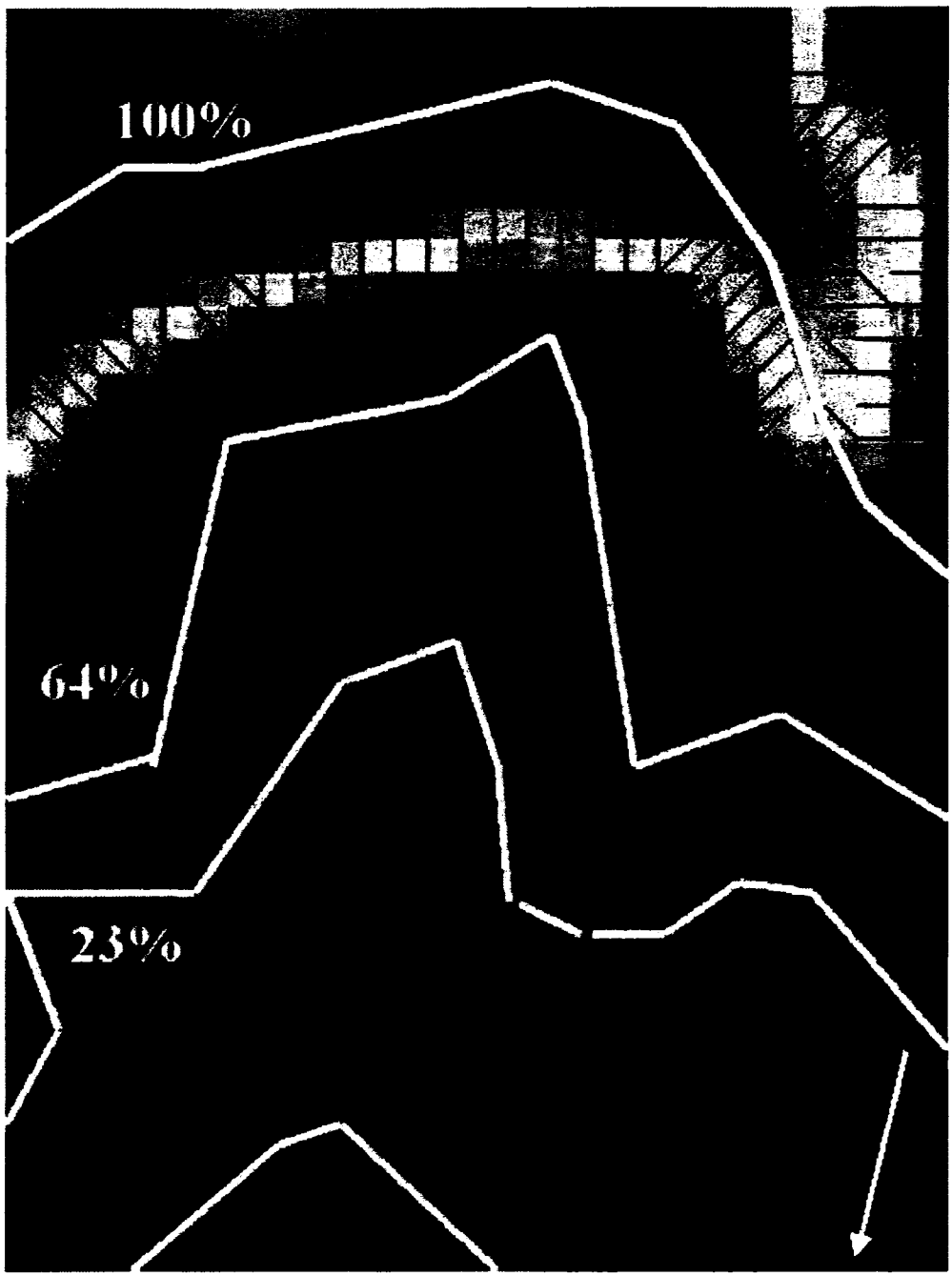

Figure 5.4: Model domain, channel network, and permafrost distribution of the 'virtual watershed.' The heavy white lines indicate the approximate permafrost/no permafrost boundary for the 18, 50, and 80% spatial distributions. The white arrow indicates the location of simulation output. The channel network for the entire model domain is displayed, with heavier lines indicating higher order channel segments. Relative DEM values are represented by the background color. Hot colors (reds and yellows) correspond to high DEM values (maximum = 721.0 m) while cold colors (dark blue and blue) correspond to low DEM values (minimum = 287.0 m).

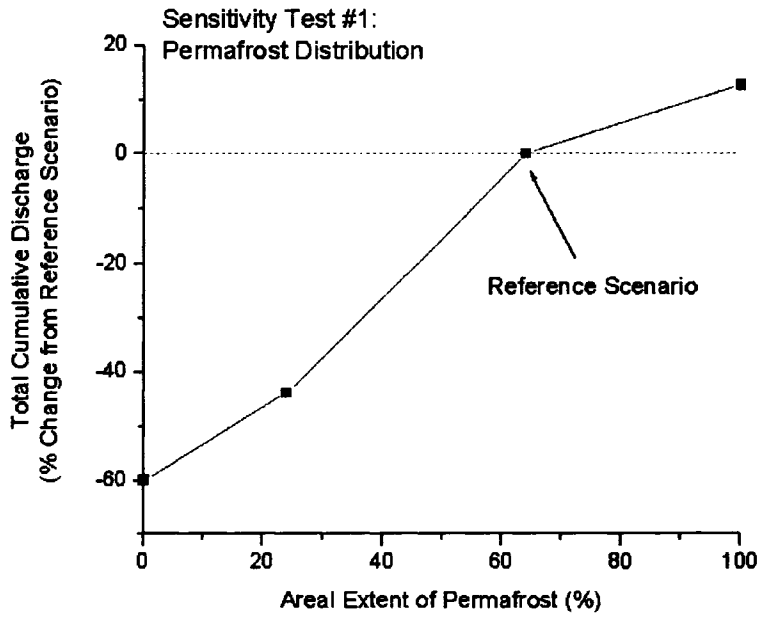

Figure 5.5. Sensitivity Test #1: Stream flow variation with changes in permafrost extent.

Results from the permafrost distribution test show that cumulative discharge increases with permafrost extent (Figure 5.5). As permafrost extent increases, the contributing area of the watershed proportionately increases. In this analysis, the percent contributing area for each precipitation event ranged from 14-66% for the 0% and 100% permafrost scenario, respectively. The percent contributing area is determined by:

$$\frac{(\Sigma Q/\Sigma P)}{Area} \cdot 100 \tag{5.5}$$

where ΣQ is the total simulated discharge $[m^3]$, ΣP is the total precipitation $[m]$, and *Area* is the watershed area, $[m^2]$.

As with the permafrost extent scenario, the maximum active layer depth scenario includes a water table that is initialized from a previous simulation (Test 2a, Figure 5.6) as well as a water table that is outputted from Test 2a (Test 2b, Figure 5.6). Results from Test 2a show little variation in total simulated stream flow with changes in the maximum active layer depth. In the simulations where the maximum active layer depth is less than the

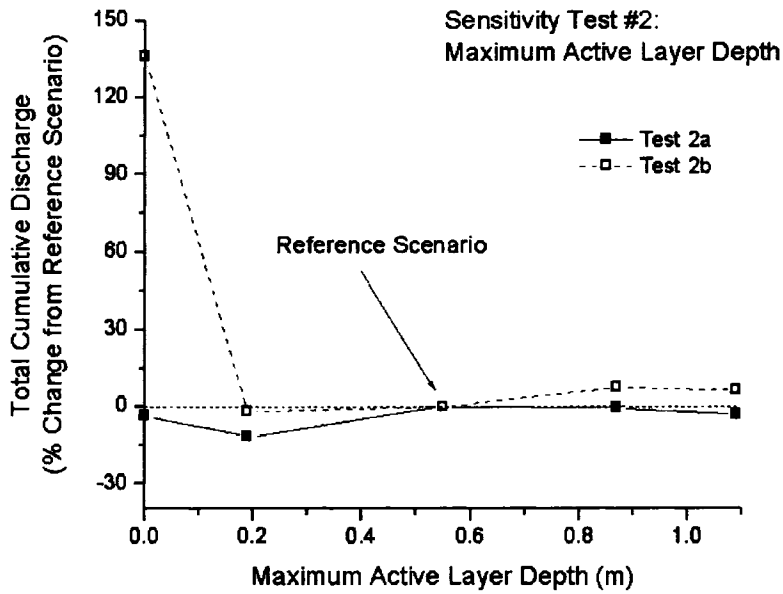

Figure 5.6: Sensitivity Test #2. Stream flow variation with changes in maximum active layer depth. In Test 2a, the water table is initialized from a previous simulation. In Test 2b, the initial water table is outputted from the results of Test 2a. The initial water table in Test 2b was located at the land surface, effectively eliminating the available soil water storage capacity.

reference scenario (maximum active layer thickness equals 0.0 and 0.19 m), the depth to the water table is located in the soils that remain frozen for the majority of the simulation period, resulting in a total cumulative discharge less than the reference scenario. The initial water table in Test 2b is initialized closer to the ground surface in the relatively higher conductive surface soils, resulting in a consistantly higher total cumulative discharge then Test 2a. The large difference between Tests 2a and 2b when the maximum active layer depth equals 0.0 meters is due to simulation initial conditions. In Test 2a, the water table in the permafrost is set below the ground surface, near the organic and mineral soil interface. In Test 2b, the water table is set at the ground surface. During the first precipitation event, the overland flow occurs in Test 2b, resulting in a much higher simulated runoff compared to Test 2a.

5.6.2 Changes in vegetation

In the boreal forest, broad-leaf aspen and birch stands evaporate at rates which approach the equilibrium rate, while in upland coniferous forests (black spruce), evaporation rates range between 25-50% of equilibrium evaporation [*Baldocchi et al.*, 2000; *Eugster et al.*, 2000]. Vegetation in Test 3a (Figure 5.7) is distributed with coniferous vegetation located in the valley bottoms, while deciduous vegetation is distributed in the uplands. During the precipitation events, the percent contributing areas (Equation 5.5) is were found to be 58%, 60%, 61%, and 61% for the 0, 24, 64, and 100% coniferous vegetation extent simulations, respectively. Simulation results indicate the only changes in model output occur when the vegetation type is altered within the contributing area. This is confirmed by reversing the vegetation distribution (i.e. deciduous vegetation located in the valley bottoms and coniferous vegetation located in the higher elevations) (Test 3b, Figure 5.7). The evapotranspiration scenarios indicate the simulated discharge is inversely proportional to the rate of evapotranspiration (Figure 5.8).

5.6.3 Changes in the evapotranspiration due to changes in temperature

Changes in temperature (air, surface, and ground) are calculated by adding or subtracting the appropriate percentage of the average measured temperature, measured over the simulation period, to the measured value. The average measured air, surface, and ground temperatures used in these scenarios are 10.1, 4.8, and 0.9°C, respectively. In these scenarios, the only hydrologic process in which temperature is used as an input variable is evapotranspiration, which is simulated in this study with a modified Priestley-Taylor (Test 5a) and energy balance (Test 5b) methods (Table ??).

The first evapotranspiration change test is simulated using the Priestley-Taylor method of evapotranspiration. The Priestley-Taylor equation for evapotranspiration used in TopoFlow is:

$$Q_{ET} = \alpha \cdot (0.406 + 0.011 T_{air}) \cdot (Q_{net} - Q_c) \tag{5.6}$$

where: α is the coefficient relating potential evaporation (the evaporation rate of a saturated land surface where there is no significant surface or physical control on evapora-

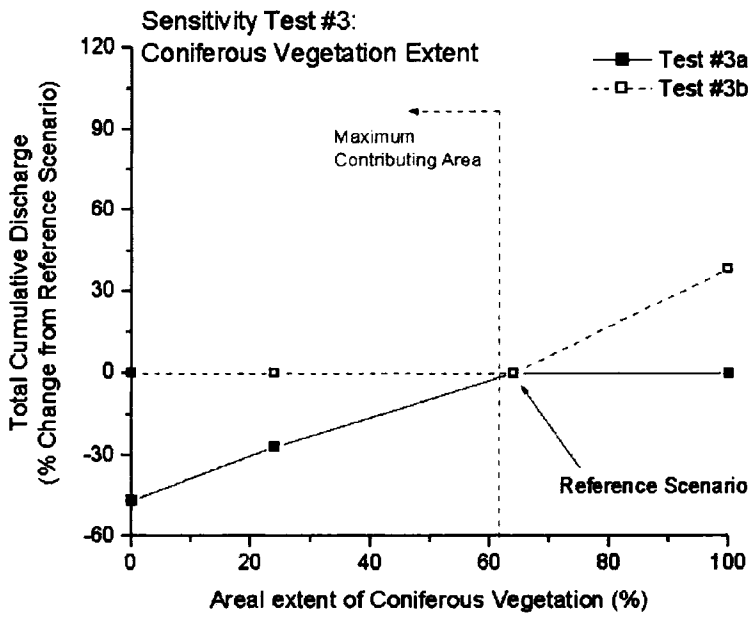

Figure 5.7: Sensitivity Test #3: Stream flow variation with changes in vegetation distribution. In Test 3a, coniferous vegetation is located in valley bottoms while deciduous vegetation is located in the uplands. In Test 3b, the vegetation distribution is reversed.

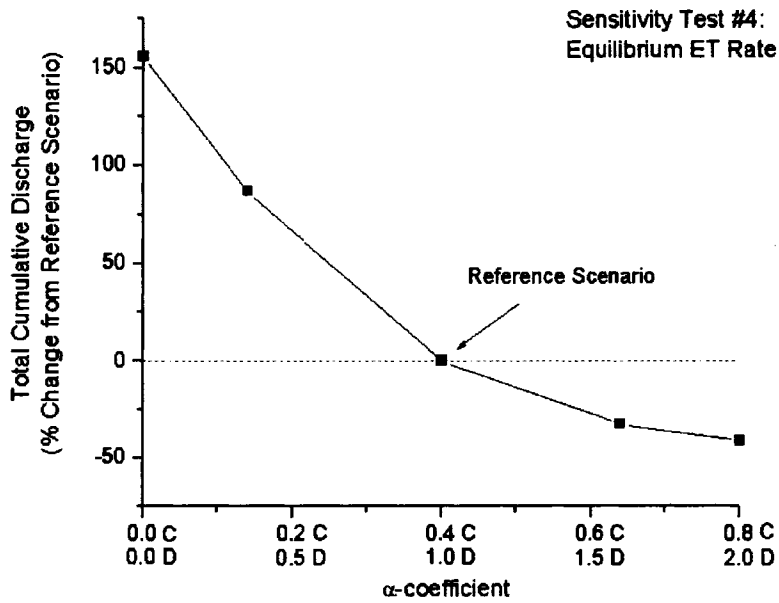

Figure 5.8: Sensitivity Test #4: Stream flow variation with changes in equilibrium evaporation rate. Note: C is the α-coefficient applied to coniferous vegetation and D is the α-coefficient applied to deciduous vegation.

tion [*Lhomme*, 1997]) to equilibrium evapotranpiration, T_{air} is the air temperature, Q_{net} is the net radiation, and Q_c is the conductive heat flux into the soil. While increases in the conductive heat flux, Q_c, will reduce the evapotranspiration rate, it can be seen that evapotranspiration rate is proportional to the air temperature. Using this method, increases in temperature results increased evapotranspiration and decreasing simulated discharge (Test 5a, Figure 5.9).

The second temperature change test, using the energy balance method of evapotranspiration, is based upon the expected $3-6^oC$ range of temperature increase reported by the *ACIA* [2005]. In this test, a uniform temperature increase or decrease is specified for each temperature variable ($\pm 3^o$, $\pm 6^o$C). In this test, increases in temperature result in slightly increased evapotranspiration and decreased streamflow. The range in difference from the reference simulation is $\pm 0.08\%$ (Test 5b, Figure 5.9).

5.6.4 Changes due to changes in precipitation

The precipitation change scenarios results indicate that the simulated discharge is proportional to change in precipitation rate (Figure 5.10). When precipitation eleminated from the test, groundwater flow is the only process contributing to stream flow. As the amount of precipitation increases, its influence on the simulated stream flow increases at a rapid rate.

5.7 Discussion and conclusions

Simulation of the hydrologic processes in the sub-arctic environment is challenging due to the rapidly changing thermal (permafrost verses non-permafrost, active layer development) and hydrologic (hydraulic conductivity and storage capacity) conditions in both time and space (x, y, and z-directions). By spatially and temporally varying only the hydraulic conductivity (proxy for permafrost distribution) and porosity (proxy for storage capacity) with thaw depth development, stream flow patterns observed in the field are simulated.

The importance of soil properties and contributing area on the stream flow process is illustrated by the sensitivity analysis. As permafrost extent was increased, the rate of increase of the contributing area was reduced. The difference in contributing area between

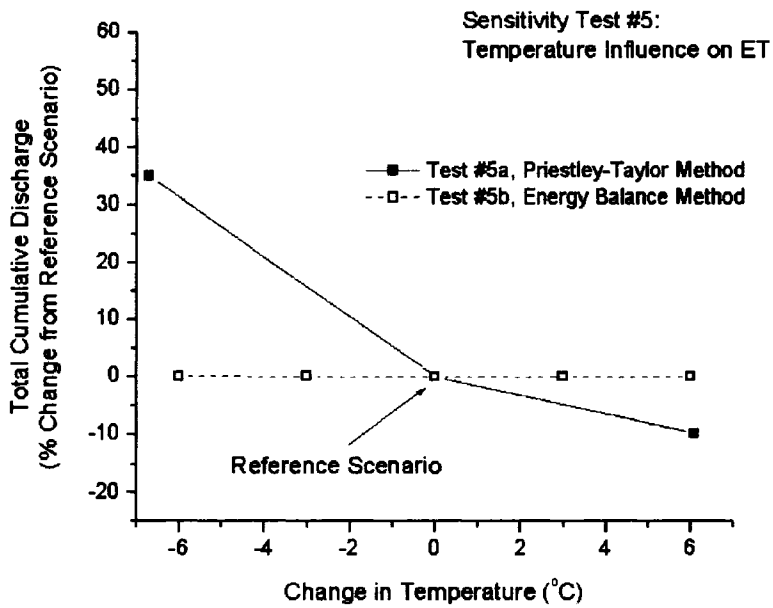

Figure 5.9: Sensitivity Test #5: Stream flow variation with changes in evapotranspiration due to changes in temperature. A modified Priestley-Taylor method of evapotranspiration is used in Test 5a and the energy balance method of evapotranspiration is used in Test 5b.

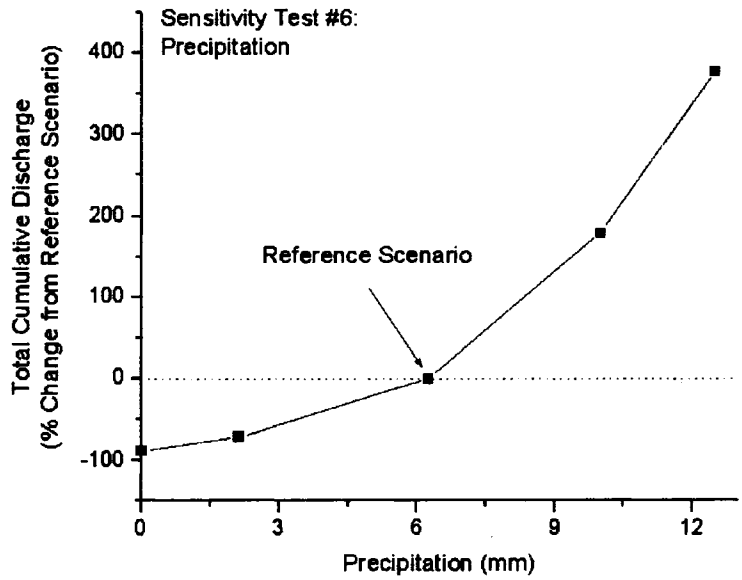

Figure 5.10. Sensitivity Test #6: Stream flow variation with changes in precipitation.

the 0% and 24% permafrost extents was approximately 20%, compared to the 5% difference between the simulations of 64% and 100% permafrost extent. This is consistent with field studies such as Dingman's [1973] study of the Glenn Creek watershed located near Fairbanks, Alaska. The second active-layer test, in which subsurface storage is limited within the contributing area by a near surface water table, resulted in a greater simulated discharge. Evaportranspiration is an important process in the sub-arctic. *Gieck and Kane* [1986] and *Bolton et al.* [2004] report that evapotranspiration can account for nearly all the summer precipitation. In this analysis, the water evaporated from the system is removed directly from the top of the water table. Given the known sensitivity to water table position, it is not suprising the difference in cumulative discharge between the -100% and +100% evapotranspiration rates is large.

The model sensitivity analysis indicates that rainfall has the largest influence on stream flow dynamics (Figure 5.11) and permafrost plays an important secondary role through its strong influence on the size of the watershed contributing area, groundwater flow, soil moisture, soil storage, and distribution of vegetation. Furthermore, if the observed

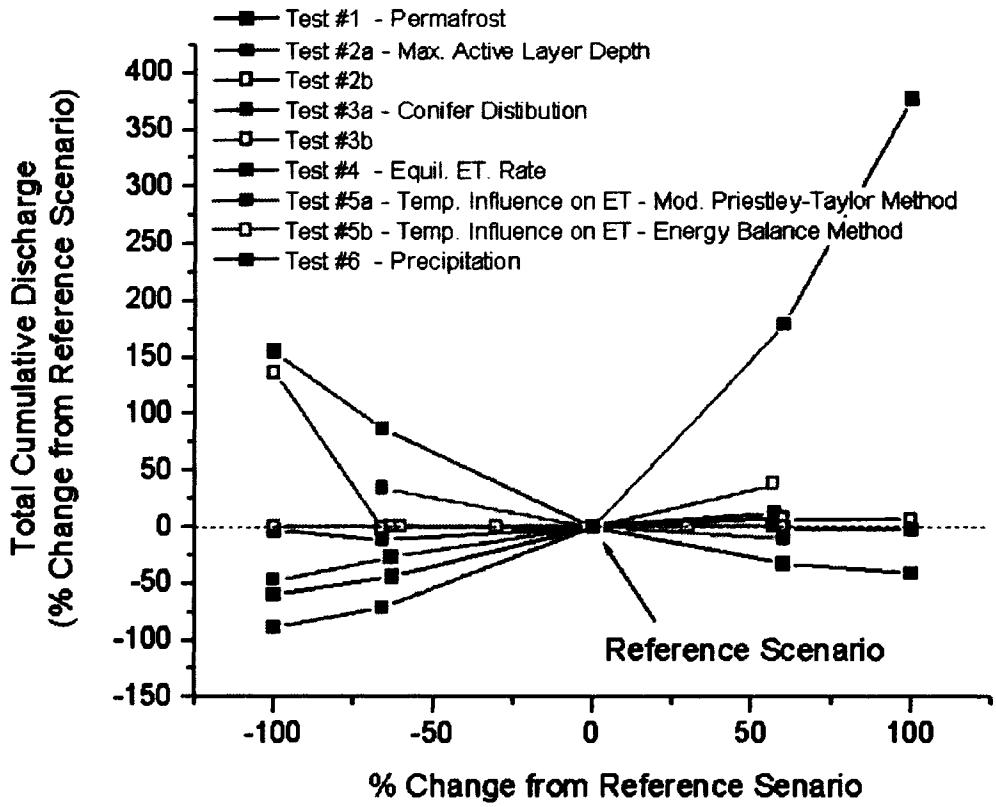

Figure 5.11: Results of sensitivity analysis. Note: In Test 5b, the % change is temperature in plotted relative to air temperature.

changes in the permafrost regime continue as expected (decrease in areal extent, increase in active layer depth), the contributing area of the watershed will decrease, reducing the area of influence to which hydrologic runoff respond.

The design of TopoFlow is well suited to the sub-arctic environment. By using a spatially distributed model, important hydrologic processes, such as the influence of vegetation in the contributing area or the impact of varying thaw depths, can be readily identified. This is not possible using typical rainfall-runoff or 'black box' models such as the HBV (Hydrologiska Byråns Vattenbalansavdelning, [*Bergström*, 1976, 1992]) model.

5.8 Acknowledgements

Support for this research was provided by the U.S. National Science Foundation Arctic System Science Program (OPP-0229705), the U.S. National Science Foundation Division of Environmental Biology under the Long Term Ecological Research Program (Grant number DEB-9211769), a fellowship from the Inland Northwest Research Alliance (U.S. Dept. of Energy contract DE-FG07-021D14277), and a grant from the Center of Global Change - University of Alaska Fairbanks.

References

ACIA (2005), *Impacts of a warming Arctic: Arctic Climate Impact Assessment*, 1046 pp., Cambridge University Press.

Andreassian, V., E. Parent, and C. Michel (2003), A distribution-free test to detect gradual changes in watershed behavior, *Water Resources Research*, *39*(9), 10–1–11.

Baldocchi, D., F. M. Kelliher, T. Black, and P. Jarvis (2000), Climate and vegetation controls on boreal zone energy exchange, *Global Change Biology*, *6*(Supplement 1), 69–83.

Bergström, S. (1976), Development and application of a conceptual runoff model for Scandinavian catchments, *SMHI Reports RHO 7*, Swedish Meteorological and Hydrological Institute, Norrköping, Sweden.

Bergström, S. (1992), The HBV model - it's structure and applications, *SMHI Reports RHO 7*, Swedish Meteorological and Hydrological Institute, Norrköping, Sweden.

Beringer, J., A. H. Lynch, F. S. Chapin, M. Mack, and G. B. Bonan (2001), The representation of Arctic soils in the land surface model: The importance of mosses, *Journal of Climate*, *14*, 3324–3335.

Boike, J., K. Roth, and P. Overduin (1998), Thermal and hydrologic dynamics of the active layer at a continuous permafrost site (Taymyr Peninsula, Siberia), *Water Resources Research*, *34*(3), 355–363.

Bolton, W., L. Hinzman, and K. Yoshikawa (2000), Stream flow studies in a watershed underlain by discontinuous permafrost, in *Proceedings Water Resources in Extreme Environments*, edited by D. Kane, pp. 31–36.

Bolton, W., L. Hinzman, and K. Yoshikawa (2004), Water balance dynamics of three small catchments in a sub-arctic boreal forest, in *Northern Research Basins Water Balance (Proceedings of a workshop held at Victoria, Canada, March 2004)*, edited by D. L. Kane and D. Yang, IAHS , Publication 290, pp. 213 – 223.

Bolton, W. R., S. D. Peckham, and L. Hinzman (This issue), Toward understanding the hydrologic processes in a watershed dominated by discontinuous permafrost, *Journal of Geophysical Research - Biogeosciences*.

Brown, R. (1973), Influence of climate and terrain factors on ground temperatures at three locations in the permafrost region of Canada, in *The North American Contribution to the Second International Conference on Permafrost, Yakutsk*, pp. 27–34, National Academy of Sciences, Washington, D.C.

Burt, T., and P. Williams (1976), Hydraulic conductivity in frozen soils, *Earth Surficial Processes, 1*, 349–360.

Carey, S. K., and M.-K. Woo (1998), Snowmelt hydrology of two Subarctic slopes, Southern Yukon, Canada, *Nordic Hydrology, 29*(4/5), 331–346.

Carey, S. K., and M.-K. Woo (2001), Slope runoff processes and flow generation in a subarctic, subalpine catchment, *Journal of Hydrology, 253*, 110–129.

Chacho, J., E.F., and S. Bredthauer (1983), Runoff from a small subarctic watershed, in *Proceedings of the Fourth International Conference on Permafrost*, pp. 115–120, National Academy of Sciences, Washington D.C.

Chapman, W., and J. Walsh (1993), Recent variations in sea ice and air temperature in high latitudes, *Bulletin American Meteorology Society, 74*, 33–47.

Dingman, S. (1973), Effects of permafrost on stream flow characteristics in the discontinuous permafrost zone of central Alaska., in *Permafrost: North American Contribution to the Second International Conference*, pp. 447–453, National Academy of Sciences, Washington D.C.

Dingman, S. (1975), Hydrologic effects of frozen ground, *Special Report 218*, U.S. Army Cold Regional Research and Engineering Laboratory.

Eugster, W., W.R. Rouse, R.A. Pielke, J.P. McFadden, D.D. Baldocchi, T.G.F. Kittel, F.S. Chapin, G.E. Liston, P.L. Vidale, E.Vaganov, and S. Chambers (2000), Land-atmosphere energy exchange in arctic tundra and boreal forest: available data and feedbacks to climate, *Global Change Biology, 6*(Supplement 1), 84–115.

Freeze, R. A., and J. A. Cherry (1979), *Groundwater*, Prentice-Hall.

Gieck, R. J., and D. Kane (1986), Hydrology of two subarctic watersheds, in *Proceedings of the Cold Regions Hydrology Symposium*, edited by D. Kane, pp. 283–291, American Water Resources Association.

Haugen, R., C. Slaughter, K. Howe, and S. Dingman (1982), Hydrology and climatology of the Caribou-Poker Creeks Research Watershed, Alaska, *CRREL Report 82-26*, US Army Corps of Engineers Cold Regions Research and Engineering Laboratory.

Hinzman, L., and D. Kane (1991), Snow hydrology of a headwater arctic basin, 2, conceptual analysis and computer modeling, *Water Resources Research*, *27*(6), 95–100.

Hinzman, L., D. Goering, and D. Kane (1998), A distributed thermal model for calculating soil temperature profiles and depth of thaw in permafrost regions, *Journal of Geophysical Research*, *103*(D22), 28,975–28,991.
72, 251–298.

Hinzman, L., N.D. Bettez, F.S. Chapin, M.B. Dyurgerov, C.L.Fastie, B. Griffith, R.D. Hollister, A. Hope, H.P. Huntington, A.M. Jensen, G.J. Jia, T. Jorgenson, D.L. Kane, D.R. Klein, G. Kofinas, A.H. Lynch, A.H. Lloyd, A.D. McGuire, F.E. Nelson, W.C. Oechel, T.E. Osterkamp, C.H. Racine, V.E. Romanovsky, R.S. Stone, D.A.Stow, M. Sturm, C.E. Tweedie, G.L. Vourlitis, M.D. Walker, D.A. Walker, P.J. Webber, J.M. Welker, K.S. Winker, and K. Yoshikawa (2005), Evidence and implications of recent climatic change in northern Alaska and other arctic regions, *Climatic Change*, *72*, 251–298.

IPCC (2001), Climate change 2001: Synthesis report. summary for policymakers., *Tech. rep.*, Intergovernmental Panel on Climate Change.

Jorgenson, M., C. Racine, J. Walters, and T. Osterkamp (2001), Permafrost degradation and ecological changes associated with a warming climate in Central Alaska, *Climate Change*, *48*, 551–571.

Kane, D., and L. Hinzman (2004), Monitoring extreme environments: Arctic hydrology in transition, *Water Resources Impact*, *6*(1), 24–27.

Kane, D., L. Hinzman, and J. Zarling (1991), Thermal response of the active layer to climatic warming in a permafrost environment, *Cold Regions Science and Technology, 19*(2), 111–122.

Kane, D., and J. Stein (1983), Field evidence of groundwater recharge in Interior Alaska, in *Proceedings of the Fourth International Conference on Permafrost*, pp. 572–577, National Academy Press.

Kane, D. L., R. D. Seifert, and G. S. Taylor (1978), Hydrologic properties of subarctic organic soils, *Tech. Rep. IWR-88*, Institute of Water Resources, University of Alaska Fairbanks.

Lhomme, J.-P. (1997), A theoretical basis for the Priestley-Taylor coefficient, *Boundary-Layer Meteorology, 82*, 179–191.

Magnuson, J., D. Robertson, B. Benson, R. Wynne, D. Livingstone, T. Arai, R. Assel, R. Barry, V. Card, E. Kuusisto, N. Granin, T. Prowse, K. Steward, and V. Vuglinski (2000), Historical trends in lake and river ice cover in the northern hemisphere, *Science, 289*, 1743–1746.

McNamara, J., D. Kane, and L. Hinzman (1998), An analysis of streamflow hydrology in the Kuparuk River basin, Arctic Alaska: a nested watershed approach, *Journal of Hydrology, 206*, 39–57.

Mölders, N., M. Jankov, and G. Kramm (2005), Application of Gaussian error propagation principals for theoretical assessment of model uncertainty in simulated soil processes caused by thermal and hydraulic parameters, *Journal of Hydrometeorology, 6*, 1046–1062.

Nelson, G. (1978), Hydrologic information for land-use planning, Fairbanks vicinity, Alaska, *Open-File Report 78-959*, U.S. Geological Society.

Nixon, J., and E. McRoberts (1973), A study of some factors affecting the thawing of frozen soils, *Canadian Geotechnical Journal, 13*, 40–57.

Osterkamp, T., and V. Romanovsky (1999), Evidence for warming and thawing of discontinuous permafrost in Alaska, *Permafrost and Periglacial Processes, 10*, 17–37.

Osterkamp, T., L. Viereck, Y. Shur, M. Jorgenson, C. Racine, A. Doyle, and R. Boone (2000), Observations of thermokarst and its impact on boreal forests in Alaska, USA, *Arctic, Antarctic and Alpine Research, 32*, 303 – 315.

Peterson, B., R. Holmes, J. McClelland, C. Vörösmarty, R. Lammers, A. Shiklomanov, I. Skiklomanov, and S. Rahmstort (2002), Increasing river discharge to the Arctic Ocean, *Science, 298*, 2171–2173.

Petrone, K., L. Hinzman, and R. Boone (2000), Nitrogen and carbon dynamics of storm runoff in three sub-arctic streams, in *Water Resources of Extreme Environments*, edited by D. Kane, pp. 167–172, American Water Resources Association.

Schramm, I. (2005), Hydrologic modeling of an Arctic watershed, Alaska, Master's thesis, Universität Potsdam, Potsdam, Germany.

Serreze, M., J. Walsh, F. Chapin, T. Osterkamp, M. Dyurgerov, V. Romanovsky, W. Oechel, J. Morison, T. Zhang, and R. Barry (2000), Observational evidence of recent change in the northern high latitude environment, *Climatic Change, 46*, 159–207.

Slaughter, C., and D. Kane (1979), Hydrologic role of shallow organic soils in cold climates, in *Canadian Hydrology Symposium: Proceedings, 79-Cold Climate Hydrology*, pp. 380–389.

Smith, L., Y. Sheng, G. MacDonald, and L. Hinzman (2005), Disappearing arctic lakes, *Science, 308*, 1429.

Terzaghi, K. (1952), Permafrost, *Journal of the Boston Society of of Civil Engineers, 39*(1), 1–50.

Washburn, A. (1979), *Geocryology: A survey of Periglacial Processes and Environments*, Wiley.

Woo, M., and P. Steer (1983), Slope hydrology as influenced by thawing of the active layer, *Canadian Journal of Earth Science, 20*, 978–986.

Woo, M.-K. (1986), Permafrost hydrology in North America, *Atmosphere-Ocean, 24*(3), 201–234.

Woo, M. K. (1990), Permafrost hydrology, in *Northern Hydrology, Canadian Perspectives. Proceedings of the Northern Hydrology Symposium*, edited by T. Prowse, C. Ommanney, and M. Woo, no. 1 in Canadian National Hydrology Research Institute Science Report, pp. 63–76.

Woo, M.-K. (2000), Permafrost and Hydrology, in *The Arctic: Environment, People, Policy*, edited by M. Nuttal and T.V. Callaghan, Chap. 3, pp. 57–96, Harwood Academic Publications.

Yoshikawa, K., W. Bolton, V. Romanovsky, M. Fukuda, and L. Hinzman (2002), Impacts of wildfire on the permafrost in the boreal forest of Interior Alaska, *Journal of Geophysical Research, 107*(8148: doe:10.1029/2001JD000438), printed 108(D1), 2003.

Yoshikawa, K., D. White, L. Hinzman, D. Goering, K. Petrone, W. Bolton, and N. Ishikawa (2003), Water in permafrost: Case study of aufeis and pingo hydrology in discontinuous permafrost, in *International Conference on Permafrost, Proceedings 8*, vol. 2, edited by M. Phillips, S. Springman, and L. Arenson, pp. 1259–1264.

Zhang, Z., D. Kane, and L. Hinzman (2000), Development and application of a spatially-distributed Arctic hydrological and thermal process model (ARHYTHM), *Hydrological Processes, 14*, 1017–1044.

Chapter 6
Conclusions

Hydrologically speaking, the presence or absence of permafrost is the defining characteristic of the sub-arctic environment. Although the distribution of permafrost is site-specific in this environment, it impacts most of the hydrologic processes including stream flow, soil moisture dynamics, ground water flow, and water storage processes. The overarching hypothesis for this research is '**in the sub-arctic environment, the presence or absence of permafrost is the dominant influence on the soil moisture regime and stream flow patterns.**' A series of research objectives and questions, presented in Chapter 1, were formulated in order to test this hypothesis. These research objectives and questions were approached through a combination of field study and computer simulation. Results from the field studies show that the presence or absence of permafrost is the dominant influence on soil moisture dynamics. Results from the sensitivity analysis suggest that rainfall has the largest influence on the stream flow regime. The distribution of permafrost and the depth of thaw play an important, but secondary, role. This research expands upon the current knowledge of the hydrologic processes, with emphasis on the stream flow and soil moisture processes, which operate in the sub-arctic environment. Results from the field and computer studies are discussed below.

6.1 Field study

In Chapters 2 and 5, the soil moisture regime in areas of discontinuous permafrost was analyzed. Based upon field measurements in the Caribou-Poker Creeks Research Watershed (CPCRW), it was found that large differences in soil moisture exist in areas underlain by permafrost and those which are free of permafrost. In areas underlain by permafrost, ice-rich pores at the permafrost table impede movement of near surface water to the subsurface, resulting in soils which are at or near saturation throughout the summer period, showing little response to precipitation events. In non-permafrost areas, soils tend to be well-drained and tend to be drier, having a greater response to precipitation events. Significant soil moisture differences were found among vegetation types (deciduous versus coniferous), permafrost conditions (permafrost verses no-permafrost), and varying topography (hillside verses valley bottom), with the largest difference occurring between the

permafrost and non-permafrost sites. In Chapter 2, the stream flow hydrographs were analyzed. Permafrost-dominated watersheds display slower response times and a higher peak specific discharge during precipitation events, a longer recession period following a precipitation event, and lower specific baseflow between precipitation events. Using hydrograph separation analysis, it is shown that, as the thaw depth develops throughout the summer, the sub-surface water contribution ('old water' held in storage) to storm hydrographs increases significantly (from approximately 20-60%) in the permafrost-dominated watersheds. In the C2 sub-basin, which is underlain by about 3% permafrost, the sub-surface contribution to storm events is fairly constant at about 70%.

In Chapter 3, the relative importance of hydrologic processes in the sub-Arctic environment was addressed. In this Chapter, a water balance in three sub-basins of CPCRW, with varying permafrost extent, was conducted over the 1978-2003 time period. For every year of the study period, the water balance was calculated from the time of maximum snow water equivalent (mid-March to early-April) to the time of winter freeze-up (late-September to mid-October). The approach we took to solving the water balance equation was to set the change in storage term, (ΔS in Equation 3.1), as the residual. In taking this approach, all associated measurement errors are lumped into this term, limiting our ability to determine the degree to which we are able to 'close' the water balance. In terms of a yearly water balance, it is clear that significant errors exist as reflected in the reported ΔS values. The ΔS term is reported as a positive value for all watersheds over most years of study - an unlikely result. The predominately positive ΔS values indicate our ability to quantify water sources entering the system is better than our ability to quantify the water sources leaving the system. This is not a surprising result as the winter baseflow and (typically) the snow melt runoff events were not taken into account. Despite the limitations of the method used, some important findings were obtained.

In terms of processes, the snowmelt period is typically a major hydrologic event each year. Over a 2-3 week period, approximately 1/3 of the annual precipitation (rain + snow), which is held in storage over 7-8 month period, is introduced to the watershed system. The snowmelt period also coincides with the time when the water storage capacity of the permafrost soils is at its lowest, as ice-rich mineral soils are completely frozen. However, the snowmelt event was hard to capture due to extensive aufeis buildup leading to disper-

sal of snow melt runoff outside the normal channel boundaries. In comparing the summer stream flow between the watersheds, it was found that the watersheds with lesser amounts of permafrost produce less runoff compared to watersheds with a larger areal extent of permafrost, although the runoff ratios between all the watersheds varied little. Differences in summer runoff between the low and high permafrost watersheds must be offset by a higher winter discharge as water is released from the deep groundwater system. The areal composition of vegetation plays an important role as evaportranspiration was found to consume between 1/3 and nearly all of the summer precipitation (depending upon the sub-basin in question). In this study, it became clear the role of the water storage processes is critically important in terms of the water balance, but is the least well quantified. Changes in the water storage processes, in particular the active layer depth (increasing the storage capacity of the soils), may lead to shift in magnitude and timing of runoff.

The runoff ratios from the CPCRW sub-basins are markedly lower than other research watersheds located in discontinuous permafrost. The runoff ratios from CPCRW range from 0.17 - 0.20, while the runoff ratio from the Scotty Creek Watershed (located in the Northwest Territories, Canada), Wolf Creek Watershed (located in the Yukon Territories, Canada), and the Iittovuoma Watershed (located in northern Finland) are reported to be 0.35, 0.39, and 0.60, respectively [*Janowicz et al.*, 2004; *Quinton et al.*, 2004; *Seuna and Linjama*, 2004]. The low runoff ratio reported for the CPCRW sub-basins is in part due our inability to adequately capture the snowmelt event. The high runoff ratio is in in the Iittovuoma Watershed is due in part to a reduced evapotranspiration. The evapotranspiration ratios for CPCRW, Scotty Creek, Wolf Creek, and Iittovuma are 0.5-0.77, 0.66, 0.76, and 0.4, respectively.

Direct comparison of the individual water balance components is difficult due to differences in methods and hydrologic environment. For example, the evapotranspiration component Iittovuoma and Scotty Creeks is determined as the difference between precipitation and runoff and assumes a ΔS term equal to 0. In CPCRW and Wolf Creek Watershed, the evapotranpiration is directly calculated and the ΔS term is determined as the residual of the other terms. There are also large differences in ecosystems. CPCRW is located in the boreal forest, with no large surface storage component. The Wolf Creek Watershed cov-

ers three ecosystems (boreal forest, sub-alpine taiga, and alpine tunda) with a large lake within its boundries. Scotty Creek is located in the boreal forest, but has a large surface storage component, as approximately 30% of the basin is classified as either fens or bogs. The Iittovuoma basin is located north of the boreal forest and is practically treeless.

As part of the FROSTFIRE experiment, I participated in a study which analyzed the role of short- and long-term effects of wildfire on permafrost in Interior Alaska (Appendix A). My role in this study was to examine the short- and long-term effects of wildfire on the soil moisture regime. It was found that in both the short and the long term, the most significant impact on the soil moisture regime was through the removal of vegetation and the surface organic layers. In the short term, the loss of vegetation results in a decreased evapotranspiration demand, resulting in wetter soils than those of adjacent non-burned sites. The increased moisture content increases the thermal conductivity of the soils. In the moderate (partial, but significant removal of the organic layer) or severe (complete removal of the organic layer) sites surveyed, the increase in thermal conductivity led to a thickening of the active layer, increasing the soil storage capacity. The long-term (>10 years) effect of wildfire in these (moderate or severe) sites were drier soils (at depth) compared to adjacent un- or lightly-burned areas.

6.2 Computer simulation

A new spatially-distributed, process-based model hydrologic model, TopoFlow, was developed to simulate the hydrologic processes in the arctic and sub-arctic environments. The TopoFlow model is very well suited to simulating the hydrologic processes in the sub-arctic environment. TopoFlow is flexible enough to handle spatial and temporal input files, which is critical in describing the soil properties in the discontinuous permafrost environment. In Chapter 4, the structure of TopoFlow was described. TopoFlow is a second-generation hydrologic model, following ARHYTHM, developed by the Water and Environmental Research Center, University of Alaska Fairbanks.

Hydrologic modeling in any environment is challenging due to site-specific conditions In the sub-arctic environment, the challenge is presented by the discontinuous permafrost condition, in which rapid changes in thermal properties of the soils (permafrost versus non-permafrost, thaw depth) and hydrologic properties (hydraulic conductivity, storage

capacity) occur over short temporal and spatial scales. In our approach to representing the discontinuous permafrost condition, TopoFlow was modified to allow spatially and temporally variable inputs of hydraulic conductivity and porosity. By continually varying the hydraulic conductivity (used as a proxy for permafrost distribution and thaw depth) and porosity (used as a proxy for storage capacity), the dynamic changes of the soil properties associated with the discontinuous permafrost environment could be adequately represented. In Chapter 5, we showed that by only varying the hydraulic conductivity and porosity over time and space, we are able to reproduce the stream flow patterns observed in watersheds of varying permafrost coverage.

An analysis was conducted to test the sensitivity of the TopoFlow model with changing climatic conditions and soil properties. The hydrologic response to changes (both positive and negative) in permafrost distribution, active layer thickness, distribution of vegetation, evapotranspiration rates, precipitation, and temperature were all tested. This analysis demonstrated that precipitation has the strongest influence on the stream flow regime. The sensitivity test also illustrates the importance of the contributing area. A hydrologic response to spatial changes in vegetation distribution was found only in simulations in which the contributing area was altered.

References

Janowicz, J.R., N. Hedtrom, J. Pomeroy, R. Granger, and S. Carey (2004), Wolf Creek Research Basin water balance studies, in *Northern Research Basins Water Balance (Proceedings of a workshop held at Victoria, Canada, March 2004)*, edited by D. L. Kane and D. Yang, IAHS Series of Proceedings and Reports Number 290, pp. 195 – 204.

Quinton, W.L., M. Hayashi, K.E. Blais, N. Wright, and A. Peitroniro, (2004), The water balance of wetland-dominated permafrost basins, in *Northern Research Basins Water Balance (Proceedings of a workshop held at Victoria, Canada, March 2004)*, edited by D. L. Kane and D. Yang, IAHS Series of Proceedings and Reports Number 290, pp. 186 –194.

Seuna, P. and J. Linjama, (2004), Water balance studies of the northern catchments of Finland, in *Northern Research Basins Water Balance (Proceedings of a workshop held at Victoria, Canada, March 2004)*, edited by D. L. Kane and D. Yang, IAHS Series of Proceedings and Reports Number 290, pp. 111 – 119.

Appendix A

Impacts of wildfire on permafrost in the boreal forests of Interior Alaska*

Abstract

The impact to permafrost during and after wildfire was studied using 11 boreal forest fire sites including two controlled burns. Heat transfer by conduction to the permafrost was not significant during fire. Immediately following fire, ground thermal conductivity may increase 10-fold and the surface albedo can decrease by 50% depending on the extent of burning of the surficial organic soil. The thickness of the remaining organic layer strongly affects permafrost degradation and aggradation. If the organic layer thickness was not reduced during the burn, then the active layer (the layer of soil above permafrost that annually freezes and thaws) did not change after the burn in spite of the surface albedo decrease. Any significant disturbance to the surface organic layer will increase heat flow through the active layer into the permafrost. Approximately 3–5 years after severe disturbance and depending on site conditions, the active layer will increase to a thickness that does not completely refreeze the following winter. This results in formation of a talik (an unfrozen layer below the seasonally frozen soil and above the permafrost). A thawed layer (4.15 m thick) was observed at the 1983 burned site. Model studies suggest that if an organic layer of more than 7–12 cm remains following a wildfire then the thermal impact to the permafrost will be minimal in the boreal forests of Interior Alaska.

A.1 Introduction

The discontinuous permafrost zone is one of the most sensitive areas to climate warming in the world. Throughout the circumpolar north, the boreal forest widely overlaps the area of discontinuous permafrost [*Péwé*, 1975; *Brown et al.*, 1997; *Osterkamp et al.*, 2000]. The thermal condition of permafrost in this region is quite unstable, as it is very close to thawing, often $-1^{o}C$ or warmer. The distribution of the permafrost is strongly influenced by local factors such as landscape, soil type, and vegetation cover [*Viereck*, 1982; *Haugen et al.*, 1982]. The presence and thickness of the surface organic layer are the most important

*K. Yoshikawa, W.R. Bolton, V.E. Romanovsky, M. Fukuda, and L.D. Hinzman, Impacts of wildfire on the permafrost in the boreal forests of Interior Alaska, *J. Geophys. Res.*, *107*, 8148, doi:10.1029/2001JD000438, 2002. [printed 108(D1), 2003]

factors controlling degradation or aggradation of permafrost [*Viereck*, 1982]. When the organic layer is removed, the surface albedo decreases and the soil thermal conductivity of the surface soil layer increases from about 0.2 to about 1.0 W/m K [*Hinzman et al.*, 1991]. Wildfire is one of the most important agents controlling the thickness of organic layer in the boreal forest.

Wildfires have been a natural part of the boreal forest ecosystems, burning an average of 1 million ha/yr in 1950 increasing to almost 3 million ha/yr in 2000 in the North American boreal forests (B. Stocks et al., The changing fire regime of Western North America submitted to *Journal of Geophysical Research*, 2002) [*Kasischke and Stocks*, 2000]. Fires in boreal forests have both immediate and long-term impacts on the ecosystem due to their effects on surface energy, water balance, and underlying permafrost. The wildfire-return interval in the boreal forest is about 29 - 300 years [*Yarie*, 1981; *Kasischke et al.*, 2000; *Dyrness et al.*, 1986] and is strongly influenced by climate and human activities (both as a source of ignition and as an agent of fire control) [*Burn*, 1998a; *Brown and Grave*, 1979; *Fastie and Mann*, 1993].

Short-term studies of the effects of fire on the soil moisture and ground thermal regime in more temperate regions as well as cold regions have been well documented. Soil moisture content increases immediately following fires due to a decrease in evapotranspiration [*Klock and Helvey*, 1976; *Tiedemann et al.*, 1979; *Moore and Keeley*, 2000]. *Klock and Helvey* [1976] also noted a decrease in soil moisture content to prefire levels after a 5 year period. However, *Liang et al.* [1991] reported lower soil moisture contents in a burned area 2 years after a fire. Numerous other studies show increasing soil moisture contents following logging operations [*Croft and Monninger*, 1953; *Zierner*, 1964; *Klock and Helvey*, 1976].

Although the net surface energy balance may not change significantly after fire, the ways in which the incoming energy is partitioned does change substantially. For example, following wildfire, the surface albedo is significantly reduced. The reduced albedo means that soils can absorb incoming shortwave radiation than before the fire, which is then converted to sensible heat, resulting in higher ground surface temperatures. The offset of this is significantly increased outgoing longwave radiation due to these higher ground temperatures and increased energy conducted into the ground. The effect of this is an actual decrease in the net radiation by about 10% [*Rouse and Mills*, 1977].

Changes in depth to permafrost and active layer thickness are well documented and have been observed in numerous experimental studies. Changes in the surface material and thermal properties allow for increased heat flow. *MacKay* [1970] reported an average 24.1 cm (149%) increase in active layer thickness at the end of the first year and 34.8 cm increase (171%) in the second autumn. *Burn* [1998b] documented more rapid thawing and delayed freeze-back of the active layer compared to unburned areas. *Brown* [1983] noted that each of these effects is directly proportional to the fire severity. In cases of more severe fires, the surface organic layer is entirely combusted exposing the mineral soil beneath. Any disturbance to the surface layer will increase heat flow through the active layer into the permafrost. After approximately 3-5 years (depending on site conditions) the active layer will increase to a thickness that does not completely refreeze the following winter forming a talik. *Viereck* [1982] reported there was no significant difference in the active layer between the burned site and unburned sites in the first summer following the 1971 Wickersham Dome fire, located near Fairbanks, Alaska. However, the time required for the active layer to become completely frozen was delayed by 1 month compared to the unburned site in the first winter after the fire (12 December to 15 January 1971). In the following summer, the active layer was 161% deeper in the burned site as compared to the unburned control area. *Viereck* [1982] also demonstrated that fire lines (mechanically removing vegetation with a bulldozer) had more impact to the active layer than the severely burned site. *Heginbottom* [1971] reported that by the summer after a fire in Northwest Canada, thaw was 9 cm deeper on a burned site as compared to a control. *Lotspeich et al.* [1970] reported that the 1966 Dennison River fire, Eastern Alaska, showed no significant difference in thaw depth between burned and unburned sites. The burn was not severe enough at any site to remove the organic layer, which remained about 20 cm thick at the study burned site. *Wein* [1971] reported the conditions of site burned in 1969 in Interior Alaska. He described the active layer as being 35-50% deeper the next spring following the fire, and 15-20% greater in fall. *Brown et al.* [1969] observed several fire sites along the Alaskan Taylor Highway. The thaw depth was increased 140-160%. *Kryuchkov* [1968] observed the active layer was actually thinner several years after a fire in case of Siberian tundra. Before the fire, the active layer was 50-70 cm deep. However, it was only 40-45 cm a few years after the fire. This decrease in summer thawing was due to higher soil

moisture (ice) contents resulting from decreased transpiration. Controlled field experiments achieved more uniform results as compared with observations following wildfires. *Dyrness* [1982] studied differences in active layer thickness under different ground surface treatments (control, lightly burned, heavily burned, half the forest floor organic layer removed, and entire organic layer removed). After the fourth summer, the only treatment that had a statistically significant effect on soil temperature and permafrost depth was the mechanical removal of all or a portion of the forest floor. *Esch* [1982] tested the impact on permafrost of removing vegetation for road construction in Alaska. Three years after treatment he observed the removal of vegetation had increased the depth to permafrost by 300-600%.

Wildfires also impact geomorphological features on small and larger scales. In the first and second years after a fire, mass wasting or landslides frequently occur on hillslopes, which are more prone to failure due to increased soil moisture content [*Brown and Grave*, 1979; *Tiedemann et al.*, 1979; *Brown*, 1983]. Several decades later, thermokarst formation may occur as a result of thawing of ice-rich permafrost [*Viereck*, 1973; *Brown*, 1983].

This investigation focused on postfire impacts to the permafrost to quantify the impacts of fire on (1) direct heat conduction and convection to the ground, (2) removing moss as an insulating material, (3) heat budget, (4) soil moisture characteristics, and (5) active layer thickness and talik formation. These agents are the major components of permafrost dynamics. The evaluation of these agents will provide a better understanding of the relationship between burn severity and permafrost response and the effects on the hydrologic regime following wildfire.

A.2 Methods

Eleven wildfire sites throughout Interior Alaska, with dates of ignition ranging from 1924 to 2000, were selected for this study (Figure A.1). At each of these sites, active layer depth, ground temperature, soil moisture content, thermal conductivity and air temperature were measured. Several historical fires are located near Caribou-Poker Creeks Research Watershed (CPCRW) 48 km north of Fairbanks, Alaska [*Fastie and Mann*, 1993; *Fastie*, 2000]. Four of these wildfire burn areas within or immediately adjacent to CPCRW were selected for study and occurred in 1999 (site 1, control, moderate, severe), 1996 (site 2, moderate, con-

trol), 1990 (site 3, moderate, control), and 1924 (site 4, severe, moderate). The July 1999 controlled burn experiment (FROSTFIRE) took place in a $9.7km^2$ subbasin underlain by discontinuous permafrost [*Hinzman et al.*, 2000]. At the 1996, 1990, and 1924 burn areas, two small pits were dug: one in a burned area and one control. In the 1924 site, one pit was located inside the severely burned area and the other inside the moderately burned area. Locations of the pits were selected to be as physically similar to each other as possible. The total depth of the pits varied between 60 and 80 cm. In each pit, the temperature and soil moisture content were measured. TDR probe and gravimetric samples were collected in the surface duff layer, in the organic layer, and at regular intervals through the mineral soil. A ground temperature transect was established between the burned and the unburned sites. Shallow surface (15-20 cm depth) temperature measurements were collected at 3 m intervals using a thermocouple. A series of thermistors were used to measure the (0-100 cm depth) ground profile temperatures along the transect. Measurements were collected at 10-20 m intervals with additional measurements made near the boundary of the burned and unburned areas. Measurements were made every other month at the 1996 site and in August 1998 at the 1990 and 1926 sites. Seasonal frost depths were also measured. At the 1999 sites (site 1, FROSTFIRE), active layer depth, ground temperature, thermal conductivity, soil moisture content, and meteorological observations were collected.

The Rosie Creek site (Bonanza Creek LTER) was located in a burn that occurred in 1983 (severe, control) located approximately 10 km southwest of Fairbanks, Alaska. The Chena Host Springs Road site was located at a controlled burn that was conducted in August 2000, approximately 25 km east of Fairbanks, Alaska. This controlled burn lasted about 3 hours, during which direct measurements were collected. The purpose of this experiment was to determine the thermal impact from direct heating by the fire. A black spruce stand, 16 m^2 X 5 m high, with woody debris on the surface was ignited on a surface of feathermoss (*Hylocumium* spp.) and *Sphagnum*. Soil moisture contents and temperatures were measured below the surface to a depth of 32 cm in 2 cm increments. Type T and type K thermocouples were installed in the organic layer. Type K thermocouples with silfa silica insulation were used at the surface and in the moss (8 cm). The deeper layers were monitored using copper-constantan (type T) thermocouples with regular polyvinyl chloride (PVC) insulation. Temperature measurements were collected every minute. Soil

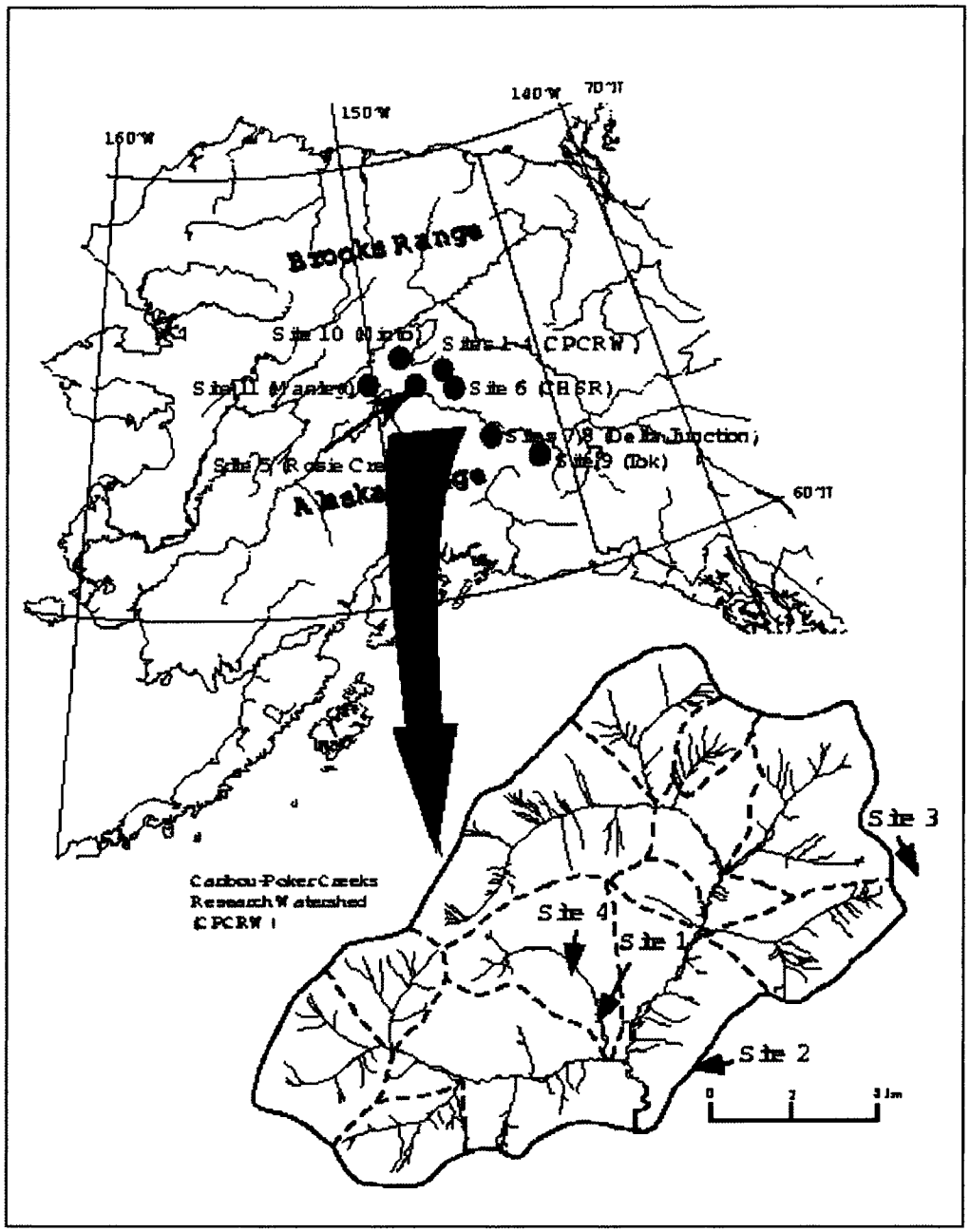

Figure A.1: Map of study sites. Eleven sites are located in Interior Alaska between the Alaska Range and the Brooks Range. Four of the 11 sites were located near CPCRW (insert map).

moisture content was measured using balanced TDR (time domain reflectometery) probes and a Tektronix model 1502B cable tester on 10 min intervals.

Two sites (sites 7 and 8) were located near Delta Junction, Alaska. The 1994 fire at Hajdukovich Creek (severe, control) and the 1999 fire at Donnely Flats (severe, moderate, control). Both fires had a variety of severities in black spruce (*Picea mariana*) with a feathermoss forest floor. The fire at site 9 occurred near Tok, Alaska in 1990 and was classified as a moderate burn with some severe areas. The final two sites are located north of Fairbanks, at Minto (site 10, 1999, moderate, control) and at Manley (site 11, 1963, severe, moderate).

At all sites, the remaining moss thickness, soil moisture content, ground temperature and thermal conductivity were measured (Table A.2). Soil moisture contents were measured using the Hydra soil moisture capacitance probe by Vitel Inc. [*Atkins et al.*, 1998]. The Campbell Scientific CS615 probe [*Bilskie*, 1997] was used to detect changing dielectric permittivity (constant). Electronic measurements were verified by gravimetric sampling and oven drying for 72 hours at 65^{o}C. Classification of organic soils and degree of humidification was based on the works of the *Soil Classification Working Group Staff* [1998] and *Pritchett and Fisher* [1987].

Ground temperatures were measured using three different methods. Routine monitoring of active layer temperatures was accomplished using NTC thermistors (Alpha thermistor 14A5001C2) and recorded on Campbell Scientific CR10X data loggers. Type K and T thermocouples with CR10X loggers were used to measure near surface temperatures directly during fire. Three shallow (20-30m) boreholes were installed at the CPCRW 1999 site (site 1) and Rosie Creek 1983 site (site 5) to periodically monitor permafrost temperature profiles. A precision thermistor was lowered slowly down the boreholes to accurately ($< 0.001^oC$ error) record permafrost temperature changes and geothermal gradients.

Thermal conductivity was measured using the heat probe method [*Shiozawa and Campbell*, 1990] made by Kona systems and Thermal Logic. Thermal conductivity was also measured in the laboratory as a function of the water content and temperature on undisturbed samples from all sites.

Incoming and reflected shortwave radiation and incoming and emitted longwave radiation were measured using a pair of calibrated pyranometers (Eppley Black and White Pyranometer Model 8-48) and a calibrated pair of pygeometers (Eppley Precision Infrared

Radiometer Model PIR), respectively. An independent estimation of net radiation was obtained using a calibrated Frischen type net radiometer (REBS Model Q7.1). A wind speed (Met One 014) dependent dome cooling correction was applied to the results. Table A.1 provides a summary of measurements and instruments at each site.

The radiation budget before and after the CPCRW controlled burn was measured using shortwave, longwave and net radiometers. Sensors measuring shortwave and longwave incoming and reflected (emitted) radiation were installed on a 3 m tower (unburned site) and a 1.5 m tower (burned site); both were higher than the black spruce canopy. The radiation balance (Q) is expressed in terms of incoming solar radiation (K↓), surface albedo α, incoming longwave radiation (L↓) and emitted longwave radiation (L↑) in the form:

$$Q = K\downarrow(1-\alpha) + L\downarrow - L\uparrow \tag{A.1}$$

Talik formation was simulated using data from Rosie Creek (site 5). Ground temperature observations and other meteorological, vegetation and soils data were obtained from the data archive of the Bonanza Creek Long-Term Ecological Research (LTER). The thermal models used for these studies were described by *Osterkamp and Romanovsky* [1996] and *Romanovsky et al.* [1997].

A.3 Results

Five categories of the impacts to the permafrost were evaluated: (1) direct fire effects, (2) removing (burned) moss as an insulating material, (3) heat budget, (4) soil moisture characteristics, and (5) active layer thickness and talik formation. All these impacts are interrelated and cannot be absolutely separated; however, the following is a discussion of the separate mechanisms and the factors that influence them.

A.3.1 Impact 1: Direct fire effects

Figure A.2 shows the ground temperature at several depths during the fire at 25 km Chena Hot Springs Road (site 6). The increase in temperature at the forest floor during the fire was quite rapid. The temperature of the forest floor (surface of the moss itself) was more than 800°C during this experimental burn by using type K thermocouple. Temperature started

Table A.1. Summary of site information and instrumentation

Site	Location	Latitude	Longitude	Year of ignitiion	Ground temperature	Soil Moisture	Active layer	Profile method	Meteorological observation
Site 1	CPCRW	65.1°N	147.3°W	1999	K, Th, Pt	CS, Vt	Thaw probe, MRC	trench, borehole (26 m)	10 m tower
Site 2	CPCRW	65.1°N	147.3°W	1996	K, Th	Vt	Thaw probe, MRC	trench	no
Site 3	CPCRW	65.1°N	147.3°W	1990	K	Vt	Thaw probe	trench	no
Site 4	CPCRW	65.1°N	147.3°W	1924	K, Th	Vt	Thaw probe	trench	no
Site 5	Rosie Creek (LTER)	64.7°N	148.1°W	1983	K, Th	CS, Vt	Thaw probe, MRC	trench, borehole (18 m)	10 m tower
Site 6	25 km east of Fairbanks	64.8°N	147.1°W	2000	K, T, Th	CS, Vt, TDR	Thaw probe, T	trench	no
Site 7	Donnely Flats	64.0°N	145.7°W	1994	K, Th	Cs, Vt	Thaw probe, Th	trench	no
Site 8	Hajdukovich Creek	64.0°N	145.7°W	1999	K, Th	Cs, Vt	Thaw probe, Th	trench	10 m tower
Site 9	Tok	63.3°N	143.0°W	1990	K, Th	CS, Vt	Thaw probe	trench	no
Site 10	Minto	65.2°N	149.3°W	1999	K	CS, Vt	Thaw probe	trench	no
Site 11	Manley	65.0°	150.6°W	1963	K	CS, Vt	Thaw probe	trench	no

K: Type K Thermocouple, T: Type T Thermocouple, Th: Thermistor (Alpha Thermistor 14A5001C2), Pt: 100 Ohm Platinum Resistor, CS: Campbell Scientific CS615 Probe, Vt: Hydra Soil Moisture Capacitance Probe by Vitel Inc., MRC: MRC Thermistor Ground Temperature Probe, TDR: Time Domain Refractometry

Table A.2. Physical and thermal properties of the organic layer at selected study sites

Site	Year of ignition	Vegetation	Observation date	Density (g/cm^3)	SMC (%vol.)	Thermal conductivity (W/m K)	Ground temperature (°C)	Type of layer	Degree of humification	Dielectric constant (100 MHz)
Site 1 Birch Stand (3 cm)	1999	*Pleurozium schrebrii*	10 July 2000	NA	NA	0.09	15.55	live moss	H1	3.1166
Site 1 Birch Stand (10 cm)	1999		10 July 2000	NA	NA	0.15	7.84	Dead moss, litter	NA	3.5529
Site 1 Birch Stand (15 cm)	1999		10 July 2000	NA	NA	NA	NA	mineral, litter	NA	12.9701
Site 1 Open Spruce (3 cm)	1999	*Sphagnum,*	10 July 2000	NA	NA	0.10	13.73	live moss	H1	3.4405
Site 1 Open Spruce (12 cm)	1999	*Pleurozium schrebrii*	10 July 2000	0.08	36.20	0.16	5.78	Fibric	H2	2.7769
Site 1 Open Spruce (20 cm)	1999		10 July 2000	NA	NA	0.24	1.12	Humic	NA	28.4742
Site 5 UB (3 cm)	>1900	*Sphagnum*	7 July 2000	0.05	2.96	0.03	21.98	live moss	H1	2.1634
Site 5 UB (10 cm)	>1900	*Pleurozium schrebrii*	7 July 2000	0.05	10.56	0.06	7.72	Dead moss		4.7433
Site 5 UB (20 cm)	>1900		7 July 2000	0.06	19.47	0.41	0.96	Humic		11.9779
Site 5 B (3 cm)	1983	*Hylocomium splendens*	7 July 2000	0.05	4.96	0.11	19.53	Dead moss	H1	2.253
Site 5 B (8 cm)	1983		7 July 2000	0.36	41.96	NA	NA	Humic	NA	16.7177
Site 5 B (13 cm)	1983		7 July 2000	0.67	60.16	0.91	19.56	Mineral, charcoal	NA	36.4338
Site 7 B (3 cm)	1994	*Ceratodon purpureum*	20 June 2000	0.79	30.58	0.49	15.0	live moss, charcoal	NA	15.94
Site 7 UB (3 cm)	>1860	*Hylocomium splendens*	20 June 2000	0.09	3.27	0.05	13.3	Dead moss	H1	NA
Site 7 UB (12–18 cm)	>1860		20 June 2000	0.09	3.67	0.03		Fibric	H3	2.78
Site 7 UB (25 cm)	>1860		20 June 2000	0.71		0.20	0.6	Humic	H7	12.60
Site 8 S (3 cm)	1999		20 June 2000	0.88	23.76	0.39	17.8	Charcoal	H3	5.92
Site 8 UB (10 cm)	>1860	*Polytrichium, lichen*	20 June 2000	0.32	24.60	0.10	10.4	live moss	H1	11.68
Site 8 UB (12 cm)	>1860		20 June 2000	1.02	71.00	0.57	1.6	Humic	H6	57.48
Site 8 M (7 cm)	1999		20 June 2000	0.09	3.27	0.04	14.8	Fibric	H2	4.22
Site 8 M (15 cm)	1999		20 June 2000	0.50	26.65	0.15	1.5	Humic	H4	19.20
Site 9_1 (8 cm)	1990	*Polytrichium commune,*	20 June 2000	0.45	28.34	0.13		Fibric	H1	18.92
Site 9_2 (8 cm)	1990	*Polytrichium spp.*	20 June 2000	1.16	35.87	0.99		Humic	H7	16.72
Site 10 B (3 cm)	1999		21 June 2000	0.20	6.54	0.05	22.0	dead moss, charcoal	H3	3.13
Site 10 B (15 cm)	1999		21 June 2000	0.86	65.19	0.58	3.1	fibric	H8	55.79
Site 10 UB (5 cm)	1999	*Hylocomium splendens*	21 June 2000	0.04	1.88	0.06	15.3	live moss	H1	2.21
Site 10 UB (15 cm)	1999	*Pleurozium schrebrii*	21 June 2000	0.09	4.50	NA	1.4	fibric	H4	3.34
Site 11 M (3 cm)	1963	*Drepanocladus sp.*	21 June 2000	0.23	16.73	0.22	6.9	live moss	H1	10.11
Site 11 M (15 cm)	1963	*Polytrichium*	21 June 2000	0.44	34.23	0.44	0.3	Humic	H5	41.03
Site 11 S (5 cm)	1963	*Polytrichium*	21 June 2000	0.08	4.29	0.06	6.3	live moss	H1	2.50
Site 11 S (15 cm)	1963		21 June 2000	0.07	3.89	0.11	2.0	Fibric	H2	3.85
Site 11 S (23 cm)	1963		21 June 2000	0.97	58.10	0.58	0.5	Humic	H7	20.67

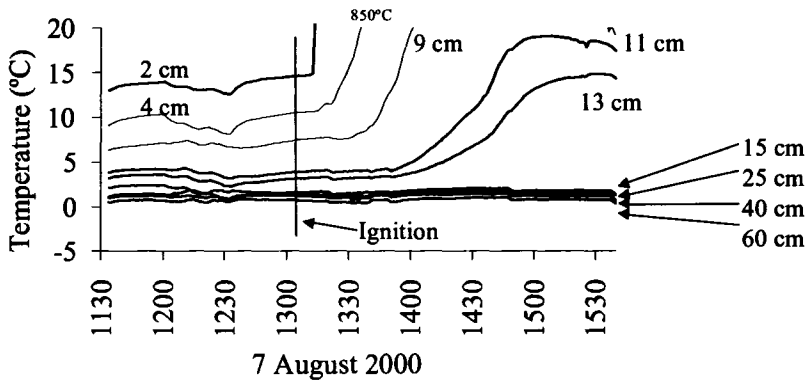

Figure A.2: Ground and surface temperatures during the fire at 25 km Chena Hot Springs Road (site 6) showing the increase in the near surface temperatures shortly after ignition. The ground temperature at this site rose only at the shallow depths(<15 cm). Most of the heat from the wildfire transfers to the ground by conduction, which does not penetrate deeply.

to rise 2 cm below the surface about 10 min after ignition. No significant increase in temperature was recorded below 15 cm at the feathermoss (*Hylocomium* spp.) and *Sphagnum* sites.

Many natural wildfires occur in forests where the floor is dominated by feathermoss (*Hylocomium* spp.) while fires in areas dominated by *Sphagnum* moss are relatively rare. The differences are due primarily to the characteristic moisture conditions both species prefer. Feathermoss (*Hylocomium* spp.) has a much lower moisture field capacity (about 20%) (C.M. Mack, Earth System Science, University of California Irvine, personal communication, 2000) and the typical water content is around 10% by volume in summer months, as compared to *Sphagnum* (40% moisture field capacity and typical levels of 30-40% by volume in summer months). The type of moss is not only an important factor in characterizing burn potential and severity, but also affects the surface thermal properties. About 70% of the volume of the live feathermoss is air and 10% is solid; consequently the thermal conductivity is strongly controlled by the water content. Increasing the water content by 40% increases the thermal conductivity 10-fold (Figure A.3). However, the typical condition of the moisture content of feathermoss is somewhat dry (usually less than 15% by volume). The thermal conductivity of the dry moss is almost the same as air (0.02 W/m K). As a result, under these conditions, fires do not transfer an immediate thermal impact

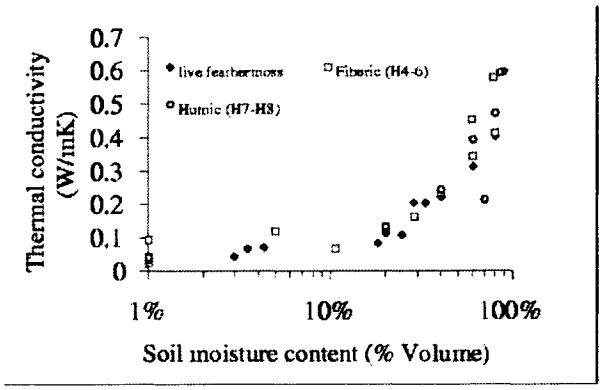

Figure A.3: The thermal conductivity of live feathermoss, fibric, and humic layers are strongly affected by moisture content. The classification of the organic layer was based on the works of *Soil Classification Working Group Staff* [1998] and *Pritchett and Fisher* [1987].

to deeper soil layers during a burn.

A.3.2 Impact 2: Removing (burned) moss as an insulating material

Removal of the organic layer exerts a serious impact to the ground thermal regime. In the first year following a fire, *Viereck* [1982] reported the thawing index of the soil surface may reach 1900 days°C in severely burned sites, as compared to 1500 days°C in unburned sites. The Mean Annual Surface Temperature (MAST) can increase by 2-3°C. The thawing index at 10 cm depth was 847 days°C (unburned site), 940 days°C (fire line) and 722 days°C (burned site). These suggest that the burn site is slightly cooler at the ground surface during the summer. However, because of of higher thermal conductivity of the surface soils of the burned site, the thawing index will be larger throughout the soil profile at the burned site as compared to similar depths in an undisturbed site.

At nearly every site we monitored, the summer ground temperatures of the burned areas were substantially warmer (by 1 - 20°C) than the adjacent complementary unburned control sites. The only exception to this trend was site 1 in the 1999 FROSTFIRE burn where the thermistors in the burned site were more shaded from the Sun as compared to the control site (Figure A.4a). In cases of fires that burned within the last 10 years, the ground surface temperature was warmer at the burned sites as compared to control sites during the early freezing period in autumn. This difference was maintained until the

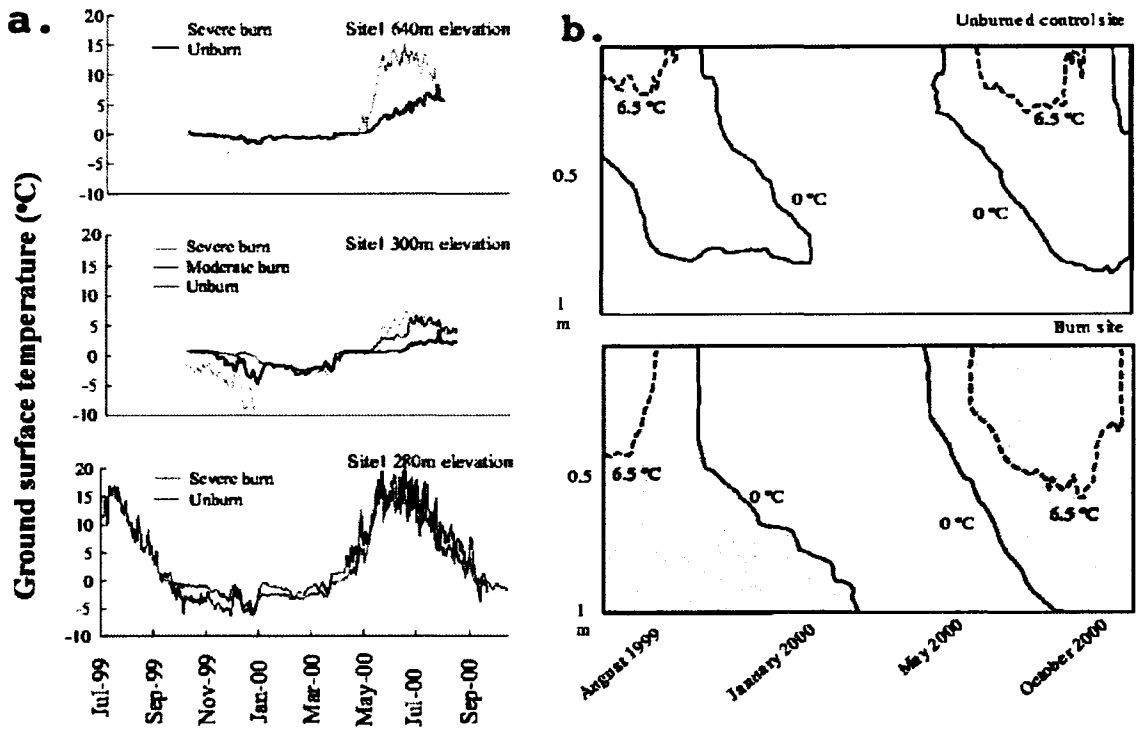

Figure A.4: Ground temperature dynamics at the FROSTFIRE site 1. (a) Annual variation of the near surface temperature in three separate locations showing warmer surface temperatures and delayed freezing in the burned sites. (b) Development of active layer in the unburned site is limited to 80 cm while the active layer in the burned site exceeds 1 m.

active layer became completely frozen. The moisture content of recent fires was higher in the burned sites, probably due to lower transpiration rates, so freezing would take longer due to larger latent heat of fusion requirements. However, in the older fires, the soils of the burned sites were somewhat drier and they would freeze faster in the fall. The depth of snow was not significantly different within sites (except in the Delta Junction area, sites 7 and 8) and is not considered to be a controlling factor for these differences. Sites where the burn severity was classified as moderate or severe also demonstrated an increased thickness in the active layer (Figure A.4b).

The most important factor controlling the active layer thickness is the thermal conductivity of the organic layer. The active layer thickness is not substantially impacted when the thickness of the organic layer is not significantly reduced during burning, even though the surface albedo is lowered. Table A.2 shows field observations of the thermal conductiv-

ity of each organic layer. In general, thermal conductivity is mainly a function of density, moisture content, and temperature; water content was particularly important in the post-fire environment. The type of moss and extent of decomposition of the organic material are important factors in controlling the soil thermal regime (Table A.2). A surficial layer of feathermoss has a lower thermal conductivity than *Sphagnum*, but after burning, feathermoss has a fibric layer that has a higher (or equal) thermal conductivity than *Sphagnum*. The thermal conductivity of the surface layer of *Sphagnum* does not change appreciably with burning, thus feathermoss has potentially larger thermal impacts after burning.

The thickness of the surface organic layer remaining after the fire and the resulting active layer were measured in CPCRW and Delta Junction areas. The active layer thickness is strongly controlled by the moss thickness, its thermal conductivity and moisture content and can be predicted based upon a relatively simple relationship. Sites that were severely burned (all or nearly all organic layer burned) always had deeper active layers than their control or adjacent lightly burned sites. A wildfire did not always affect the underlying permafrost. An organic layer with a thickness of 10 cm provided adequate thermal resistance to protect the frozen mineral soil.

A.3.3 Impact 3: Heat budget

After the prescribed burn at the FROSTFIRE site 1, the total net radiation decreased compared to an unburned site (97.7 at a moderate burn site compared to 160.2 MJ/m^2 at the control site between 23 July and 10 August 1999) as a result of the increase in the longwave emission (424-438 W/m^2). On the other hand, the albedo dramatically decreased from ~ 0.14 to ~ 0.05 (Figure A.5) yielding greater absorbtion of shortwave radiation at the ground surface. The daily variation of the net radiation (Q) was more variable at the unburned site (max 537 W/m^2, min -48.7 W/m^2) than the burned site (max 458 W/m^2, min -37.6 W/m^2). The radiation balance components are given in Table A.3 in terms of 100 units of incoming shortwave.

Radiation efficiency (Re) was calculated as the ratio of incoming shortwave radiation to net radiation, $Re = Q/K_d$. The radiation efficiency of the site 1 (moderately burned) was 50% (at noon) while the control unburned site has a Re of 75%. This indicates that the burned site was 25% less efficient at retaining incoming radiation. *Chambers and Chapin III*

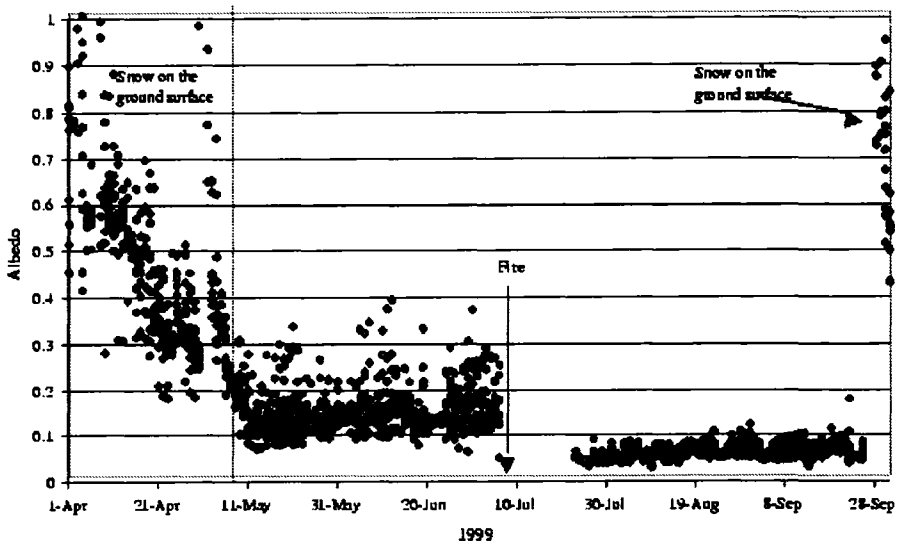

Figure A.5: Differences in albedo before and after wildfire. There are strong differences in albedo before and after wildfire. During snowmelt, the albedo ranges from 0.2 to 0.9 or more, decreasing to about 0.14 on a feathermoss surface prior to the fire. The albedo drops to 0.07 at a moderately burned site after the fire. Plotted data are the daytime (0600–1700 AST) averages.

Table A.3: Radiation balance of burned and control areas at site 1 (From 23 July to 10 August 1999 (sensor height 1 m at burned, 1.5 m unburned))

Radiation	K↓	K↑	α (%)	L↓	L↑	Re	Q	ΣQ (MJ/m^2)	Max. (W/m^2)	Min W/m^2)
Burned (site 1)	100	4.6	0.05	105	122	0.47	47.43	97.7	458	-37.6
Unburned (site 1)	100	13.5	0.14	105	118	0.74	73.59	160.2	537	-48.7

Net Radiation Q, Incoming Solar Radiation K↓, Reflected Shortwave Radiation K↑, Surface Albedo (%) α, Incoming Longwave Radiation L↓, Emmitting Longwave Radiation L↑, Radiation Efficiency Re, Total Net Radiation ΣQ.

[1999] reported somewhat similar results of radiation efficiency being 75% of efficiency at moderate burn site and 78% at an unburned site. The energy absorbed at the ground surface divides into sensible, latent, ground heat fluxes and energy storage. The daytime sensible heat flux is large and comprises at least 20% of K↓ (38% according to *Chambers and Chapin III* [1999]). The large sensible heat flux from the fresh burn manifests itself visibly on a sunny day [*Rouse and Mills*, 1977]. The Bowen ratio of a freshly burned site in the FROSTFIRE study was reported at $\beta = 4.5 \pm 3.3$ [*Chambers and Chapin III*, 1999]. Using this value of β, the ground heat flux and energy storage at our site 1 increased from an unburned area (0.07Q: 18.5 W/m^2) to (0.16Q : 29 W/m^2 or more) at the burned site. The ratio of ground heat flux to net radiation increased following fire. The distribution of the energy balance components shifted before and after fire. The increasing sensible heat and ground heat flux was balanced by decreasing the latent heat flux. As a result, ground temperatures were increased and wetter conditions became established despite the total net radiation decrease.

A.3.4 Impact 4: Soil moisture characteristics

During burning, the soil moisture content of the soils becomes drier than an adjacent unburned area (Figure A.6). Burned soils can develop a near surface hydrophobic layer [*DeBano*, 2000] that can resist surface water infiltration. Precipitation occurred during the 2 days following the CHSR Fire (site 6). In the control area, a significant increase in the soil moisture content was observed; while in the burn area, little change was observed. At the end of the observation period, the apparent hydrophobic layer was decreasing and the soil moisture content in the burned soils began to increase. It is unclear if the hydrophobicity effect is very important in the Alaskan soils that are usually somewhat moist to wet.

Prior to the CPCRW fire (site 1), the soil moisture contents at two adjacent sites were nearly the same. However, following the fire, the burned area displayed a noticeable increase in soil moisture content compared to the unburned control area (Figure A.7). However, all of the older fire sites (>10 years) tend to display drier soils as compared to the unburned (or lightly burned) control sites. At several sites, the soil moisture content was measured in burned areas and adjacent unburned areas at the same depth. Figure A.8 shows that the burned sites were always wetter at corresponding depths (active layer 0-50

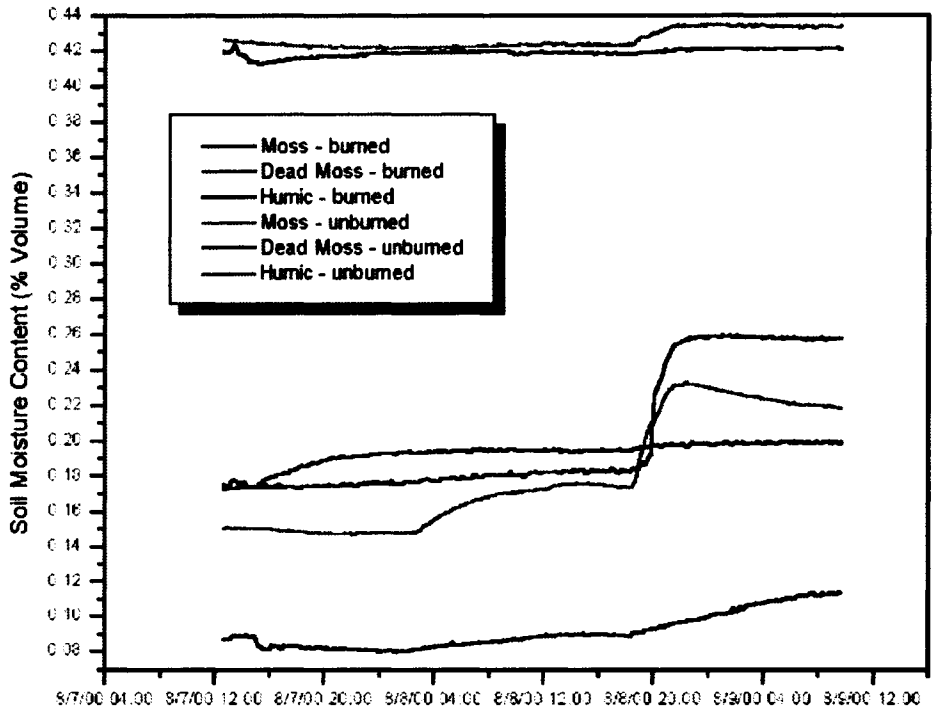

Figure A.6: Soil moisture content during and immediately following wildfire, 2000 CHSR, site 6

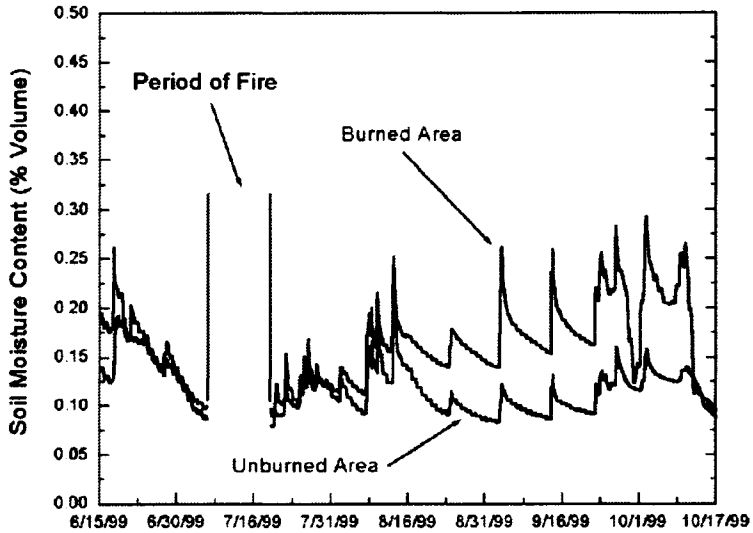

Figure A.7: Short-term near surface soil moisture content following wildfire at FROST-FIRE, site 1

cm) in the 1996 and 1994 burns. On the other hand, older burn sites were always drier at any depth. At the 1990 burn (site 3) the moisture content was about the same in the burned and unburned sites. The results of this study indicate the time required for severely burned soils to transition from having higher soil moisture contents to lower soils moisture contents to be about one decade.

A.3.5 Impact 5: Active layer thickness and talik formation

Both increased soil moisture contents as well as soil temperatures affect the active layer at the severe burn sites. Figure A.4b shows the active layer temperature profile for two thaw cycles in the FROSTFIRE severe burn area. There appears to be clear evidence of a change due to the fire in the first summer. The active layer was greater in locations where most of the organic material was burned to mineral soil. At the 1999 Minto fire (site 10), 50 random random active layer depths were measured in both the moderate burned area and unburned areas. The average active layer thickness was virtually identical (29.9 cm

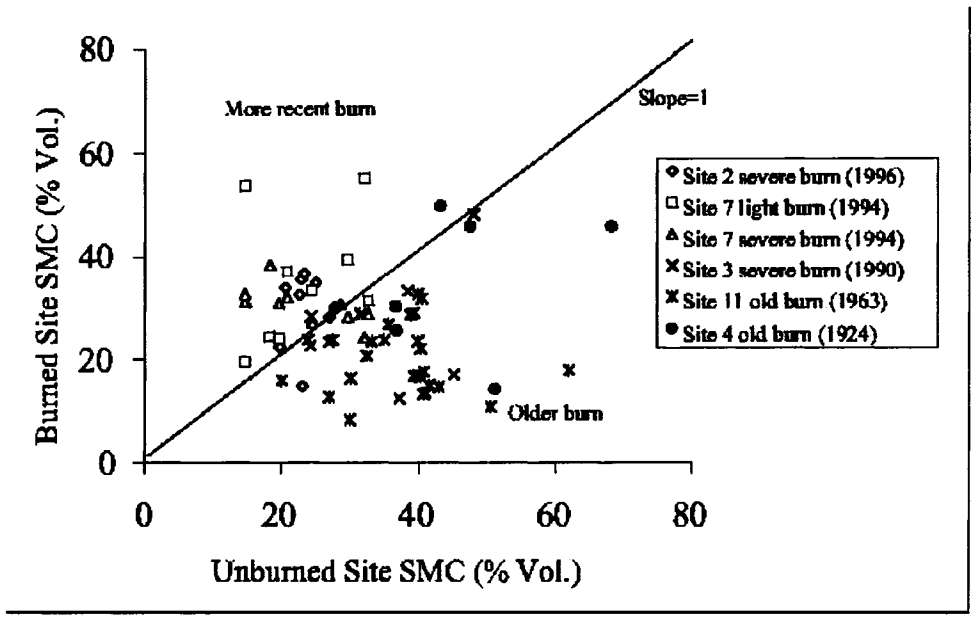

Figure A.8: Comparison of soil moisture contents between burned areas and adjacent unburned areas at fires of various ages (sites 2, 3, 4, 7, and 11) shows that in general more recent fires have higher mineral soil moisture contents in burned areas while older fires have higher mineral soil moisture contents in unburned areas.

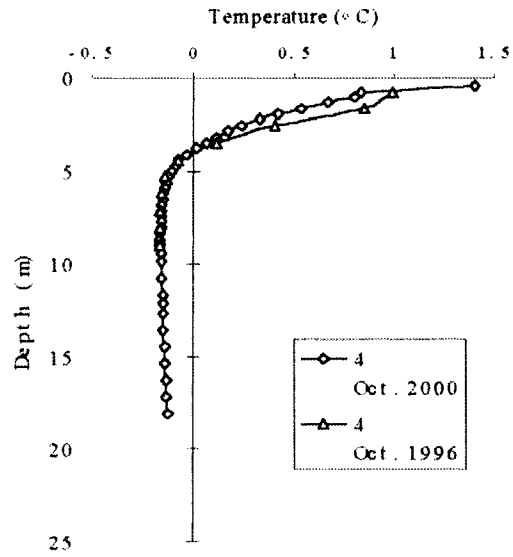

Figure A.9: Ground temperature profile at site 5 borehole. The permafrost starts 4.15 m below the surface (4 October 2000). The permafrost is very warm and close to thawing with the coldest temperature only –0.16°C at 8.6 m.

burned area versus 29.2 cm unburned area on 21 June 2000). The permafrost has degraded to a depth 4.15 m from the surface at the severe burned area of Rosie Creek (site 5) since 1983. The maximum annual depth of seasonally frozen ground is about 2 m, so the layer of unfrozen soil between the seasonally frozen ground and the permafrost is a talik. The thawing of the permafrost seems to have slowed or ceased as evidenced by the year 2000 ground temperature profile being nearly identical (below 4 m) to the year 1996 ground temperature profile (Figure A.9). There are many permafrost-free areas (or deep taliks) in areas where one would expect thick permafrost. Some of these permafrost-free anomalies correspond with fire scars indicating previous disturbances impart long lasting impacts to the permafrost. In light of the recent climatic conditions, we hypothesize that it will be difficult for permafrost to recover once thawed following a severe fire in this area.

A.4 Discussion

The permafrost distribution and ground surface heat balance are closely related. It is possible to determine a simple heat balance based upon the freezing index (I_f) and thawing

index (I_t) at the ground surface. The freezing and thawing indices are calculated based upon an accumulation of freezing or thawing degree days throughout the positive and negative daily mean temperature periods. $I_t = \Sigma t_s$ when ($t_s > 0$) and $I_f = \Sigma t_s$ when ($t_s < 0$) where t_s is the mean daily ground surface temperature. I_f and I_t were calculated at each burn and control site based on hourly data. The boundary conditions of permafrost presence is calculated using the following formula [*Lunardini*, 1981; *Romanovsky and Osterkamp*, 1995]:

$$I_t \leq (\lambda_f / \lambda_t) I_f \tag{A.2}$$

where λ_f and λ_t are frozen and thawed thermal conductivities. The ground surface I_f (freezing degree days) ranges between 500 (on south facing slopes) and 3000 (at the base of the north facing slopes) in CPCRW. On the other hand, I_t (thawing degree days) does not vary greatly (Ca. 1400) compared to the freezing degree days [*Yoshikawa et al.*, 1998]. Thus I_f is a key factor in determining the presence or absence or permafrost. *Van Cleve and Viereck* [1983] suggested that I_t measured at 10 cm ground depth is a good indicator of permafrost presence. On a black spruce forest floor, I_t averages about 500-800°C days. Less than 5 years after a fire, I_t increased to 1000-1250. If the organic layer and original trees recover, the active layer may return to its original thickness within 25–50 years [*Van Cleve and Viereck*, 1983].

Wildfire affects frozen ground systems primarily through the removal of vegetation and the surface organic layer. The loss of vegetation increases the soil moisture content due to reduced evapotranspiration. The thermal conductivity of an organic layer is a function of the moisture content, temperature, and density. If the organic layer remaining after a fire is adequately thick, the active layer thickness will not be depressed, in spite of dramatically lowered albedo. As a result, thickness and type of organic layer are the most important agents influencing the permafrost response to wildfire. Figure A.10 shows the relationship between active layer thickness and a function of the thermal properties of the soil (ξ). This function is thermal resistance divided by the local thawing index:

$$\xi = \frac{\sum_i \frac{d_{org}^i}{\lambda_i}}{\sqrt{I_t}} \tag{A.3}$$

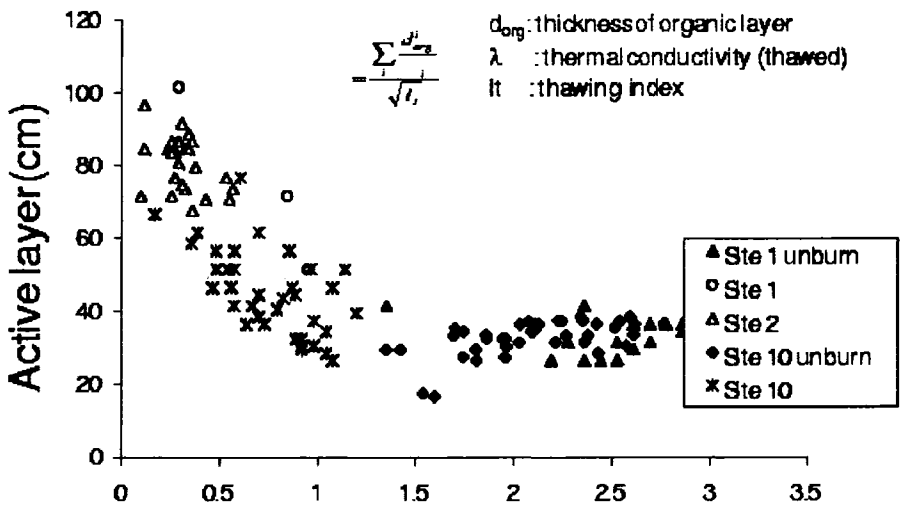

Figure A.10: Active layer thickness is affected by organic (living and dead moss, fibric, humic) layer thickness and composition, its thermal conductivity, and the thawing index. Data from sites 1, 2, and 10 in July 1999 demonstrate increasing active layer thickness with thinner organic layers.

where d^i_{org} is the thickness of organic layers (moss and peat, cm), λ_i is thermal conductivity of organic layers (W/m K) and I_t is thawing index of the ground surface (°C days). Thermal conductivity is strongly affected by the moisture content of the moss (Figure A.3). The thermal conductivity of moss and peat was determined by field and laboratory measurements [*Burwash*, 1972; *Andersland and Anderson*, 1978; *Farouki*, 1981]. In an unburned forest where permafrost is present, the function of thermal properties of organic soil (ξ) is usually greater than one. In areas where the fire severity was rated as low or moderate (organic soil was only lightly burned) such as site 10, the function of thermal properties of organic soils (ξ) will be between 0.7 and 1. As the severity of the fire increases, the function of thermal properties of organic soils (ξ) decreases. A ξ value of 0.7 or above appears to be a threshold as to when the permafrost will be adversely impacted by a wildfire. In Interior Alaska, the typical patterns of organic soils will yield thermal properties in the range of λ = 0.25–0.45 and I_t = 1400. Thus, after wildfire, if more than 7–12 cm of organic soil remain, the active layer thickness in the burned area will not be greater than that in the adjacent unburned area.

Heat transfer processes other than by conduction do occur and have been documented in many studies [*Hinkel and Outcalt*, 1994; *Kane et al.*, 2001; *Outcalt et al.*, 1990, 1997; *Woo*, 1982]. Nonconductive heat transfer processes occur in soils primarily in association with water movement, either in vapor or liquid phase. The processes increase in importance in soils with large pore sizes and large thermal or moisture gradients. Some heat movement coupled with vapor transport may have occurred in the active layer, decreasing the effective thermal conductivity [*de Vries*, 1974] and lowering the amount of heat transferred by conduction. It is difficult to quantify heat transfer by convection from measurements of soil moisture because the latent heat of vaporization is so large (approx. 2.5 MJ/kg). Relatively small changes in moisture may accompany significant heat flux. However, we do not believe that convective transport played a major role in accounting for the differences observed among these field sites, except for brief periods when the near surface soils were quite wet and the near surface temperature gradient was quite large (such as on sunny spring days when the active layer was still frozen near the surface). In general the pore size of these soils is quite small following a fire, greatly limiting free convection [*Russell*, 1935]. The most noticeable nonconductive thermal effect is produced by snowmelt water, which during the spring can infiltrate into the upper moss layer and into the frozen soils using the thermal cracks as flow paths. However, the annually averaged effect of this process on permafrost temperatures is minimal because the infiltrating water cannot transport any significant amount of sensible heat due to small differences in temperatures of this water and surrounding material. The latent heat of refreezing water can noticeably increase soil temperatures at this time but the same amount of latent heat will be consumed during the melt of this additional ice in the active layer during its thawing. So, the annual heat balance in the active layer will not be changed and the thermal effect on permafrost will be negligible.

A.5 Modeling

To investigate the effects of forest fire on permafrost temperature regime, we applied numerical modeling of the active layer and permafrost temperature field dynamics at the 1983 Rosie Cree fire (Bonanza Creek LTER, site 5). The models used for these studies were described by *Osterkamp and Romanovsky* [1996] and *Romanovsky et al.* [1997]. Daily air tem-

peratures and snow depth records for the last 46 years from the Fairbanks International Airport meteorological station were used for the upper boundary conditions. The lower boundary was placed at the approximate base of the permafrost at this site (54 m). A constant heat flux of 0.04 W/m^2 was used for the lower boundary condition. The models include the effects of latent heat and unfrozen water in the active layer and permafrost since it was found that the thermal response of the active layer and permafrost could not be successfully modeled without doing so [*Riseborough*, 1990; *Burn*, 1992; *Romanovsky and Osterkamp*, 2000]. Time steps in these calculations were 15 min, while the 200 vertical steps were changed from 1 cm within the upper 1 m of soils to 1 m at the lower boundary of the spatial domain (54 m). Site specific calibration of the models was accomplished using annually measured temperature profiles at this site and daily mean temperatures measured at the ground surface and at several depths in the upper meter of soil. Daily air temperatures and snow cover thickness from the Fairbanks International Airport were used to complete the model calibration and to extend the calculations back in time. Drilling records were used to determine the lithology and the initial approximate thermal properties of the soils in the thawed and frozen states. The thermal properties (including unfrozen water content curves) were refined using a trial and error method [*Romanovsky et al.*, 1997]. The results of modeling for the undisturbed site were discussed by *Osterkamp and Romanovsky* [1999]. Here we will compare these results with calculations for the site within the LTER Bonanza Creek research area where a severe forest fire occurred in the summer of 1983 (Rosie Creek fire).

As a result of this fire, the entire moss layer and most of the peat layer were destroyed. The model was modified to reflect these changes in soil properties. Other parameters of the model and driving variables such as air temperature and snow cover thickness were kept the same as in simulations of the undisturbed site. Calculations were started in the summer 1983 and the temperature profile from the no-disturbance simulation at the time of fire ignition were used as initial conditions. The calculation results are shown in Figure A.11. Immediately after the fire, the ground surface and active layer temperatures increased significantly and the long-term permafrost thawing began. As is shown in Figure A.11, the mean annual temperatures at the ground surface and at 1 m depth increased by 3–3.5°C during the first 5 years after the fire. This difference then decreased to 1.5–2°C during the

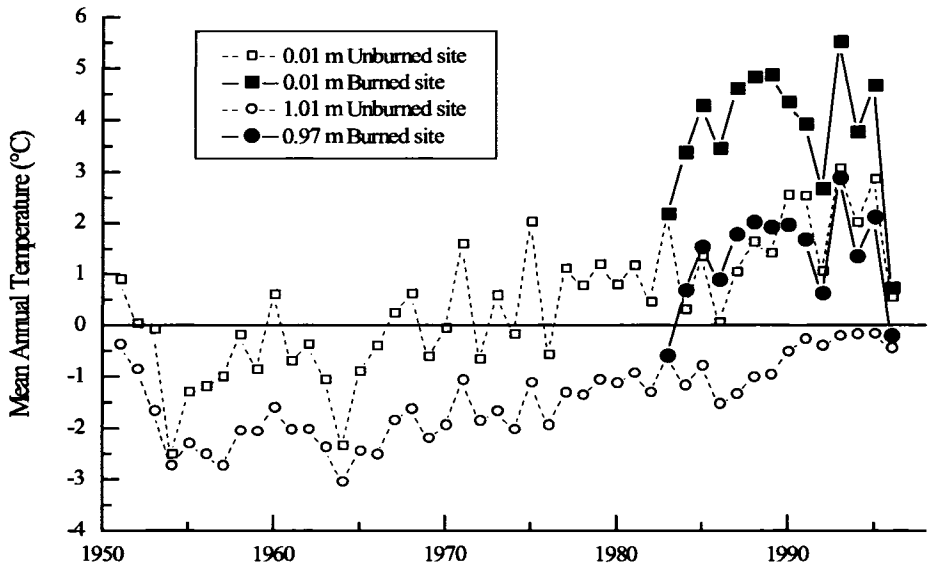

Figure A.11: Modeled mean annual temperature at the ground surface (open and filled squares) and at 1 m depth (open and filled circles) at an unburned site (open symbols) and at burned site 5 (filled symbols).

1990s.

The modeled permafrost thawing progression and a talik development at site 5 are shown in Figure A.12. The thawing of the permafrost was especially rapid during the first 5 years. By the end of this period, the depth of talik was 3.4 m. During the last 8 years of calculations, the talik increased by only 0.8 m, totaling 4.15 m in depth by 1996. Recent measurements (Figure A.9) show that during the rest of the 1990s, the talik did not increase with the permafrost table position practically stationary at the 4.15 m depth.

The organic soil was completely burned at site 5 (Table A.2). In the case of a light burn (simulation of a 16 cm moss layer, $\lambda = 0.7$ W/m K, $\xi = 1.2$), this model study suggests that maximum active layer reaches only 98 cm instead of the 4.15 m observed and simulated following a severe burn (simulation of a 6 cm moss layer, $\xi = 0.75$). The active layer depth of the area around site 5 is usually 60–70 cm at the unburned control area, while the burned area was about 20 cm deeper. Simulation results indicate that at the end of the 1989–1990 winter, the seasonal frost depth did not completely reach the top of the permafrost forming a 10–20 cm thick talik. Model simulations indicate the talik continues to increase in thickness for 5 years. The modeling study suggests that severity of burn (e.g. thickness

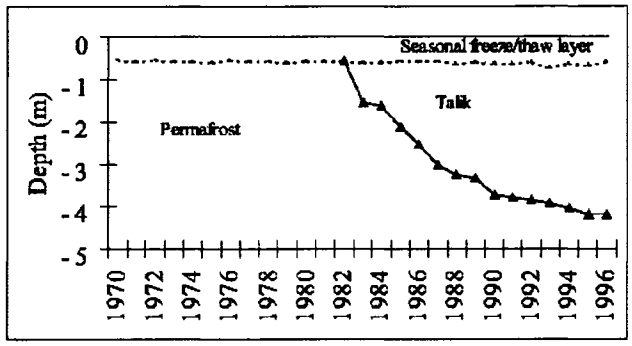

Figure A.12: Simulated active layer dynamics at an undisturbed site (dashed line) and talik formation at a burned site (solid line) at site 5 from 1970 to 1996.

of remaining organic layer) is an important factor controlling active layer thickness and talik formation. Observations and simulation results of the site 5 area indicate permafrost degradation due to fire is about 10 years in both the lightly and severely burned sites under the current climate conditions.

A.6 Conclusions

Depending on burn severity, wildfires result in an immediate impact upon the permafrost and ground thermal regime. In permafrost regions, the soils in a burned site will be warmer than in an adjacent unburned site for many decades. In the short term, wildfires will decrease rates of transpiration causing increasing soil moisture contents. In the long-term (more than a decade), the increased thickness of the active layer and recovery of vegetation will cause decreases in soil moisture content in burned sites as compared to control sites. However, after a light burn, where most of the fibric layer and some of dead moss remains, the permafrost is not significantly impacted in spite of a decrease in surface albedo to less than half that of an undisturbed forest. The thermal conductivity of the soils is greatly increased by increases in soil moisture content. There appears to be a threshold of organic material remaining after a fire that determines the degree of influence of the wildfire on frozen grounds. This threshold value is a function of the thickness of the moss, thermal conductivity of moss, and thawing index at the ground surface.

In the case of severe fire, the active layer begins to increase immediately following the

fire, but heat from the fire itself does not affect the active layer. Formation of talik depends on the thickness of the organic layer. Entirely removing an organic layer would very quickly initiate talik formation in this region. After a talik has formed, it is unlikely that the permafrost will recover under present climate conditions. The impact of the wildfires may influence the permafrost on a more global scale as well. With increased global warming (increasing ground surface thawing index), fire frequencies and severities may increase. Since permafrost temperatures in Interior Alaska are at or near 0^{o}C, the influence of wildfires may have a far-reaching impact on the landscapes, ecological impacts on the vegetation types, and enhanced feedback to global warming.

Acknowledgments. The authors are grateful to Tom Osterkamp (University of Alaska Fairbanks) for providing borehole temperature measurement equipment and a wealth of advice and information in support of this work. We also thank Nobuyoshi Ishikawa (Hokkaido University), Eric Kasischke (University of Maryland), Michelle Mack (University of California Irvine), Jennifer Harden (U.S. Geologic Survey), Shawna Laderach, Trevor White, Andrew Monaghan, and Jeremiah Drage (University of Alaska Fairbanks) for providing important suggestions and field assistance. Support for this research was provided by the U.S. National Science Foundation, Division of Environmental Biology, TECO program (DEB-9707461) and NSF LTER program (DEB-9211769) and the Japanese New Energy and Industrial Development Organization.

References

Andersland, O., and D. Anderson (Eds.) (1978), *Geotechnical Engineering for Cold Regions*, McGraw-Hill.

Atkins, T., R. Pangburn, R. Ates, and B. Brockett (1998), Soil moisture determination using capacitance probe methodology, *Special Report 98-2*, CRREL.

Bilskie, J. (1997), Using dielectric properties to measure soil water content, *Sensors*, pp. 26–32.

Brown, J. (1983), *The Role of Fire in Northern Circumpolar Ecosystems*, chap. Effects of fire on permafrost ground thermal regime, pp. 97–100, John Wiley.

Brown, J., and N. Grave (1979), Physical and thermal disturbance and protection of permafrost, *CRREL Report 79-5*.

Brown, J., W. Rickard, and D. Vietor (1969), The effect of disturbance on permafrost terrain, *Special Report 138*, CRREL.

Brown, J., O. Ferrians Jr., J. Heginbottom, and E. Melnikov (1997), Circum-Arctic map of permafrost and ground-ice conditions, *USGS Circum-Pacific Map Series CP-45*, U.S. Geological Survey.

Burn, C. (1992), *Periglacial Geomorphology*, chap. Recent ground warming inferred from the temperature in permafrost near Mayo, Yukon Territory, pp. 327–350, John Wiley.

Burn, C. (1998a), Field investigations of permafrost and climatic change in northwest North America, in *Proceedings of the Seventh International Conference on Permafrost*, vol. 57, edited by A. Lewkowicz and M. Allard, pp. 107–120.

Burn, C. (1998b), The response (1958-1997) of permafrost and near-surface ground temperatures to the forest fire, Takhini River Valley, southern Yukon Territory, *Canadian Journal of Earth Science, 35*, 184–199.

Burwash, A. (1972), Thermal conductivity of peat, in *Preceedings 4th International Peat Congress*, International Peat Society.

Chambers, S., and F. Chapin III (1999), Fire effects on surface-atmosphere energy exchange in black spruce forests of interior Alaska, in *Proceedings of the 50th AAAS Arctic Science Conference*, American Association for the Advancement of Science.

Croft, A., and L. Monninger (1953), Evapotranspiration and other water losses on some aspen forest types in relation to water available for stream flow, *EOS Transactions of the American Geophysical Union, 34*.

de Vries, D. (1974), *Heat and Mass Transfer in the Biosphere: Transfer Processes in Plant Environment*, chap. Heat transfer in soils, pp. 5–28, John Wiley.

DeBano, L. (2000), The role of fire and soil heating on water repellency in wildland environments: A review, *Journal of Hydrology, 231-232*, 195–206.

Dyrness, C. (1982), Control of depth to permafrost and soil temperature by the forest floor in black spruce/feathermoss communities, *Research Note PNW-396*, USDA Forest Service, Pacific Northwest Forest and Range Experiment Station.

Dyrness, C., L. Viereck, and K. Van Cleve (1986), *Forest Ecosystems in the Alaskan Taiga*, chap. Fire in taiga communities of interior Alaska, pp. 74–86, Springer-Verlag.

Esch, D. (1982), Permafrost prethawing by surface modification, *Tech. Rep. FHWA-AK-RD-83-23*, USDT Highway Administration.

Farouki, O. (1981), Thermal properties of soils, *CRREL Monograph 81-1*, Amry Cold Regions Research and Engineering Laboratory.

Fastie, C. (2000), Fire history of the C4 and P6 basins of the Caribou-Poker Creeks Research Watershed, Alaska, in *FROSTFIRE Synthesis Workshop, The Role of Fire in the Boreal Forest and its Impacts on Climatic Processes*, no. 00.03 in INE/WERC Report, pp. 21–23.

Fastie, C., and D. Mann (1993), A preliminary fire history for the Caribou-Poker Creeks Research Watershed, Alaska, unpublished memorandum, 8 pp.

Haugen, R., C. Slaughter, K. Howe, and S. Dingman (1982), Hydrology and climatology of the Caribou-Poker Creeks Research Watershed, Alaska, *CRREL Report 82-26*, US Army Corps of Engineers Cold Regions Research and Engineering Laboratory.

Heginbottom, A. (1971), *Proceedings of a Seminar on the Permafrost Active Layer*, chap. Some effects of a forest fire on the permafrost active layer, pp. 31–36, Technical Memo 103, NRCC.

Hinkel, K., and S. Outcalt (1994), Identification of heat transfer processes during soil cooling, freezing, and thaw in central Alaska, *Permafrost and Periglacial Processes*, *5*, 217–235.

Hinzman, L., D. Kane, R. Gieck, and K. Everett (1991), Hydrologic and thermal properties of the active layer in the Alaskan Arctic, *Cold Regions Science and Technology*, *19*, 95–110.

Hinzman, L., K. Yoshikawa, V. Romanovsky, W. Bolton, and K. Petrone (2000), Effects of forest fires on surface hydrologic and thermal processes, in *FROSTFIRE Synthesis Workshop, The Role of Fire in the Boreal Forest and its Impacts on Climatic Processes*, no. 00.03 in INE/WERC Report.

Kane, D., K. Hinkel, D. Goering, L. Hinzman, and S. Outcalt (2001), Non-conductive heat transfer associated with frozen soils, *Global Plantary Change*, *29*.

Kasischke, E., and B. Stocks (2000), *Fire, Climate Change, and Carbon Cycling in the Boreal Forest*, Springer-Verlag.

Kasischke, E., N. French, K. O'Neill, D. Richter, L. Bourgeau-Chavez, and P. Harrell (2000), *Fire, Climate Change and Carbon Cycling in the Boreal Forest*, chap. Influence of fire on long-term patterns of forest succession in Alaskan boreal forests, pp. 214–238, Springer-Verlag.

Klock, G., and J. Helvey (1976), Soil-water trends following wildfire on the Entiat Experimental Forest, in *Annual Proceedings Tall Timbers Fire Ecologic Conference*, 15, pp. 193–200.

Kryuchkov, V. (1968), Soils of the far north should be conserved (in Russian), *Priroda*, *12*, 72–74, translated and reproduced in Brown et al., 1969.

Liang, L.-H., Y.-W. Zhou, and J. Wang (1991), Changes to the permafrost environment after forest fire, da xi'an ridge, Gu Lian mining area, China, *Permafrost and Periglacial Processes*, *2*, 253–257.

Lotspeich, F., E. Mueller, and P. Frey (1970), Effects of large scale forest fires on water quality in interior Alaska, *Tech. rep.*, US Dept. of Interior, Fed Water Pollu. Control Admin, Alaska Water Lab.

Lunardini, E. (1981), *Heat Transfer in Cold Climates*, Van Nostrand Reinhold.

MacKay, J. (1970), Disturbances to the tundra and forest tundra environment of the western Arctic, *Canadian Geotechnical Journal*, *7*, 420–432.

Moore, C., and J. Keeley (2000), Long-term hydrologic response of a forested catchment to prescribed fire, in *Proceedings Water Resources in Extreme Environments*, edited by D. Kane, pp. 37–42, American Water Resources Association, Anchorage, Alaska.

Osterkamp, T., and V. Romanovsky (1996), Characteristics of changing permafrost temperatures in the Alaskan Arctic, USA, *Arctic Alpine Research*, *28*(3), 267–273.

Osterkamp, T., and V. Romanovsky (1999), Evidence for warming and thawing of discontinuous permafrost in Alaska, *Permafrost and Periglacial Processes*, *10*, 17–37.

Osterkamp, T., L. Viereck, Y. Shur, M. Jorgenson, C. Racine, A. Doyle, and R. Boone (2000), Observations of thermokarst and its impact on boreal forests in Alaska, USA, *Arctic, Antarctic and Alpine Research*, *32*, 303 – 315.

Outcalt, S., F. Nelson, and K. Hinkel (1990), The zero-curtain effect: Heat and mass transfer across an isothermal region in freezing soil, *Water Resources Research*, *26*(7), 2509–2516.

Outcalt, S., K. Hinkel, and L. Miller (1997), *International Symposium on Physics, Chemistry, and Ecology of Seasonally Frozen Soils*, chap. Modeling the magnitude and time dependence of non-conductive heat-transfer effects in taiga and tundra soils, pp. 98–104, Cold Regions Research and Engineering Laboratory.

Péwé, T. (1975), Quaternary geology of Alaska, *Professional Paper 835*, U.S. Geological Survey.

Pritchett, W., and R. Fisher (1987), *Properties and Management of Forest Soils*, 2 ed., John Wiley.

Riseborough, D. (1990), Soil latent heat as a filter of the climate signal, in *Proceedings of the Fifth International Conference on Permafrost*, vol. 54, pp. 199–206.

Romanovsky, V., and T. Osterkamp (1995), Interannual variations of the thermal regime of the active layer and near surface permafrost in northern Alaska, *Permafrost and Periglacial Processes*, *6*, 313–335.

Romanovsky, V., and T. Osterkamp (2000), Effects of unfrozen water on heat and mass transport processes in the active layer and permafrost, *Permafrost and Periglacial Processes*, *11*, 219–239.

Romanovsky, V., T. Osterkamp, and N. Duxbury (1997), An evaluation of three numerical models used in simulations of the active layer and permafrost temperatures, *Cold Regions Science and Technology*, *26*, 195–203.

Rouse, W., and P. Mills (1977), A classification of fire effects on the microclimate of forest and tundra ecosystems, *Tech. Rep. R71-19/2*, Indian and North. Affairs, Ottawa.

Russell, H. (1935), Principals of heat flow in porous insulators, *J. Am. Ceram. Soc.*, *18*(1), 1–5.

Shiozawa, S., and G. Campbell (1990), Soil thermal conductivity, *Remote Sensing Review*, *5*, 301–310.

Soil Classification Working Group Staff (1998), *The Canadian System of Soil Classification*, 3 ed.

Tiedemann, A., C. Conrad, J. Dieterich, J. Hurnbeck, W. Megahan, L. Viereck, and D. Wade (1979), Effects of fire on water – a state-of-knowledge review, *General Technical Report WO-10*, U.S. Department of Agriculture Forest Service, 28 p.

Van Cleve, K., and L. Viereck (1983), A comparison of successional sequences following fire on permafrost-dominated and permafrost-free sites in Interior Alaska, in *Permafrost: Proceedings of the 4th International Conference*, pp. 1286–1291, National Academy Press.

Viereck, L. (1973), Ecological effects of river flooding and forest fires on permafrost in the taiga of Alaska, in *Permafrost: The North American Contribution to the 2nd International Conference*, pp. 60–67, National Academy of Science, Yakutsk, USSR.

Viereck, L. (1982), Effects of fire and firelines on active layer thickness and soil temperatures in Interior Alaska, in *Proceedings of the 4th Canadian Permafrost Conference*, pp. 123–134, Ottawa.

Wein, R. (1971), *Fire in the Northern Environment: A Symposium*, chap. Fire and resources in the subarctic-panel discussion, pp. 251–253, Pacific Northwest Forest and Range Experimental Station.

Woo, M. (1982), Flux of vapor from frozen materials in the high Arctic, *Cold Regions Science and Technology*, *5*, 269–274.

Yarie, J. (1981), Forest fire cycles and life tables: A case study from interior Alaska, *Canadian Journal of Forest Research*, *11*, 554–562.

Yoshikawa, K., L. Hinzman, N. Ishikawa, C. Collins, and V. Lunardini (1998), Air and ground temperature models at Caribou-Poker Creeks Research Watershed, in *Proceedings of the 49th AAAS Arctic Science Conference*, Fairbanks, Alaska.

Zierner, R. (1964), Summer evapotranspiration trends as related to time after logging of forests in Sierra Nevada, *Journal of Geophysical Research*, *69*, 615–620.